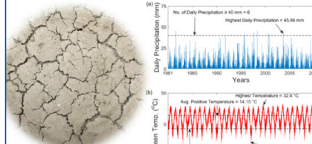


MOUNTAIN-PLAINS CONSORTIUM

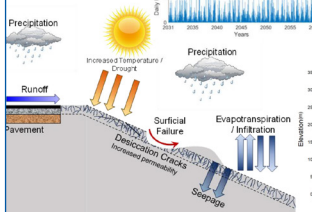
MPC 24-530 | A. Banerjee and D. Ghosh

ENHANCING THE RESILIENCY OF PAVEMENT INFRASTRUCTURE BUILT ON SULFATE-RICH EXPANSIVE SOIL SUBJECTED TO CLIMATE CHANGE

Slope Failures due to Desiccation Cracking and Extreme Weather



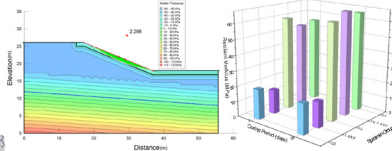
Sulfate-rich Expansive Soil



Advanced Soil Characterization and Testing



Modeling using Advanced Test Data



Additives: Biopolymers and Stabilizers



A University Transportation Center sponsored by the U.S. Department of Transportation serving the Mountain-Plains Region. Consortium members:

Colorado State University
North Dakota State University
South Dakota State University

University of Colorado Denver
University of Denver
University of Utah

Utah State University
University of Wyoming

Technical Report Documentation Page

1. Report No. MPC-687	2. Government Accession No.	3. Recipient's Catalog No.	
4. Title and Subtitle Enhancing the Resiliency of Pavement Infrastructure Built on Sulfate-Rich Expansive Soil Subjected to Climate Change		5. Report Date July 2024	
		6. Performing Organization Code	
7. Author(s) Aritra Banerjee, Ph.D., P.E. Debayan Ghosh, Graduate Research Assistant		8. Performing Organization Report No. MPC 24-530	
9. Performing Organization Name and Address South Dakota State University Civil & Environmental Engineering Crothers Engineering Hall 318, Box 2219 Brookings, SD 57007		10. Work Unit No. (TRAIS)	
		11. Contract or Grant No.	
12. Sponsoring Agency Name and Address Mountain-Plains Consortium North Dakota State University PO Box 6050, Fargo, ND 58108		13. Type of Report and Period Covered Final Report	
		14. Sponsoring Agency Code	
15. Supplementary Notes Supported by a grant from the US DOT, University Transportation Centers Program			
16. Abstract The study aimed to understand the impacts of extreme climatic conditions such as prolonged droughts and intense precipitation due to climate change on the resilience of civil infrastructures like embankments. The knowledge of unsaturated soil mechanics and soil chemistry is integrated to determine the impact of climate change on the stability of embankment slopes built with sulfate-rich expansive soils based on various emission predictions and climate models. An advanced suction-controlled triaxial setup that can determine the shear strength under varying moisture conditions and the resilient modulus of soils, was installed and calibrated. This setup is essential to study the impact of climate change. A series of suction-controlled triaxial tests were performed to demonstrate the behavior of clayey soil from the region with varying suction levels. The stability of an embankment was analyzed based on low to moderate emissions and high emissions till the end of the century. It was observed that for the high emissions scenario, the stability of embankment slopes decreased significantly, which demonstrated the need for resilience of embankments to address the stresses caused by climate change. An alternative treatment method using biopolymers and cement was identified as a potential candidate for the treatment of sulfate-rich expansive soils.			
17. Key Word climate change, disaster resilience, flexible pavements, modulus of resilience, pavement distress, soil stabilization, subgrade (pavements), sulfates, swelling soils, triaxial shear tests		18. Distribution Statement Public distribution	
19. Security Classif. (of this report) Unclassified	20. Security Classif. (of this page) Unclassified	21. No. of Pages 130	22. Price n/a

Enhancing the Resiliency of Pavement Infrastructure Built on Sulfate-Rich Expansive Soil Subjected to Extreme Weather

Prepared by:

Aritra Banerjee, Ph.D., P.E.

Assistant Professor

and

Debayan Ghosh

Graduate Research Assistant

Department of Civil and Environmental Engineering

South Dakota State University

Brookings, South Dakota

July 2024

Acknowledgments

The work presented in this report was conducted with support from South Dakota State University and the Mountain-Plains Consortium (MPC), a University Transportation Center (UTC) funded by the U.S. Department of Transportation. The authors would like to thank the support of the Department of Civil and Environmental Engineering and Jerome J. Lohr College of Engineering at South Dakota State University in Brookings, South Dakota for assisting in the procurement of the advanced triaxial system and supporting a graduate student who worked on this study. The assistance from Mr. Jay Tople at the South Dakota Department of Transportation at Pierre, South Dakota in helping the authors to obtain soil from different sites is greatly appreciated. The authors would also like to thank graduate students Avishek Ghosh and Niraj Neupane for their efforts and input during this study.

Disclaimer

The contents of this report reflect the views of the authors, who are responsible for the facts and the accuracy of the information presented. This document is disseminated under the sponsorship of the Department of Transportation, University Transportation Centers Program, in the interest of information exchange. The U.S. Government assumes no liability for the contents or use thereof.

NDSU does not discriminate in its programs and activities on the basis of age, color, gender expression/identity, genetic information, marital status, national origin, participation in lawful off-campus activity, physical or mental disability, pregnancy, public assistance status, race, religion, sex, sexual orientation, spousal relationship to current employee, or veteran status, as applicable. Direct inquiries to Vice Provost, Title IX/ADA Coordinator, Old Main 100, [\(701\) 231-7708](tel:7012317708), ndsu.eoaa@ndsu.edu.

ABSTRACT

The study aimed to understand the impacts of extreme climatic conditions such as prolonged droughts and intense precipitation due to extreme weather on the resilience of civil infrastructures like embankments. The knowledge of unsaturated soil mechanics and soil chemistry is integrated to determine the impact of extreme weather on the stability of embankment slopes built with sulfate-rich expansive soils based on various emission predictions and climate models. An advanced suction-controlled triaxial setup that can determine the shear strength under varying moisture conditions and the resilient modulus of soils, was installed and calibrated. This setup is essential to study the impact of extreme weather on the behavior of soils. A series of suction- controlled triaxial tests were performed to demonstrate the behavior of clayey soil from the region with varying suction levels. The stability of an embankment was analyzed based on low to moderate emissions and high emissions till the end of the century. It was observed that for the high emissions scenario, the stability of embankment slopes decreased significantly, which demonstrated the need for resilience of embankments to address the stresses caused by extreme weather. An alternative treatment method using biopolymers and cement was identified as a potential candidate for the treatment of sulfate-rich expansive soils.

TABLE OF CONTENTS

1. INTRODUCTION	1
2. UNSATURATED SOIL MECHANICS FUNDAMENTALS	4
2.1 Introduction.....	4
2.2 Saturated and Unsaturated Soils.....	4
2.3 Soil Suction in Unsaturated Soils.....	5
2.4 Surface Tension	6
2.5 Capillary Phenomenon.....	7
2.6 Soil Water Characteristic Curve (SWCC).....	8
2.6.1 General	8
2.6.2 Air-Entry Value.....	11
2.6.3 Residual Soil Suction	11
2.6.4 Hysteresis Effect	11
2.6.5 Techniques for SWCC Measurement	12
2.6.6 Mathematical Models for SWCC	15
2.7 Shear Strength.....	16
2.7.1 Shear Strength of Saturated Soil.....	17
2.7.2 Shear Strength of Unsaturated Soil	18
2.8 Types of Triaxial Tests.....	21
2.8.1 Unconsolidated Undrained (UU) Tests.....	21
2.8.2 Consolidated Undrained (CU) Tests.....	21
2.8.3 Consolidated Drained (CD) Tests.....	21
2.8.4 Constant Water (CW) Tests.....	22
2.8.5 Unconfined Compression (UC) Tests:	22
2.9 Methods to Control Suction	23
2.9.1 Axis Translation Technique	23
2.9.2 Osmotic Suction Technique	27
2.9.3 Vapor Equilibrium Technique.....	28
2.10 Modified Unsaturated Soil Triaxial Testing System.....	30
2.10.1 Independent Pore Water and Pore Air Pressures Control and Measurement.....	30
2.10.2 Volume Measurement	34
2.11 Summary.....	39
3. ADVANCED TRIAXIAL TESTING TO DETERMINE THE SHEAR STRENGTH OF UNSATURATED SOILS	40
3.1 Modifications to the base pedestal to implement the axis-translation technique.....	42
3.1.1 Double-walled triaxial cell	43
3.1.2 Automatic volume change device	44

3.1.3	Saturation of Ceramic Disc	44
3.2	Saturated Soil Triaxial Testing	45
3.2.1	General	45
3.2.2	Saturation of the specimen	45
3.2.3	Isotropic Consolidation of the specimen	46
3.2.4	Shearing under Drained conditions	46
3.3	Unsaturated Soil Triaxial Testing	48
3.3.1	General	48
3.3.2	Stress Variables and Shear Strength of Unsaturated Soils.....	48
3.3.3	Testing Procedure.....	49
3.3.4	Test Program	51
3.4	Mechanical Response under Suction-controlled Shearing.....	51
3.5	Summary.....	54
4.	IMPACT OF EXTREME WEATHER ON EXPANSIVE SOIL.....	55
4.1	Introduction.....	55
4.2	Incorporating Extreme Weather Data in Geotechnical Engineering.....	59
4.3	Climate Data	61
4.3.1	Historical Climate Data	61
4.3.2	Future Climate Dataset.....	63
4.3.3	Extreme Events	64
4.4	Numerical Modeling and Analysis.....	64
4.4.1	Soil Properties	64
4.4.2	Geometry of the Section.....	67
4.4.3	Numerical Modeling of Unsaturated Soil.....	67
4.4.4	Results and Discussion.....	68
4.5	Summary.....	71
5.	NUMERICAL ANALYSIS OF THE IMPACT OF EXTREME WEATHER ON EXPANSIVE SOIL EMBANKMENT IN SOUTH DAKOTA.....	73
5.1	Location of Interest.....	73
5.2	Soil Properties.....	73
5.3	Geometry of the Slope	75
5.4	Climate Dataset.....	76
5.4.1	Baseline Climate	76
5.4.2	Future Precipitation	78
5.4.3	Extreme Events	78
5.5	Results and Discussion.....	79
5.6	Conclusions.....	81

6.	PERFORMANCE OF CEMENT- AND BIOPOLYMER-TREATED SULFATE-RICH EXPANSIVE SOIL	82
6.1	Introduction.....	82
6.2	Materials	83
6.2.1	Expansive Soil.....	83
6.2.2	Additives	85
6.2.3	Cement	85
6.2.4	Biopolymer.....	85
6.3	Specimen Preparation	86
6.4	Experimental Program	87
6.4.1	Strength Studies	87
6.4.2	Determination of Stiffness Properties.....	88
6.4.3	Study of Swelling and Shrinkage Properties	88
6.4.4	pH Test.....	89
6.4.5	Study of the Microstructural Changes.....	89
6.4.6	Freeze-Thaw Test.....	89
6.5	Combined effect of cement and biopolymers in soil stabilization	90
6.5.1	Change in compaction characteristics.....	90
6.5.2	Comparison of stabilization effect of soil treatment.....	91
6.5.3	Change in pH due to the additives.....	92
6.5.4	Swelling-shrinkage characteristics of treated soil compared to control soil.....	93
6.5.5	Effect of stabilization on the strength characteristics	95
6.5.6	Effect of cement- and biopolymer-treatment on the resilient modulus.....	96
6.5.7	Microstructural studies of the treated soil.....	98
6.5.8	Study on the effect of the freeze-thaw (F-T) cycles	99
6.6	Summary.....	104
7.	CONCLUSIONS.....	105
7.1	Findings from the current study	105
7.2	Recommendations for Future studies.....	106
8.	REFERENCES	107

LIST OF TABLES

Table 2.1	Techniques to determine the various types of suction (modified from Lu and Likos 2004 and Murray and Sivakumar 2010)	13
Table 2.2	Empirical models used to best fit SWCC data.....	16
Table 2.3	Types of triaxial tests for soils (modified from Fredlund et al. 2012)	23
Table 4.1	Comparison of different GCMs in relation to baseline climate	62
Table 4.2	Soil properties used in the study	65
Table 5.1	Soil properties used for the numerical study.....	75
Table 5.2	Comparison of GCMs and NOAA climate normals	77
Table 5.3	Comparison of factor of safety (FOS) for different scenarios.....	80
Table 6.1	Basic geotechnical properties of the soil used in this study.....	84
Table 6.2	Expansive and Chemical properties of the soil used in the study	85

LIST OF FIGURES

Figure 1.1	Map of swelling clay in the continental U.S., in the northern-mountain-plains region, and South Dakota	1
Figure 1.2	Scanning electron microscope (SEM) image of ettringite formation.....	3
Figure 2.1	Schematic diagram of the variation of pore water pressure with depth	5
Figure 2.2	A schematic of the surface tension at air-water interface	6
Figure 2.3	Surface tension on a warped membrane	7
Figure 2.4	A typical Soil Water Characteristic Curve.....	10
Figure 2.5	Effect of initial density on SWCCs.....	10
Figure 2.6	Schematic of SWCCs depicting hysteresis due to drying and wetting cycle.....	12
Figure 2.7	Calibration curves for Whatman No. 42 filter paper	14
Figure 2.8	WP4 chilled water Potentiometer	15
Figure 2.9	A typical Mohr-Coulomb Failure Envelope for saturated OC clayey soils	17
Figure 2.10	Extended Mohr-Coulomb Failure Envelope.....	20
Figure 2.11	Schematic representation of the air-water interface in HAE disc	24
Figure 2.12	High air-entry disk ring arrangement.....	25
Figure 2.13	Chamber to saturate a ceramic filter disc.....	26
Figure 2.14	Saturation of HAEV ceramic disc in a test cell	27
Figure 2.15	Osmotic suction technique to impose suction in soil specimen.....	28
Figure 2.16	General Layout of automatic humidity control system.....	29
Figure 2.17	Relative humidity setup for triaxial testing.....	29
Figure 2.18	Modified triaxial setup for unsaturated soil testing	31
Figure 2.19	Modifications to (a) base platen, and (b) top cap assembly	31
Figure 2.20	(a) General setup of medium-sized triaxial apparatus and (b) Structure of top cap and base pedestal	33
Figure 2.21	Schematic plot of triaxial setup for unsaturated soils	35
Figure 2.22	Schematic of new triaxial setup to measure the volume change of the specimen.....	36
Figure 2.23	Modified triaxial testing equipment.....	37
Figure 2.24	Proposed triaxial testing system: (a) photograph of the setup; (b) schematic plot.....	38
Figure 3.1	Panoramic view of the (a) fully automated double-walled triaxial test setup and (b) repeated load triaxial setup.	40
Figure 3.2	A schematic diagram of the fully automated double-walled triaxial setup.....	41
Figure 3.3	A closer view of the experimental setup and soil sample (a) before and (b) after the completion of a test	42
Figure 3.4	The different pressure units for independent control of overburden pressure and matric suction within a soil sample	43
Figure 3.5	The ceramic disks used to maintain matric suction via axis translation technique	43
Figure 3.6	Automated volume change device.....	44
Figure 3.7	Deviator stress response of saturated silt for varying effective confining pressure	47
Figure 3.8	Determination of peak shear strength parameters for saturated silt specimen using Mohr-Coulomb failure criterion	48

Figure 3.9	Schematic of procedure to perform an unsaturated triaxial test at a net confining pressure of 200 kPa and matric suction of 250 kPa under drained conditions	50
Figure 3.10	Saturated and suction-controlled CTC stress paths in $p:q:s$ space.....	51
Figure 3.11	Deviatoric stress response of consolidated specimen at induced matric suction of 200 kPa under drained condition.....	52
Figure 3.12	Determination of peak shear strength parameters for unsaturated silt specimen using modified Mohr-Coulomb failure criterion.....	53
Figure 3.13	Critical state lines in $p-q$ space for saturated and unsaturated soils.....	53
Figure 4.1	Normalized plot of suction (in kPa) with depth for dry and wet conditions	56
Figure 4.2	(a) Desiccation crack formation of expansive soil, (b) surficial failure of expansive soil embankment.....	57
Figure 4.3	Schematic of climatic interactions with slope and surficial failure	59
Figure 4.4	SSP scenarios and their five SSP families	60
Figure 4.5	Baseline climatic conditions between 1981 and 2010: (a) daily precipitation, (b) daily mean temperature.....	62
Figure 4.6	Modeled future daily precipitation from GFDL ESM4 dataset: (a) SSP2-4.5 2031-2060, (b) SSP5-8.5 2031-2060, (c) SSP2-4.5 2071-2100, and (d) SSP5-8.5 2071-2100	63
Figure 4.7	Depth-duration-frequency curves for the site.....	64
Figure 4.8	Soil-water characteristics curve of the soil plotted using FX model.....	66
Figure 4.9	Hydraulic conductivity function of soil plotted using VG model.....	66
Figure 4.10	Profile and mesh structure of the embankment	67
Figure 4.11	FOS with PWP distribution at the end of the precipitation event for the different scenarios for historical data	69
Figure 4.12	FOS with PWP distribution at the end of the precipitation event for the different scenarios in the future for SSP2-4.5.	70
Figure 4.13	FOS with PWP distribution at the end of the precipitation event for the different scenarios in the future for SSP5-8.5.....	70
Figure 4.14	Change in FOS with temporal variations for 24 h precipitation for the baseline and future climate.....	71
Figure 5.1	(a) Hyprop, (b) WP4C setup for SWCC and HCF determination.....	73
Figure 5.2	Soil-Water Characteristics Curve of soil collected from Jones County.....	74
Figure 5.3	Hydraulic Conductivity Function Curve of soil collected from Jones County	74
Figure 5.4	Mesh structure of the slope for the study.....	76
Figure 5.5	Baseline climate data for study location in central South Dakota	77
Figure 5.6	Predicted future daily precipitation from CESM2 dataset of the study location in South Dakota: (a) SSP2-4.5 2031-2060, (b) SSP5-8.5 2031-2060, (c) SSP2-4.5 2071-2100, and (d) SSP5-8.5 2071-2100.	78
Figure 5.7	Depth-duration-frequency curves for location in South Dakota.....	79
Figure 5.8	PWP distribution of slope under SSP5-8.5 2071-2100 daily precipitation event	80
Figure 6.1	Particle Size Distribution of the native soil.	84
Figure 6.2	Molecular structure of guar gum	86
Figure 6.3	Equipment used for UCS, RLT tests, and microstructural studies.....	87

Figure 6.4	Experimental Set-up for the freeze-thaw cycles.	89
Figure 6.5	Compaction curves for control and treated soil from (a) Harvard miniature compaction and (b) Standard proctor compaction tests.....	91
Figure 6.6	Comparison of (a) Atterberg limit and (b) plasticity index with different treatment methods for soils	92
Figure 6.7	Variation of pH with treatment for different curing periods (0, 7, and 14 days)	93
Figure 6.8	Comparison of (a) 1D-swell and (b) linear shrinkage strain with treatment of different types.....	94
Figure 6.9	Variation of the swelling strain of different treatments with curing	94
Figure 6.10	Unconfined compressive strength for different biopolymer content after 7 days of curing	95
Figure 6.11	Unconfined Compressive Strength (UCS) test results of the treated soil for a curing period of 7 & 28 days compared to control soil.....	96
Figure 6.12	Variation of resilient modulus (MR) with confining pressure for constant peak deviatoric stress ($\sigma_d = 41.4$ kPa) for: a) CS, b) 1.5BP, c) 3C, d) 6C, e) 3C-1.5BP	97
Figure 6.13	Resilient modulus (MR) test results for constant confining pressure ($\sigma_3 = 27.6$ kPa) and deviatoric stress ($\sigma_d = 41.4$ kPa) of the control and treated soil for different curing periods	98
Figure 6.14	Field Emission Scanning Electron Microscopy (FE-SEM) images: (a) CS (2k Mag.), (b) 3C (2k Mag.), (c) 6C (2k Mag.), (d) 1.5BP (3k Mag.), and (e) 3C-1.5BP (10k Mag.).....	99
Figure 6.15	a. Moisture content loss, b. Volumetric strain, and c. Mass loss with F-T cycles for untreated and treated soil	101
Figure 6.16	Variation of a. UCS, and b. Strain at failure, ϵ_f with F-T cycles for untreated and treated soil.	102
Figure 6.17	Variation of MR with confining stresses: a. 41.4 kPa, b. 27.6 kPa, and c. 13.8 kPa with F-T cycles for control and treated soil for a peak deviatoric stress of 41.4 kPa	103

EXECUTIVE SUMMARY

The presence of expansive soil has resulted in significant damage to civil infrastructure like dams, levees, pavements, bridges, retaining walls, and others. Traditional calcium-based stabilizers like lime and cement are used to enhance the strength of soil, reduce the plasticity of clays, and reduce the volumetric changes in soils. However, calcium-based stabilizers have been known to be counterproductive for stabilizing sulfate-rich soils like the clayey soils from the Pierre shale formation. It is known that the soil derived from Pierre shale has layers of gypsum, which is a rich source of sulfate as evidenced by a few local soil samples in the western part of the state. The calcium from stabilizers reacts with alumina and sulfate from such soils to form ettringite and thaumasite in the presence of water. These are highly expansive minerals that are known to cause significant issues in different parts of the US due to their swell-shrink properties, and the resulting heave is termed sulfate-induced heave. The understanding of swell-shrink characteristics and variation of strength of soils with moisture is dependent on unsaturated soil mechanics, which is typically not used by Geotechnical professionals due to the complexities involved in testing and lack of equipment. The objective of the study is as follows: (a) assemble an integrated suction-controlled repeated load triaxial setup that can determine the resilient modulus and the shear strength of saturated and unsaturated soils; (b) evaluate the behavior of native and treated sulfate-rich expansive soil that is imperative for designing pavement sections by determining the variation of resilient modulus with moisture content; (c) establish the volumetric changes expected with wetting and drying of native and treated sulfate-rich expansive soils; (d) recommend design guidelines for stabilizing sulfate-rich expansive soils for enhancing the performance of pavement structure that may include using new stabilization procedures.

The study was divided into different segments to manage the workload for a complex study. The first part of the study focuses on unsaturated soil mechanics and how it relates to the study of the effect of extreme climatic conditions and variation of moisture regime. Different experimental setups were discussed and the assembly of a new advanced suction-controlled triaxial setup has been completed as a part of this study at the Geomechanics laboratory at South Dakota State University. The system was calibrated to perform suction-controlled triaxial tests on soil specimens using the axis-translation technique and to conduct repeated-load triaxial (RLT) tests on soil specimens to determine the resilient modulus of soils at different moisture levels. A series of triaxial tests and RLT tests have been demonstrated in the study.

The impact of extreme weather has been analyzed in this study for different regions with expansive soil problems. Extreme weather models were used to predict future climatic conditions and understand the additional climatic stresses that will be impacting the resilience of civil infrastructures like embankments. The most suitable climatic model was selected based on the comparison of past predictions and actual data for temperature and precipitation at the selected sites.

Based on the future emissions levels, two cases: (a) low to moderate emissions (SSP2-4.5); and (b) high emissions (SSP5-8.5) have been considered for the assessment of stability of embankment slopes in the future. The unsaturated soil properties such as soil water characteristics curve, hydraulic conductivity function, and variation of strength with suction of soil were used in the analysis. It was observed that future climatic conditions under high emission levels (SSP5-8.5) may be severe enough to trigger shallow slope failures due to prolonged periods of droughts followed by extreme precipitation. The desiccated slopes are a result of droughts and shrink-swell characteristics of expansive and high-plasticity soils. Though traditional stabilizers like cement may be suitable in enhancing the resilience of slopes built using expansive soils, however, for sulfate-rich soils such measures may be counter-productive due to the formation of ettringite.

Biopolymers such as guar gum in powdered form were used in the study to understand the potential of biopolymers to be used as stabilizers in different proportions and curing periods. Even though the volume changes were restricted due to swelling and shrinkage in biopolymer-stabilized soils, the strength increase was not significant. As an alternative treatment method, biopolymer was used as a co-additive to cement. This was the first attempt to stabilize such problematic soils using cement and biopolymers. The cement dosages were reduced to minimize the environmental impacts of using cement and biopolymers such as guar gum were used to allow crosslinking of biopolymer network with smaller concentrations of cement. The strength and resilient modulus of the soil were observed to increase significantly and at times even surpass the resilient modulus of the highest concentration of cement. The volume changes were also reduced to acceptable levels. Future studies have been recommended to explore the potential of crosslinking of biopolymers to stabilize problematic soil. The freeze-thaw studies also demonstrated the resilience of soils stabilized with a combination of biopolymers and cement, which fared better than the other stabilizers. This is a significant finding and future studies on this aspect of crosslinking of biopolymers may be suitable to stabilize not only sulfate-rich expansive soils but also other problematic soils.

1. INTRODUCTION

Expansive soils are identified by their proclivity to swell and shrink in response to changes in moisture levels due to high cation exchange capacity (CEC) and specific surface area of the dominant clay minerals, such as montmorillonite. These soils are found in many places around the world including Australia, Canada, Egypt, India, South Africa, Spain, and the U.S.A (Banerjee 2017) (Chen 1975; Jones and Holtz 1973; Puppala et al. 2003, 2013). Due to the presence of expansive soils, the parts of the western and southern United States and the Northern Great Plains have faced a multitude of problems involving the civil and transportation infrastructure (Chen 1975; Nelson and Miller 1997; Taher et al. 2020). For the NGP region, the issue of freezing and thawing causes additional distress to the pavement. Civil infrastructure including embankments and pavements are highly vulnerable to damage due to the shrink-swell behavior of expansive soils. It may not be feasible to avoid expansive soil during the construction of such civil infrastructure. Therefore, soil stabilization is frequently employed to mitigate the detrimental effects of shrink-swell behavior (Petry and Little 2003). The swelling shrinkage potential is significantly influenced by clay mineralogy (Mitchell and Soga 2005). When the surface charge density is at a moderate level with a cation exchange capacity (CEC) of 80-150 meq/100 g, the silicate layers can easily attract polar molecules (Mitchell and Soga 2005). The cations that are adsorbed may undergo hydration in smectite and vermiculite, leading to the separation and expansion of the silicate layers (Marshall 1964). Expansive soil is primarily composed of active clay minerals such as montmorillonite, vermiculite, and illite. A double-diffused layer of water and a high affinity of water are characteristics of such clay minerals (Banerjee et al. 2021; Mitchell and Soga 2005; Puppala et al. 2017). Desiccation or wetting-drying cycles can cause cracks in expansive clay due to its inherent shrinkage and swelling properties (Alonso et al. 2005; Lu et al. 2019). The prevalence of expansive soils in the continental US is illustrated in Figure 1.1, highlighting their occurrence in Dakotas, Wyoming, Montana, Colorado, Louisiana, Texas, and others.

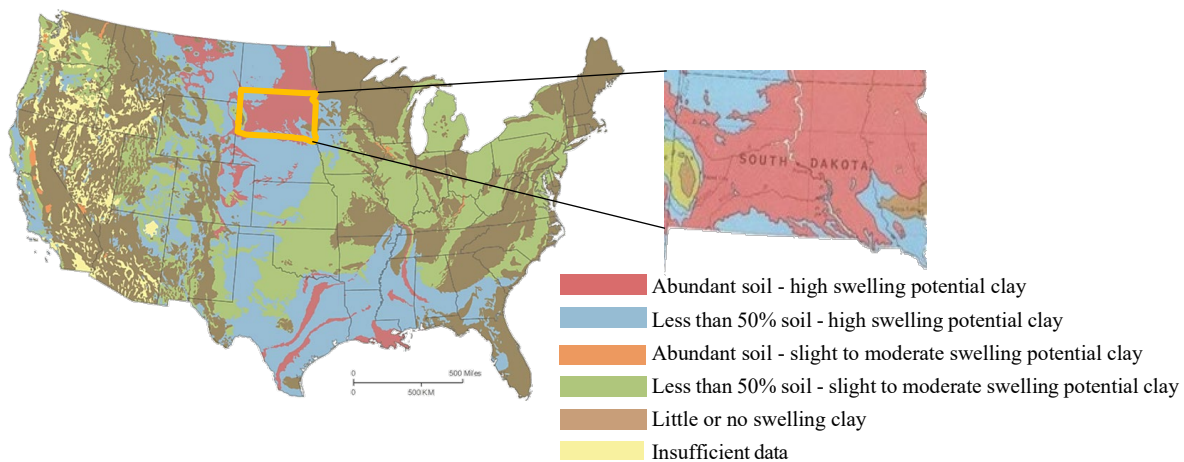


Figure 1.1 Map of swelling clay in the continental U.S., in the northern-mountain-plains region, and South Dakota (adapted from Olive et al. 1989)

Expansive clays, considered as problematic soil are commonly stabilized by using moisture-control methods such as ponding or prewetting, as well as by removing and replacing the soils. In addition, mechanical or chemical stabilization techniques are also used. Moisture management strategies are used to maintain the water content of a soil mass, thereby preventing fluctuations in water content that could cause the soil to swell and shrink. Chemical stabilization involves the incorporation of chemical additives into the soil, which modifies the physico-chemical characteristics of the soil and consequently improves its engineering properties (Petry and Little 2003). The application of chemical stabilization techniques to soils has been found to enhance their mechanical properties, specifically in terms of strength and stiffness. These improvements are observed through increased values of parameters such as unconfined compressive strength and resilient modulus. Additionally, chemical stabilization has been shown to effectively mitigate the swelling potential of soils (Puppala et al. 2003). Traditionally, lime, cement, and fly ash are widely employed as chemical soil stabilizers. Traditional stabilizers have demonstrated considerable effectiveness and represent a cost-effective solution for mitigating expansive soils.

In the past several decades, conventional calcium-based stabilizers, like lime and cement, have been used to enhance the engineering properties of expansive soils and address the issues brought on by the fluctuations in the moisture regime and low strength and stiffness of soft clays (Little and Nair 2009). Cement stabilization rapidly decreases the plasticity of the soil due to the release of calcium ions during the initial hydration reactions of cement. A cation exchange reaction or the accumulation of extra cations onto the clay particles may be involved in the process, or both mechanisms may be in effect (Puppala et al. 2003; Ross and Adaska. 2020). Both processes change the electrical charge density of the clay particles, causing them to be electrically attracted to one another (Bugge and Bartelsmeyer 1961). This causes the clay particles to flocculate or aggregate. When small amounts of cement stabilizer are added to soils, the aggregation process starts quickly (Bugge and Bartelsmeyer 1961). The hydration process of cement stabilization of soil forms calcium-silicate-hydrates (C-S-H), calcium-aluminate-hydrates (C-A-H), and calcium hydroxide ($\text{Ca}(\text{OH})_2$). Similar to the lime treatment of soil, strength is developed due to pozzolanic reactions of silica and alumina in clay minerals with calcium ions to produce cementing agents such as C-S-H ($3\text{CaO}\cdot 2\text{SiO}_2\cdot 3\text{H}_2\text{O}$) and C-A-H ($3\text{CaO}\cdot \text{Al}_2\text{O}_3\cdot 12\text{H}_2\text{O}$) in cement stabilized soil (Croft 1967).

Several previous studies have reported increased swelling potential of cement-stabilized soil with high sulfate content which sometimes leads to failure of transportation infrastructure (Puppala et al. 2004; Yong and Ouhadi 2007). This failure can be attributed to the formation of detrimental calcium-alumino-sulfate mineral, ettringite, which makes the cement stabilization insufficient or sometimes counterproductive (Little and Nair 2009). In alkaline environments with a pH of more than 10.5, the dissolution of clay releases alumina, which then reacts with Ca^{+2} from Ca-based stabilizers and soluble sulfates to form ettringite ($\text{Ca}_6(\text{Al}(\text{OH})_6)_2(\text{SO}_4)_3\cdot 26\text{H}_2\text{O}$) (Biswas et al. 2021, 2023; Chakraborty et al. 2022; Little et al. 2005). The volumetric expansion can reach up to 250% in calcium-based stabilization of sulfate-rich soil due to hydration reaction and crystal growth (Puppala and Cerato 2009). The phenomenon is known as sulfate-induced heave.

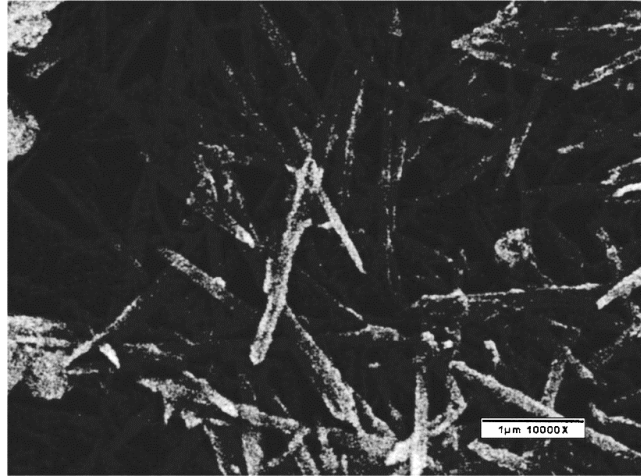


Figure 1.2 Scanning electron microscope (SEM) image of ettringite formation (Adopted from Puppala et al. 2005)

Multiple studies have been conducted to observe the effect of calcium-based traditional stabilization on sulfate-rich soil. The extent of damage resulting from the formation of ettringite is contingent upon various factors. These factors encompass (a) the thermodynamic propensity for ettringite precipitation in particular soil types; (b) the amount of limiting reactants that govern the mass of ettringite produced in a stoichiometric manner; (c) the movement of water, sulfate, and other ions that facilitate ongoing ettringite nucleation; (d) the durability of the pozzolanic or cementitious matrix; and (e) the spatial distribution of ettringite crystals within the soil matrix (Little et al. 2005). Ettringite has the potential to develop within voids that possess sufficient space to accommodate its growth without significant expansion. Ettringite crystals have the potential to grow within a compact matrix that lacks sufficient space for their expansion (Little et al. 2005).

For pavement systems, strength is not a critical parameter for design, the stiffness of pavement layers is used for current design standards (Banerjee 2017). Resilient modulus (M_R) is an important engineering parameter of soil that effectively correlates stress and strain in subgrade soils subjected to recurrent dynamic loading produced by traffic (Yang et al. 2008). In 2004, the AASHTO Mechanistic-Empirical Pavement Design Guide (MEPDG) recommended the use of resilient modulus as a design parameter for pavement systems in place of soil strength parameters (Banerjee 2017; NCHRP 2004). The American Association of State Highway and Transportation Officials pavement structure design guide (AASHTO 2008) and the mechanistic-empirical pavement design guide (M-EPDG) (NCHRP 2004) have both established and advocated the utilization of resilient modulus (M_R) for the structural design and analysis of pavements with regard to subgrade soils (Nazzal and Mohammad 2010; Rout et al. 2012). The repeated load triaxial (RLT) test was used in the previous studies to estimate the long-term performance of subgrade soil under traffic loadings and design pavement systems built over highly plastic and expansive soil (Banerjee et al. 2020a; Cary and Zapata 2011).

In this study different chapters discuss the importance of unsaturated soil mechanics in studying the response of soils due to variation in climatic conditions, the advancement of testing in regards to the suction-controlled triaxial testing to determine the shear strength parameters of unsaturated soils, the impact of extreme weather on the stability of embankments subjected to climatic stresses based on current extreme weather models, and the use of biopolymers to address some of these concerns for the need of sustainable stabilizers. Overall, they integrate the need for the study of unsaturated soil mechanics, soil chemistry, and the advancement of nature-based solutions to address the challenges of extreme weather and efficiently design critical infrastructure systems like embankments.

2. UNSATURATED SOIL MECHANICS FUNDAMENTALS

2.1 Introduction

The understanding of the response of expansive soils to the variation of moisture regime is partly dictated by the behavior of unsaturated soil. The fundamental concepts involved in unsaturated soils are complex involving solid mechanics, hydraulics, and interfacial physics (meniscus). Therefore, this chapter is devoted to the explanation of the theories of unsaturated soil mechanics.

The concept of thermodynamics plays an important role in the behavior of unsaturated soils, as it controls the meniscus formed at the air and water interface (Lu and Likos 2004). It involves the knowledge of vapor pressure, evaporation, precipitation, suction, and cavitation. Thermal agitation causes the water molecules, present within the soil, to escape from the air-water interface. Higher temperature results in higher kinetic energy, which causes a larger number of water molecules to escape from the liquid phase to the vapor phase. The vapor pressure increases till the number of molecules of water leaving and entering the water phase attains equilibrium, which is known as the saturated vapor pressure (Giancoli 1985). The evaporation of water from the soil causes the air-water interface to initially develop and gradually curve due to the pressure difference between the air and water phases in the soil (Fredlund et al. 2012).

The rate of evaporation primarily depends on the temperature, vapor pressure, water content, and concentration of salts. The suction developed due to the presence of dissolved solutes in pore water is known as osmotic suction. The concentration of salts decreases the vapor pressure and results in an increase of osmotic suction, which results in a slower rate of evaporation at a given temperature (Fredlund and Rahardjo 1993). Conversely, precipitation results in an increase in water content and a decrease in vapor pressure, resulting in a decrease in soil suction.

The behavior of the soil depends on the equilibrium of the inter-molecular and intra-molecular forces existing among the soil solids, pore water pressure, pore air pressure, and the air-water interface (Laloui 2010). Since the principles of thermodynamics affect these forces, the behavior of soil varies significantly due to the drying or wetting of soil (Fredlund et al. 2012). In other words, the behavior of saturated and unsaturated soils is significantly different due to thermodynamics. Henceforth, the constitutive relations or parameters required to predict the behavior of unsaturated soils are different from those required for saturated soils.

2.2 Saturated and Unsaturated Soils

A brief overview of the saturated and unsaturated soils is provided in this section, in order to clarify their differences. Figure 2.1 shows a schematic diagram of the location of saturated and unsaturated soils and their phase diagrams. The variation of pore water pressure with depth, with reference to the groundwater table and capillary fringe, is shown. Generally, it is assumed that the groundwater table defines the separation of the unsaturated and saturated soil mediums. There is an additional layer above the water table, which is almost saturated, known as the capillary fringe. This layer has minuscule and discontinuous pore air voids, and the pore water pressure is negative. The soil above the water table, consisting of the capillary fringe and the unsaturated soil, is commonly referred to as the vadose zone. The vadose zone media has a negative pore water pressure.

The saturated soil, which lies beneath the water table, has no air voids and forms a two-phase system consisting of soil solids and pore water. In this layer, the pore water pressure is positive and increases linearly with depth from the groundwater table level.

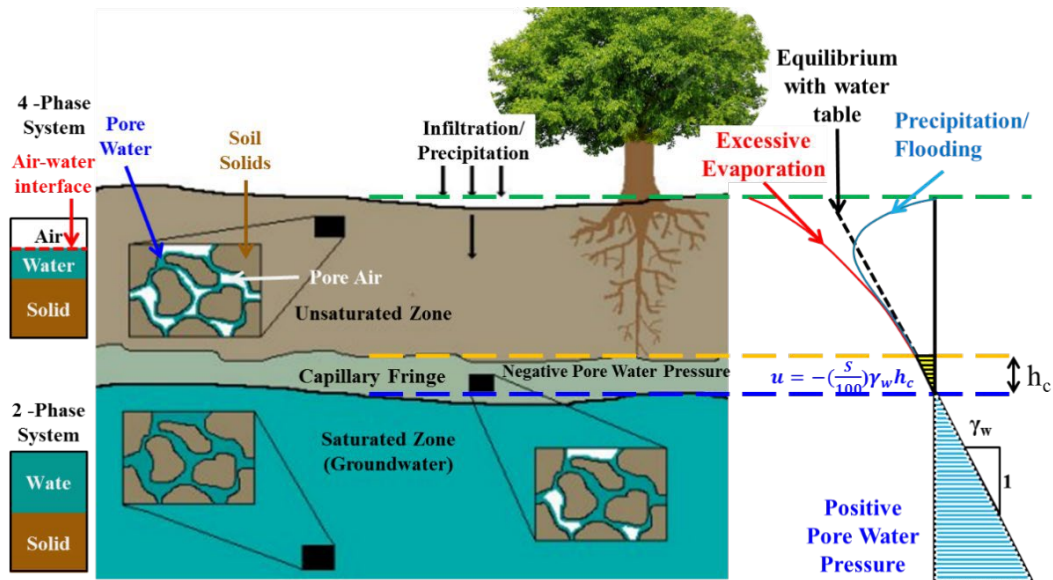


Figure 2.1 Schematic diagram of the variation of pore water pressure with depth

The unsaturated soil layer, which lies above the capillary fringe, has a four-phase system comprising soil solids, pore water, pore air, and the air-water interface, commonly known as the meniscus. The degree of saturation and the soil suction determines the continuity of the pore water and pore air. At a very low degree of saturation (less than 20% or 30%), the pore air phase is generally continuous and is referred to as “Pendular saturation” (Lu et al. 2009)).

For a higher degree of saturation (greater than 85% or 90%) the air voids are occluded within the continuous water phase (Schuurman 1966); (Fredlund and Morgenstern 1977). This state is referred to as “insular air saturation” or “capillary regime” (Lu et al. 2009)). Whereas, the transition state, where both air and water phases are continuous, is known as “Funicular saturation” (Lu et al. 2009). The variation of pore water pressure in the unsaturated zone is predominantly dependent on the climatic conditions.

Near the ground surface (in the vadose zone), the increase in temperature causes excessive evaporation which results in an increase in the magnitude of the negative pore water pressure. Conversely, precipitation or very high humidity conditions have the opposite effect. The variation of pore water pressure in this zone is thus non-linear (Fredlund et al. 2012). This non-linearity, coupled with negative values and the time-varying nature of pore water pressure results in difficulties in the measurement of these pressures in the field (Fredlund et al. 2012).

High-temperature conditions over a prolonged period of time increase the pore water pressure, causing desaturation-induced volume shrinkage cracks. This is referred to as desiccation cracking (Peron et al. 2009; Robinson and Vahedifard 2016; Tang et al. 2021; Vahedifard et al. 2024). On the other hand, when there is precipitation under these circumstances, the sudden decrease in the magnitude of pore water pressure might cause surficial failure.

2.3 Soil Suction in Unsaturated Soils

Soil suction is defined as the free energy state of the soil water, which can be computed in terms of the partial vapor pressure of the pore water. The total suction (ψ) of a soil has mainly two components: matric suction ($u_a - u_w$) and osmotic suction (π). The suction developed due to the combined effects of capillarity

and short-range adsorption is collectively known as matric suction (Lu and Likos 2004). The word *matric* reflects the prior usage of the term *matrix*, which symbolizes suction due to interactions between pore water and soil solids (Lu and Likos 2004).

The suction developed due to the presence of dissolved solutes is known as osmotic suction. Generally, in non-plastic soils, matric suction is a major component of total suction. Expansive soils demonstrate high activity due to mineral composition and dissolved solutes. Hence, the osmotic suction component constitutes a considerable portion of total suction.

2.4 Surface Tension

Air-water interface exhibits a phenomenon called surface tension. Surface tension arises from unbalanced intermolecular forces acting on molecules of the liquid phase, which is water in this case (Lu and Likos, 2004). Figure 2.2 shows a schematic diagram of the generation of surface tension from unbalanced forces at the air-water interface. Any water molecule present in the liquid phase (away from the air-water interface) experiences equal tensile forces from all directions due to hydrogen bonds between adjacent water molecules. Therefore, no unbalanced forces are present, and the water molecule is in static equilibrium.

Conversely, any water molecule at or very near the air-water interface experiences tensile forces from adjacent water molecules, but as these forces are not equally distributed, they result in unbalanced forces, and the resultant tension acts towards the interior of a water body. This resultant unbalanced force leads to the phenomenon of surface tension. The same property causes a water droplet to appear as a spherical mass which gets distorted due to gravitational forces. Surface tension acts as an elastic membrane at the air-water interface and it acts tangentially to the air-water interface (Figure 2.3).

The pressure difference (Δu) across a warped three-dimensional surface with radii of curvature of two orthogonal principal planes, R_1 and R_2 , and surface tension, T_s (Figure 2.3) is given by the following relation:

$$\Delta u = T_s \left(\frac{1}{R_1} + \frac{1}{R_2} \right) \quad (2.1)$$

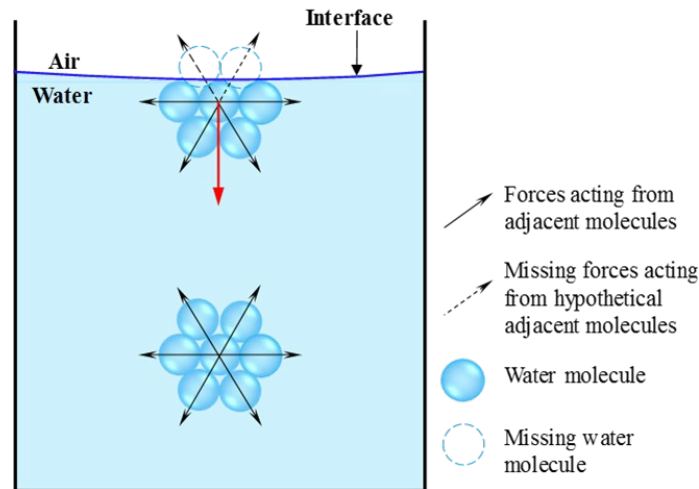


Figure 2.2 A schematic of the surface tension at the air-water interface (Banerjee 2017)

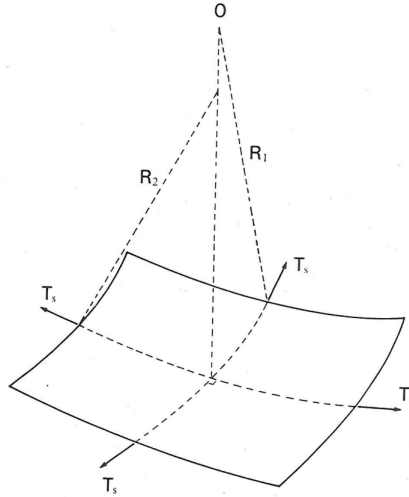


Figure 2.3 Surface tension on a warped membrane (Fredlund and Rahardjo 1993)

When the radius of curvature is the same in all directions ($R_1 = R_2 = R_s$), the equation 2.1 reduces to:

$$\Delta u = \frac{2T_s}{R_s} \quad (2.1)$$

In unsaturated soils, this pressure difference is the matric suction ($u_a - u_w$) which causes the contractile skin of the air-water interface to curve, in accordance with the following relationship:

$$(u_a - u_w) = \frac{2T_s}{R_s} \quad (2.2)$$

2.5 Capillary Phenomenon

Capillarity occurs when liquid rises in narrow tubes or is drawn into small openings such as those between grains of soil. Generally, the capillary force comprises two components: (i) the surface tension acting along the water-soil particle contact line, and (ii) the pressure difference across the bridge acting on the cross-sectional area (Pietsch and Rumpf 1967; Schubert 1984; Kim and Sture 2008). Capillary action causes the water to move (against gravity) from the water table into the soil pores. The height up to which the waterfront rises above the water table is known as the height of capillary rise, which depends on the dimension of the pore spaces. Generally, fine-grained soils with small pore sizes have a higher capillary rise as compared to coarse-grained soils. Physically, the maximum capillary height represents the decrease in pressure head across the air-water interfaces in the soil pores.

The rate of capillary rise depends on the hydraulic conductivity of the soil medium. When the capillary rise is greater than the air-entry head for that soil, the unsaturated hydraulic conductivity determines the rate of capillary rise. The unsaturated hydraulic conductivity depends on the degree of saturation and it may be 5 to 7 orders of magnitude lower than that of saturated hydraulic conductivity (Lu and Likos 2004).

The capillarity can be demonstrated by the capillary tube model, where the water rises in a tube of a small diameter when the tube is immersed in water. The capillary tube model can be used to predict the air-entry suction in the soil (Fredlund and Rahardjo 1993); (Lu and Likos 2004). Since the in-situ soil is comprised of particles of different sizes and has complex geometries, analytical solutions for the height of

capillary rise are too complicated. Hence, direct measurement of the height of capillary rise is the most reliable method, though often empirical relations, based on soil types, are used in real practice.

2.6 Soil Water Characteristic Curve (SWCC)

2.6.1 General

The soil-water characteristic curve (SWCC) provides a relationship between the water content (w) and the suction (ψ) for a specific soil. It portrays the thermo-dynamic capability of pore water in the soil with respect to that of the free water as a function of the measure of water adsorbed by the soil system (Lu and Likos 2004). The SWCC mainly depends on the soil type, gradation, void ratio, presence of salt concentration, temperature, and drying or wetting cycle of testing. The SWCC is used to develop correlations with various parameters, like shear strength, stiffness, and permeability.

The fundamentals and behavioral understanding of the SWCC have been developed by the agriculture-related research communities, like soil science and agronomy. Due to the varied disciplines using the water content – soil suction relationship, various other terminologies have been used to define the relationship, like Soil Water Retention Curve (SWRC), and moisture retention curve. Also, the amount of water in soil can be defined using various terms, such as gravimetric water content (w), volumetric water content (θ), degree of saturation (S), ratio of the volume of water to the original volume of the specimen (V_w/V_o).

Gravimetric water content, w is mostly used in geotechnical engineering and is defined as:

$$\text{Gravimetric water content, } w = \frac{M_w}{M_s} \quad (2.3)$$

where,

M_w = mass of water, and

M_s = mass of soil solids.

Volumetric water content, θ is usually used in the field of agricultural engineering and deals with the volumes of water, voids, and solids. It is defined as:

$$\text{Volumetric water content, } \theta = \frac{V_w}{V_v + V_s} \quad (2.4)$$

where,

V_w = volume of water

V_v = volume of voids, and

V_s = volume of soil solids.

The degree of saturation, S is the ratio of the volume of water, V_w to the volume of voids, V_v .

$$\text{Degree of Saturation, } S = \frac{V_w}{V_v} \quad (2.5)$$

Other terms to represent the amount of water present in soil include the dimensionless gravimetric water content, Θ , which is defined as the ratio of gravimetric water content at any degree of saturation, w to the initial saturated gravimetric water content, w_{sat} :

$$\text{Dimensionless gravimetric water content, } \Theta = \frac{w}{w_{sat}} \quad (2.6)$$

Each of the above terms has its advantages and disadvantages for determination of the amount of water in the soil. The gravimetric water content is the most commonly used measure of the water content of a soil sample in which the reference is made with respect to the mass of soil solids (which remains constant). However, it does not account for the changes in the volume of soil and the degree of saturation. The volumetric water content is often used in transient seepage in unsaturated soils, but volume measurements are complicated, and its usage is quite unfamiliar to geotechnical engineers. The degree of saturation properly designates the air-entry value and controls the behavior of unsaturated soils. Though it involves the measurement of the volume of soil solid, it does not incorporate the overall change in volume of the soil sample (Fredlund and Rahardjo 1993).

The SWCC can be portrayed in terms of matric suction, osmotic suction, and/or total suction. For practical considerations, the soil suction is considered to vary from zero to 10^6 kPa or 1 GPa. The Gibbs free-energy state equations for water vapor form the basis for the upper limit of the soil suction (Gibbs 1873); (Edlefsen and Anderson 1943). The Gibbs free-energy state equation is a thermodynamic relationship between partial water vapor pressure (i.e., relative humidity) and the soil suction. Relative humidity (RH) is defined as the ratio of the partial pressure of water vapor to the saturation pressure of pure water vapor at a given temperature condition. Hence, the Gibbs free-energy state equation is presented in the following (Sposito, 1981):

$$\psi = -\frac{RT}{v_{wo} \omega_v} \ln\left(\frac{u_v}{u_{vo}}\right) = -\frac{RT}{v_{wo} \omega_v} \ln(RH) \quad (2.8)$$

where,

ψ = total suction, kPa,

T = Absolute temperature, K,

R = Universal gas constant (8.31432 J mol⁻¹ K⁻¹),

v_{wo} = Specific volume of water (i.e. reciprocal of density, m³/kg),

ω_v = molecular mass of water vapor (18.016 kg/kmol),

u_v = partial pressure of water (or pore-water) vapor (kPa), and

u_{vo} = saturation pressure of pure water vapor (kPa).

The lowest and highest suction states provide important information about the soil and hence the suction values need to be plotted on a single graph on a logarithmic scale. Generally, the matric suction denotes the lower suction range (to 1500 kPa), while the total suction represents the higher suction range.

A typical SWCC is shown in Figure 2.4, where the various states of saturation are delineated by the air-entry value of the soil and the residual soil suction. The effect of the initial density of the SWCC is shown in Figure 2.5.

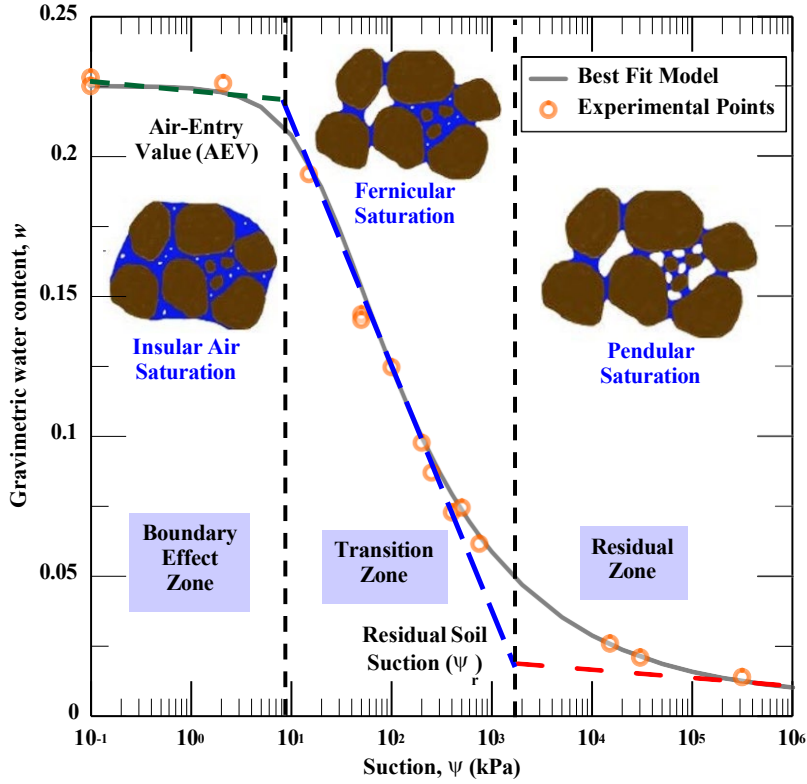


Figure 2.4 A typical Soil Water Characteristic Curve (Banerjee 2017)

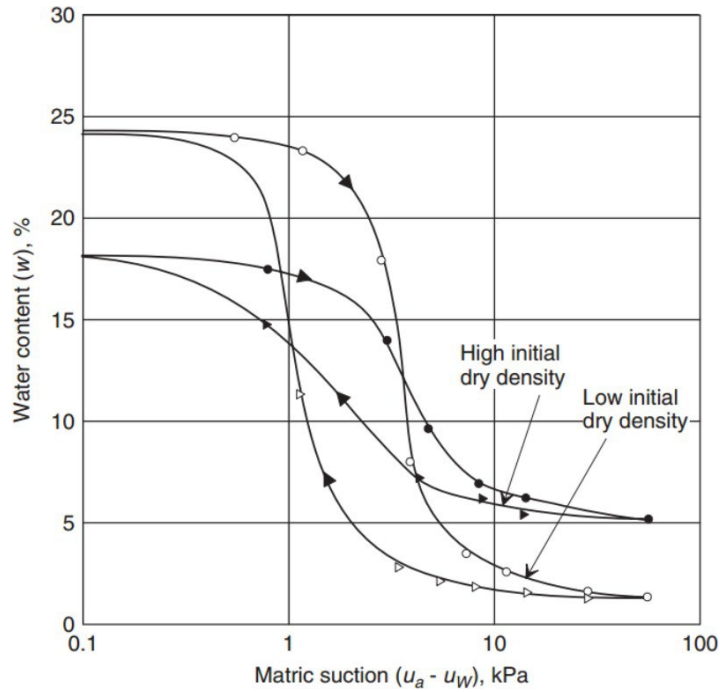


Figure 2.5 Effect of initial density on SWCCs (Croney and Coleman 1954)

2.6.2 Air-Entry Value

The air entry value (AEV) of a soil is defined as the value of matric suction at which upon drying, the pore water is replaced by the air entering the soil (Lu and Likos, 2004). The AEV demarcates the boundary effect zone, which has insular air saturation, from the transition zone, which comprises fernicular saturation. The permeability of the soil until the AEV is almost the same as the saturated hydraulic conductivity, but upon further desaturation, the permeability decreases exponentially (Fredlund and Rahardjo 1993). The AEV is determined by the intersection of the extrapolated portion of the linear part of the SWCC and the saturated portion of the SWCC as shown in Figure 2.4.

2.6.3 Residual Soil Suction

The suction at and beyond which the drying of soil barely decreases its water content is termed residual soil suction. Beyond the value of the residual suction, the water is present in the soil system by means of adsorption and not by capillarity (Vanapalli et al. 1996). The pore water phase becomes intermittent and isolated with thin films of water, which is difficult to remove with an increase in suction. The permanent wilting point is generally assumed to be the water content of the soil at the residual suction state (van Genuchten 1980). The residual soil suction is obtained by the intersection of the extrapolated section of the linear portion of the SWCC and the tangent extended from the SWCC at the maximum suction, which is practically considered as 1 GPa (as shown in Figure 2.4).

2.6.4 Hysteresis Effect

The drying and wetting cycles of the SWCCs are significantly different (as shown in Figure 2.6). In many scenarios, it becomes essential to evaluate the properties of soil separately for drying and wetting cycles. Geotechnical engineers need to consider the conditions that the soil will experience in real conditions and accordingly use the properties of either of the two cycles (Tami et al. 2004). The drying cycle is easier to perform and hence most commonly conducted in the laboratory. The hysteresis behavior of the drying and wetting cycles has been studied in detail by (Pham et al. 2003).

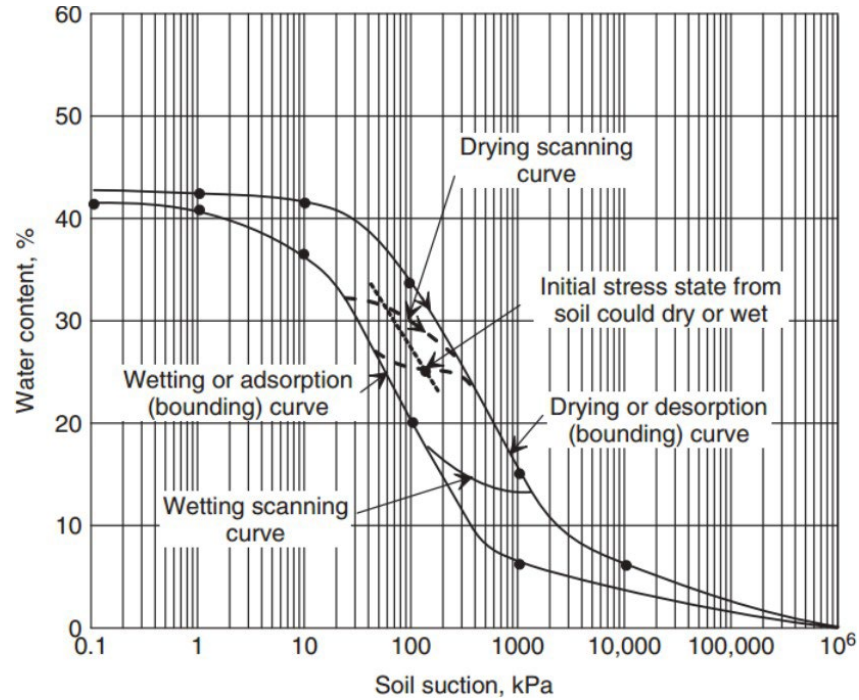


Figure 2.6 Schematic of SWCCs depicting hysteresis due to the drying and wetting cycle (Fredlund and Rahardjo 1993)

2.6.5 Techniques for SWCC Measurement

There are many techniques to determine the SWCC of soil. Some of the techniques and equipment are suitable for laboratory testing, while others are appropriate for use in the field. Some suction measurement devices measure total suction, while others record the matric or osmotic suction. The suction measurement techniques are broadly classified into two categories: (i) direct measurement techniques, where the suction is directly measured from the equilibrium of the soil-water system; (ii) indirect measurement techniques, where another parameter is measured which has been equilibrated within the soil-water system. Correlations and/or calibration charts are then used to determine the suction from that measured parameter. Table 2.1 lists some of the most commonly used suction measurement devices and their limitations.

Table 2.1 Techniques to determine the various types of suction (modified from Lu and Likos 2004 and Murray and Sivakumar 2010)

Suction Component Measured	Device / Technique	Typical range (kPa) (Area of Usage)	Limitations
Matric Suction	Pressure plate and Tempe cell	0 – 1,500 (Lab)	Long equilibration time and induced suction limited by AEV of ceramic disc
	Contact filter paper method	3000 – 100,000 (Lab)	Very sensitive to measurements
	Tensiometer	0 – 100 (Lab and Field)	Cavitation at absolute zero pressure limits the range
	Electrical/thermal conductivity sensors	0 – 400 (Lab and Field)	High failure rate; fragile and needs regular calibration
Osmotic Suction	Electrical conductivity of pore water extracted using pore fluid squeezer	Entire range (Lab)	Sensitive to extraction pressure; otherwise other equipment is required to determine the total and matric suction
Total Suction	Thermocouple psychrometer	100 – 8,000 (Lab and Field)	Sensitive to temperature fluctuations
	Chilled mirror hygrometers	1,000 – 450,000 (Lab)	Sensitive to dust and temperature
	Non-contact filter paper method	3,000 – 100,000 (Lab and Field)	Calibration is sensitive to time for equilibration
	Relative humidity apparatus	5000 – 500,000 (Lab)	High suction range

2.6.5.1 Fredlund's SWCC Device

Fredlund's SWCC device is similar to the pressure plate device, with the added advantage that the overburden pressure can be applied and the entire SWCC can be obtained without disassembling the device. It works based on the principle of the axis-translation technique. It can induce matric suction up to the air-entry value of the ceramic disk (generally, 500 kPa or 1500 kPa).

2.6.5.2 Filter Paper Technique

The filter paper technique is an indirect method of measuring suction. The suction measurement is based on the moisture equilibration between the filter paper and the adjacent soil. Contact and non-contact filter paper techniques can be used to measure the matric and total suction, respectively. The 'contact' here refers to the direct interaction of the filter paper with the soil-water system within an enclosed space.

The filter paper absorbs moisture until the equilibrium has been achieved with the water content of the soil for the contact technique and the relative humidity inside the container for the non-contact technique. After equilibrium has been achieved between the filter paper and the relative humidity in the enclosed space, the adsorbed water content provides a correlation with the suction in the filter paper, based on the calibration charts. This technique is used to measure both total and matric suction for a soil specimen. The calibration chart has been shown in Figure 2.7 for the most used filter paper, i.e., Whatman 42.

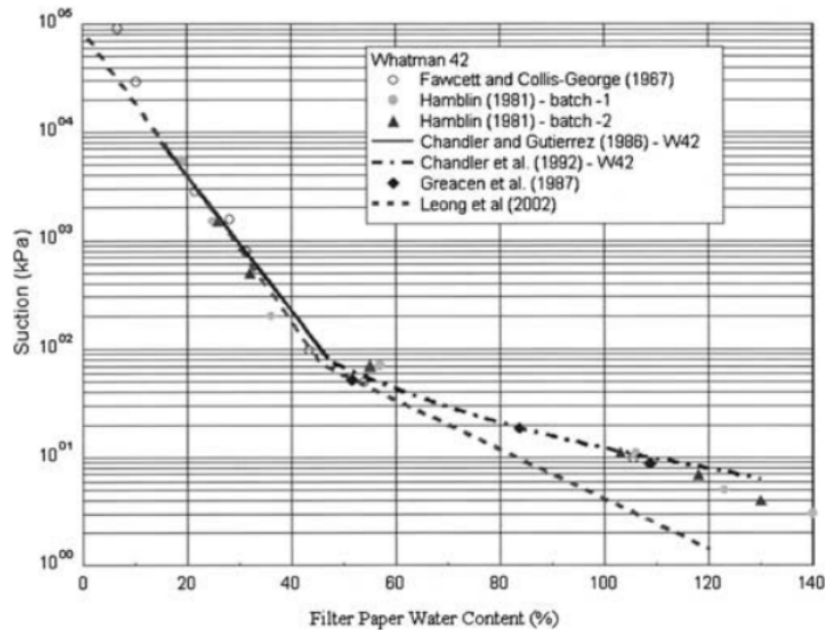


Figure 2.7 Calibration curves for Whatman No. 42 filter paper (Marinho and Oliveira, 2006)

2.6.5.3 Dew Point Potentiometer

The WP4C dew point potentiometer (Figure 2.8) measures water potential by determining the relative humidity of the air above a sample in a closed chamber, using the principle of the chilled-mirror technique (ASTM D6836-16 2016; Banerjee 2017; Banerjee et al. 2020a). The sealed block chamber comprises of the following: (i) a mirror; (ii) an optical sensor that is used to detect the dew formation on the mirror; (iii) a temperature sensor that measures the dew point temperature of the air; (iv) a thermopile to measure the temperature of the sample; and (v) a fan, which enhances the equilibration of the sample with the chamber environment (Banerjee 2017).



Figure 2.8 WP4 chilled water Potentiometer

2.6.6 Mathematical Models for SWCC

The measurement of SWCC over the entire suction range and at close intervals is not practical, due to the high expenditure, lack of replicates of soil specimens, and time constraints. Henceforth, closed-form empirical relationships are mostly used to obtain best-fit curves using the discrete data points obtained from the laboratory tests. Some of the empirical relationships commonly used have been tabulated in Table 2.2.

A dimensionless parameter, Θ , is often used and is obtained by normalizing the volumetric water content with respect to saturated and residual conditions, and is expressed as below:

$$\Theta = \frac{\theta - \theta_r}{\theta_s - \theta_r} \quad (2.7)$$

where,

θ = volumetric water content at any degree of saturation

θ_s = saturated volumetric water content

θ_r = residual volumetric water content

The normalized water content, Θ , varies from zero, for the residual condition, to 1, in the case of the saturated condition. Also, if the residual water content is zero, the dimensionless parameter for water content Θ converges to the value of the degree of saturation, S .

Table 2.2 Empirical models used to best fit SWCC data

Reference	Equation for Model	Parameters Involved
Brooks and Corey (1964)	$\theta = \begin{cases} 1, & \psi < \psi_b \\ \left(\frac{\psi_b}{\psi}\right)^\lambda, & \psi \geq \psi_b \end{cases}$	ψ = soil suction; ψ_b = air-entry suction value of soil; λ = Pore size distribution index that varies with the type of soil and its texture
van Genuchten (1980)	$\theta = \left[\frac{1}{1 + \left(\frac{\psi}{\alpha}\right)^n} \right]^m$	α , n and m are fitting parameters based on the AEV of soil, the rate of water extraction from the soil for suction greater than AEV, and residual water content, respectively.
Fredlund and Xing (1994)	$\theta = C(\psi)\theta_s \left[\frac{1}{\ln \left\{ e + \left(\frac{\psi}{a}\right)^n \right\}} \right]^m$ <p>where</p> $C(\psi) = \left[1 - \frac{\ln \left(1 + \frac{\psi}{\psi_r} \right)}{\ln \left(1 + \frac{10^6}{\psi_r} \right)} \right]$	ψ = suction θ_s = saturated volumetric water content a , n , and m are the fitting parameters based on the AEV of soil, the rate of water extraction from the soil for suction greater than AEV, and residual water content, respectively e = the natural logarithmic constant $C(\psi)$ = correction factor based on the suction corresponding to residual water content

Many other empirical relationships have also been developed in order to facilitate the SWCC modeling (Gould et al. 2012; Houston et al. 2006; Leong and Rahardjo 1997; Pham et al. 2003). Recently other tools have been used in the form of data mining, neural networks, and genetic programming-based tools for determining soil suction-water content relationships (Ahangar-Asr et al. 2012).

2.7 Shear Strength

The shear strength of soil describes the magnitude of maximum shear stress it can sustain and hence is an essential parameter for geomechanics and geotechnical engineers (Holtz and Kovacs 1981). The safety of many engineering structures depends on the strength of the underlying soil. Applications of shear strength of soil include problems like bearing capacity, slope stability, lateral earth pressure, pavement design, and foundation design (Holtz and Kovacs 1981; Lu and Likos 2004). The general concepts associated with the shear strength of soil remain similar for saturated and unsaturated conditions. For instance, the increase in cohesion, internal friction angle of the soil, and application of confining pressure increase the strength in both cases. Similarly, the concepts of dilation and changes in the shear strength of soil with strain are similar for both saturated and unsaturated conditions (Fredlund and Rahardjo 1993).

2.7.1 Shear Strength of Saturated Soil

Most of the theories of shear strength were postulated after considering the limitations of the equation of shear strength of saturated soils to predict the strength of unsaturated soil. Henceforth, a brief review of the shear strength relations for saturated soils is presented.

The Mohr-Coulomb theory of shear strength of saturated soil, initially advocated by (Coulomb 1776) and later generalized by Mohr (1914), is the most widely used relationship. Coulomb assumed that the normal stress acting on any plane had a linear relationship with the shear strength available on that plane, which is known as Coulomb's law and is expressed as follows:

$$\tau = c + \sigma \tan \phi \quad (2.10)$$

where, c and ϕ are cohesion and angle of internal friction of the soil, respectively.

The relation for the total strength parameter (Eqn. 2.10) was modified, as it was postulated by Terzaghi that shear strength is a function of effective stresses. The modified relation is as follows:

$$\tau = c' + \sigma' \tan \phi' \quad (2.11)$$

where, c' and ϕ' are effective cohesion and effective angle of internal friction of the soil, respectively. The parameters c' and ϕ' are known as the effective shear strength parameters. A typical Mohr-Coulomb Failure Envelope for a saturated over consolidated clay is shown in Figure 2.9. Three hypothetical triaxial tests, i.e. A, B, and C were performed on replicates of the same specimen at varying effective confining pressures, which failed at an effective axial stress of σ'_{1A} , σ'_{1B} , and σ'_{1C} , respectively. Therefore, at failure, a shear stress of τ_f and a normal stress of σ'_f were acting along the failure plane. Other relations are available for the shear strength of saturated soils, but those are beyond the scope of this discussion.

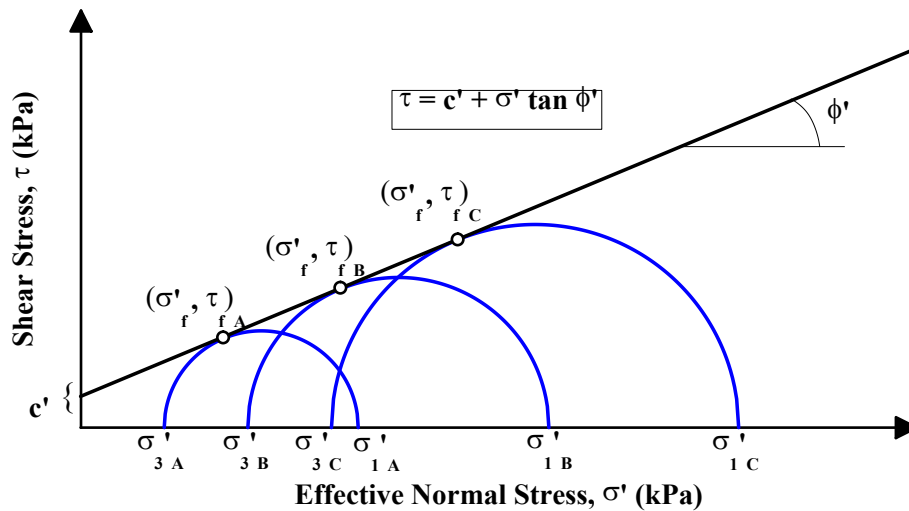


Figure 2.9 A typical Mohr-Coulomb Failure Envelope for saturated OC clayey soils

2.7.2 Shear Strength of Unsaturated Soil

The strength and deformation attributes of unsaturated soil are complex and unpredictable. Material behavior is affected by alteration in wetting, drying, loading, and unloading, and by time. The debate over the most suitable stress state variables applicable to unsaturated soil has impeded the development of the subject.

The success of the concept of classical effective stress introduced by Terzaghi (1936), given mathematically by equation 2.11, drove researchers to endeavor an extension of the equation to unsaturated soils. Attempts have been made to use a single-value stress state variable, to predict the behavior of unsaturated soils. Due to the limitations of the single-valued stress state variable approach, the independent stress variable approach was proposed. Meanwhile, researchers have worked on the development of modified stress-variable approaches.

2.7.2.1 Bishop's Effective Stress

Bishop (1959) proposed such an equation for effective stress, σ' :

$$\sigma' = (\sigma - u_a) + \chi(u_a - u_w) \quad (2.12)$$

where,

σ is the total stress,

u_a is the pore air pressure,

u_w is the pore water pressure, and

χ is a soil parameter related to the degree of saturation of the soil and the wetting or drying cycle.

The parameter $(\sigma - u_a)$ is referred to as the net normal stress, while $(u_a - u_w)$ is known as matric suction. The parameter, χ is a material variable and is generally considered to vary between zero, in the case of dry soil, and unity, in the case of saturated soil.

When the expression for effective stress for unsaturated soil is integrated with the classical Mohr-Coulomb failure criterion, the shear strength, τ_f of unsaturated soil is expressed as below:

$$\tau_f = c' + [(\sigma - u_a)_f + \chi_f(u_a - u_w)_f] \tan \phi' \quad (2.13)$$

where, c' and ϕ' are effective cohesion and effective angle of internal friction of the saturated soil, respectively.

However, it was observed that the relationship between χ and the degree of saturation, S is not unique; and the soil type and stress path had a noteworthy effect on the relationship. Thus, the use of Equation 2.12, and Equation 2.13 were debated by many researchers (Bishop and Blight 1963; Jennings and Burland 1962). Jennings and Burland (1962) argued that Equation 2.13 could not comprehensively clarify the volumetric behavior of most unsaturated soils below a certain degree of saturation and collapse upon wetting. Bishop and Blight (1963) postulated a theory that the mechanical behavior of unsaturated soil is independently correlated to the net normal stress and the matric suction. Thus, the limitations of the parameter χ to capture the behavior of unsaturated soil, its lack of one-to-one correspondence with the

degree of saturation, and the difficulties associated with the determination of χ in the laboratory, demonstrate the shortcomings of Bishop's approach.

2.7.2.2 Independent two-stress state variable approach

The limitations of the single-value stress state variable approach resulted in the consideration of an independent two-state stress variable approach. Fredlund and Morgenstern (1977) postulated the use of net normal stress and matric suction as independent stress state variables, for capturing the response of unsaturated soil. A series of "null" triaxial tests showed that when the net normal stress and the matric suction are kept constant while varying other parameters, the volume of the soil specimen practically remained the same. These "null" triaxial tests supported the proposed approach. The shear strength at failure, τ_f , provided by the modified Mohr-Coulomb failure criterion (Fredlund and Morgenstern 1977) is as follows:

$$\tau_f = c' + (\sigma - u_a)_f \tan \varphi' + (u_a - u_w)_f \tan \varphi^b \quad (2.14)$$

where, c' and φ' are effective cohesion and effective angle of internal friction of the saturated soil, respectively, and φ^b is the friction angle, which is due to the contribution of the matric suction on the shear strength of the soil. Due to a lack of experimental evidence, initially, the value of φ^b was considered as a constant for a specific soil by Fredlund et al. (1987). This assumption led to the conclusion that the soil strength increases consistently with the increase in suction. However, the increase in shear strength due to matric suction decreases with an increase in suction, which became evident with additional experimental results over a wide range of suction and on different types of soils (Escario and Sáez 1986). Equation 2.14 can be simplified to:

$$\tau_f = c' + c''(\sigma - u_a)_f \tan \varphi' \quad (2.15)$$

where c'' is the capillary cohesion, which arises due to capillary effect, and is as follows:

$$c'' = (u_a - u_w)_f \tan \varphi^b \quad (2.16)$$

Also, total apparent cohesion is the sum of c' and c'' .

The extended Mohr-Coulomb failure envelope, based on an independent two-state stress variable approach, is shown in Figure 2.10. Instead of a two-dimensional plot between effective stress and shear stress, as in the case of saturated soil; the extended MC failure envelope requires a three-dimensional plot, among the net normal stress, matric suction, and shear stress. Additionally, the MC failure envelope transforms from a line (for saturated soils) to a surface (for unsaturated soils).

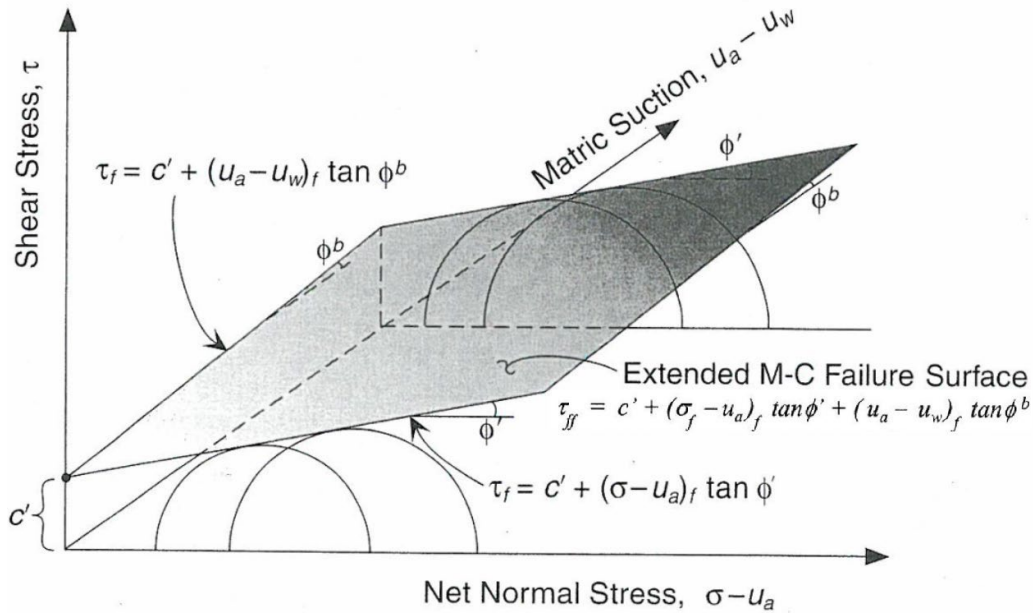


Figure 2.10 Extended Mohr-Coulomb Failure Envelope (Fredlund and Morgenstern 1977; Fredlund and Rahardjo 1993; Lu and Likos 2004)

2.7.2.3 Alternative approaches

The concept of suction stress was introduced by (Lu and Likos 2006) to facilitate the use of the suction stress characteristic curve. Suction stress is composed of four components, which originate from different water retention mechanisms: (i) van der Waals attraction, (ii) electric double layer forces, (iii) tensile pore water pressure, and (iv) surface tension (Lu and Likos 2006; Lu et al. 2009). van der Waals forces occur due to attractive or repulsive forces between molecules or atomic groups that do not have covalent or ionic bonds (Lu and Likos 2006; Lu et al. 2009). The correlations in the fluctuating polarizations of adjacent molecules are the main cause of the generation of these forces. The van der Waals forces decrease exponentially when the distance between the molecules increases or when the degree of saturation increases.

Electric double-layer forces arise between charged objects across liquids, like water. The first layer refers to the charged surface, and the charges originate from the adsorbed ions. The second layer corresponds to the diffused layer, which consists of a neutralizing charge comprising depleted co-ions or counter-ions. The potential difference between these two layers generates the difference in ionic concentration. This difference results in osmotic pressure (Lu and Likos 2006; Lu et al. 2009).

The van der Waals forces and the electric double-layer forces can be safely neglected in sands and non-plastic silts. Capillarity, which includes the latter two mechanisms, is the major reason for sand and non-plastic silt to exhibit cohesiveness or attractive forces (Lu et al. 2009; Lu and Likos 2006). However, very limited studies have been conducted independently to validate this hypothesis of the suction stress concept. The concept of the independent two-stress state variable approach by (Fredlund and Morgenstern 1977) is still the most widely used relationship for the shear strength of unsaturated soils. Various researchers have attempted to develop alternative approaches, which enable the development of constitutive models for predicting the behavior of unsaturated soils, including (Alonso et al. 1990; Chiu and Ng 2003; Gallipoli et al. 2003; Khalili and Khabbaz 2002; Manzanal et al. 2011; Patil et al. 2018).

2.8 Types of Triaxial Tests

The most common triaxial test performed in the laboratory follows the Conventional Triaxial Compression (CTC) stress path, where a constant effective confining pressure is maintained, while the soil specimen is loaded axially. The axial loading may be stress-controlled or strain-controlled. Strain-controlled tests can be continued even after the specimen has failed; thereby the post-peak or the residual behavior can be determined. However, strain-controlled test setups are more expensive than stress-controlled test setups. Based on the drainage conditions allowed during the application of confining pressure and shearing, the triaxial tests are classified into three categories:

2.8.1 Unconsolidated Undrained (UU) Tests:

There is no provision for drainage during the entire testing process. The soil is not allowed to consolidate, and no volume changes are allowed during shearing. The testing procedure for cohesive soils has been discussed in ASTM D2850-23 standards. The total stress path is obtained during this test. This is a quick test, generally completed within 30 - 45 minutes. Field applications of UU tests include scenarios where the rate of loading during consolidation and shearing is much faster than the rate of dissipation of excess pore water pressure. The rapid construction of an embankment of soft clay; the construction of footing and super-structure on a clay deposit; bearing capacity of deep foundations, like piles, on soft clay may be considered (Holtz and Kovacs 1981).

For unsaturated specimens, the procedure for conducting the unconsolidated undrained test is similar to that for saturated specimens. The sample is not consolidated, and it is sheared at its original suction state. The pore air and pore water valves are closed throughout the test. Since air pressure is not applied, a conventional triaxial setup may be used to conduct a UU test of unsaturated specimens (Banerjee 2017).

2.8.2 Consolidated Undrained (CU) Tests:

Drainage is permitted during the application of confining pressure, thereby allowing the consolidation of the soil specimen. However, drainage is not allowed during the loading stage. The generation of excess pore water pressure is measured during the loading phase. The testing procedure for cohesive soils has been explained through ASTM D4767-11 standards. The total stress path is directly obtained from this test; while the effective stress path may be calculated by deducting the excess pore pressure measured during shearing. This is a slower test when compared to the UU test (Holtz and Kovacs 1981). Field application includes situations where the soil is allowed to consolidate, and then the additional form of loading is applied. Examples include the rapid drawdown of an embankment dam and slopes of reservoirs; rapid construction of a structure on top of an embankment or raising the height of an existing embankment (Holtz and Kovacs 1981).

For unsaturated specimens, the pore-air and pore-water lines are open during consolidation, and target values of cell pressure, pore air pressure, and pore water pressures are gradually applied. During shearing, the pore air and pore water valves are closed, and their values are measured (Fredlund et al. 2012). Consolidated Undrained tests on unsaturated specimens were conducted by a few researchers (Khosravi et al. 2011; Saeedy and Mollah 1988; Soranzo 1988).

2.8.3 Consolidated Drained (CD) Tests:

Drainage is allowed throughout the consolidated drained (CD) test. In other words, the drainage valves are open during the application of confining pressure (i.e., consolidation) and loading. Thus, the soil specimen is allowed to consolidate for the confining pressure applied, and then the soil is loaded gradually, to allow proper dissipation of excess pore water pressure. Henceforth, the volume change of

the specimen is permitted during the test, and it is recorded via proper volume measurement devices. It is of primary importance to determine the proper rate of loading so that the excess pore water pressure can properly dissipate during the loading sequence. The testing procedure has been explained through ASTM D7181-20 standards. The effective stress path and the drained shear strength parameters can be computed from this test. As there is no generation of excess pore water pressure during the loading sequence, the total stress path is the same as the effective stress path. This is the slowest among the UU, CU, and CD tests and usually takes days to complete a test, and the duration is highly dependent on the permeability of the soil (Holtz and Kovacs 1981). Practical applications of CD tests comprise of cases where the loading rate is smaller than the rate of dissipation of excess pore water pressure generated during shearing. The CD tests are mostly applicable for long-term stability analyses. Examples of CD tests include slow construction of embankment over soft clay; stability analysis of embankment having steady seepage condition; and long-term stability of a natural slope or an excavation (Holtz and Kovacs 1981).

For unsaturated specimens, the pore air and pore water lines are open throughout the stages of consolidation and shearing (Fredlund et al. 2012). The respective targets of cell pressure, pore air pressure, and pore water pressure are gradually applied throughout the test. CD tests on unsaturated specimens were performed by other researchers (Banerjee et al. 2020b; Escario and Sáez 1986; Gulhati and Satija 1981; Leong et al. 2013; Ma et al. 2016; Patil et al. 2016a; Rahardjo et al. 1995a, 2004; Rosone et al. 2016).

2.8.4 Constant Water (CW) Tests:

The Constant water (CW) test is the same as the consolidated undrained test for saturated specimens. However, for unsaturated specimens, the CW test is categorized as a separate test. The consolidation of the unsaturated specimen is carried out in a similar way to the consolidated drained or consolidated undrained test. In other words, the pore air and pore water drainage valves are kept open during consolidation to permit the change in volume of the specimen and to prevent the generation of excess pore water pressure (Fredlund et al. 2012). Henceforth, the induced matric suction prior to the commencement of consolidation is maintained after the specimen has been consolidated.

During shearing, the pore water drainage valves are closed, but the pore air pressure value is kept open (Fredlund et al. 2012). Therefore, the pore air pressure is maintained at the same level as after consolidation. However, the pore water pressure is not controlled during shearing, which results in varying matric suction. The behavior of matric suction is dependent on the previous stress history of the soil, its preconsolidation pressure, and the effective confining pressure. CW tests were performed on unsaturated soils by researchers (Gulhati and Satija 1981; Li and Zhang 2015; Rahardjo et al. 2004).

2.8.5 Unconfined Compression (UC) Tests:

The unconfined compression (UC) test procedure is comparable to that of the UU test, with the exception that the confining pressure is not applied in the UC test. It is one of the most basic tests to estimate the strength of a soil specimen. Generally, an axial load is applied monotonically from a simple loading frame to shear the specimen (Fredlund et al. 2012). Table 2.3 summarizes triaxial conditions and pressures that are controlled or measured during the various types of triaxial tests.

Table 2.3 Types of triaxial tests for soils (modified from Fredlund et al. 2012)

Test Method	Consolidation Stage	Shearing Stage				
		Drainage		Pore Air Pressure	Pore Water Pressure	Soil Volume Change
		Pore Air	Pore Water			
CD	Yes	Yes	Yes	Controlled	Controlled	Measured
CW	Yes	Yes	No	Controlled	Measured	Measured
CU	Yes	No	No	Measured	Measured	No change
UU	No	No	No	N/A	N/A	No change
UC	No	No	No	N/A	N/A	N/A

2.9 Methods to Control Suction

2.9.1 Axis Translation Technique

The application and control of matric suction are pivotal for any suction-controlled triaxial test. The measurement and the control of high magnitudes of negative pore water pressure are limited due to cavitation (Fredlund and Rahardjo, 1993). Cavitation is the process of vapor nucleation in water when the absolute pore-water pressure is less than the vapor pressure of water (Lu and Likos 2004). Due to the entrapment of air within the liquid (water) phase, the continuity of the liquid phase is lost. This causes erroneous pore water pressure readings. Since matric suction is the difference between pore-air and pore water pressures, inaccurate pore water pressure would make it difficult or problematic to control matric suction.

Hilf (1956) introduced the concept of using the axis-translation technique to measure and control matric soil suction. The term “axis translation” refers to the procedure of increasing the pore air pressure above the atmospheric pressure, while maintaining a constant pore water pressure at or near the atmospheric pressure (Lu and Likos 2004). This concept alleviated the problem caused due to cavitation at a pore-water pressure below absolute zero pressure, i.e. -1 atm with reference to the atmospheric pressure. Henceforth, the datum of determining air pressure is shifted from atmospheric pressure to a higher value. Using the axis-translation technique, the matric suction higher than 1 atm ≈ 101.3 kPa can be applied or controlled, which is required for many soil types and applications.

2.9.1.1 High-Air Entry Ceramic Disk

In conventional saturated tests, the porous stone and the filter paper prevent the soil from entering the water line, but the flow of water is allowed either from or to the specimen, due to the high permeability of the porous stone and filter paper. However, due to the presence of pressurized air in unsaturated testing using the axis translation technique, the use of low air entry porous stone to separate the saturated pore water pressure line from the unsaturated soil is not feasible. Henceforth, a very low permeable and hydrophilic material, known as a High Air-Entry (HAE) ceramic disk is essential to isolate the saturated pore water pressure line from the pressurized air present in the unsaturated soil.

The HAE ceramic material generally has uniform pore sizes. After saturation of the ceramic disk, due to the hydrophilic nature of the ceramic material, the water can flow through it, but the passage of air flowing through it is prevented till the air pressure exceeds the air-entry value of the material. The HAE disks are made of materials like sintered ceramics and have an air-entry value of up to 1500 kPa (Lu and Likos 2004).

The contractile skin which forms at the interface of air and water present in pores of the HAE disk, resists the flow of air through the disk. This resistance is dependent on the surface tension, T_s , of the contractile

skin (Fredlund and Rahardjo 1993). The contractile skin acts as a thin membrane connecting the minute pores of radius, R_s , on the ceramic disc surface (as shown in Figure 2.11). The matric suction is induced due to the difference between air pressure, u_a , above the contractile skin, and water pressure, u_w , below the contractile skin.

The maximum matric pressure, which can be controlled across the contractile skin of the HAE disc is known as its air-entry value, $(u_a - u_w)$ (Lu and Likos, 2004). The air-entry value can be represented by the Young-Laplace equation, which is applicable to the capillary tube model (Lu and Likos, 2004):

$$(u_a - u_w)_d = \frac{2T_s}{R_s} \quad (2.8)$$

It is evident from Equation 2.17, that as the size of the largest pore of the HAE disc decreases the air-entry value increases. The pore sizes of the ceramic material are dependent upon the casting process and sintering technique of the ceramic material (Fredlund et al. 2012).

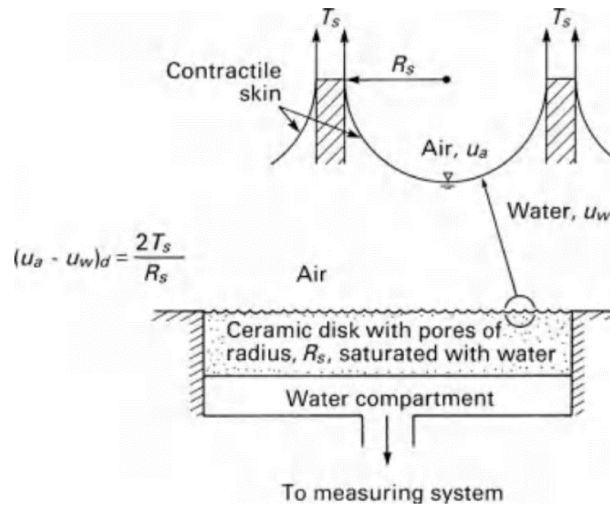


Figure 2.11 Schematic representation of the air-water interface in HAE disc (Fredlund and Rahardjo 1993)

The HAE ceramic disc can be attached to conventional triaxial equipment to perform unsaturated soil testing. The HAE disc is generally mounted on the base pedestal and it is glued to the stainless-steel ring, which fits in the base pedestal. Figure 2.12 shows the schematic section and plan of two types of shapes for HAE ceramic discs and the glue that attaches the steel ring to the HAE disc. The proper bond between the glue and the ring is pivotal for maintaining a suitable seal, thereby assuring that water passes only through the ceramic disc and there is no leakage.

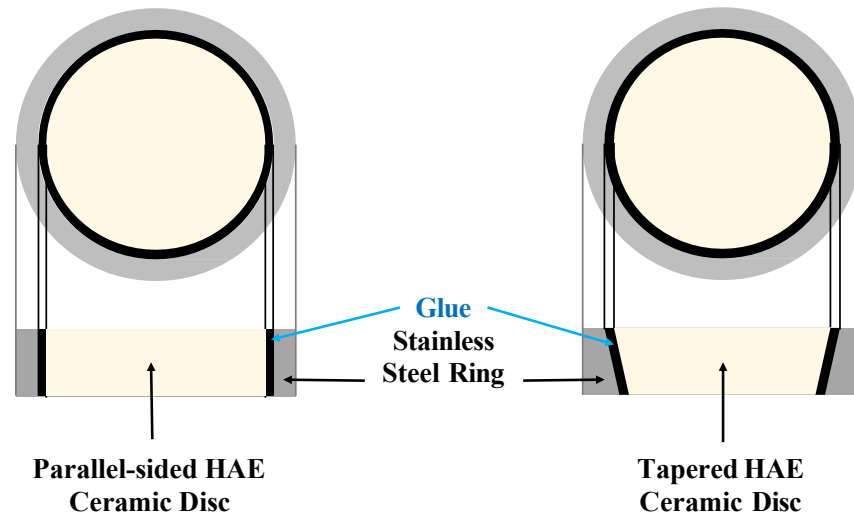


Figure 2.12 High air-entry disk ring arrangement

2.9.1.2 Saturation of HAE Ceramic Disc

The saturation of the ceramic disc is essential, before any test. The permeability of each ceramic disc is dependent on its air-entry value. Different water pressures for varying durations of time should be applied to different types of HAE ceramic discs in order to saturate the disc. Sivakumar (1993) suggested a technique to saturate the ceramic disc having an AEV of 500 kPa. The saturation process was started by placing the disc in a chamber as shown in Figure 2.13. The ceramic disc was fitted to the base pedestal which had the facility to flush water from beneath the ceramic disc. The drainage lines were saturated, and the chamber was sealed. The chamber was filled with de-aired water and pressurized beyond the air-entry value of the ceramic disk. After maintaining the pressure for a couple of days, one of the drainage lines was opened, and the water was allowed to flow for a day. Subsequently, the applied pressure in the chamber was gradually reduced to atmospheric pressure, i.e., zero pressure, and the water was removed. This process was repeated by introducing fresh de-aired water and re-pressuring the water to 600 kPa and maintaining it for a day. One of the drainage lines was again opened for another day and finally, the pressure was gradually reduced. Thereafter, the HAE disc was removed.

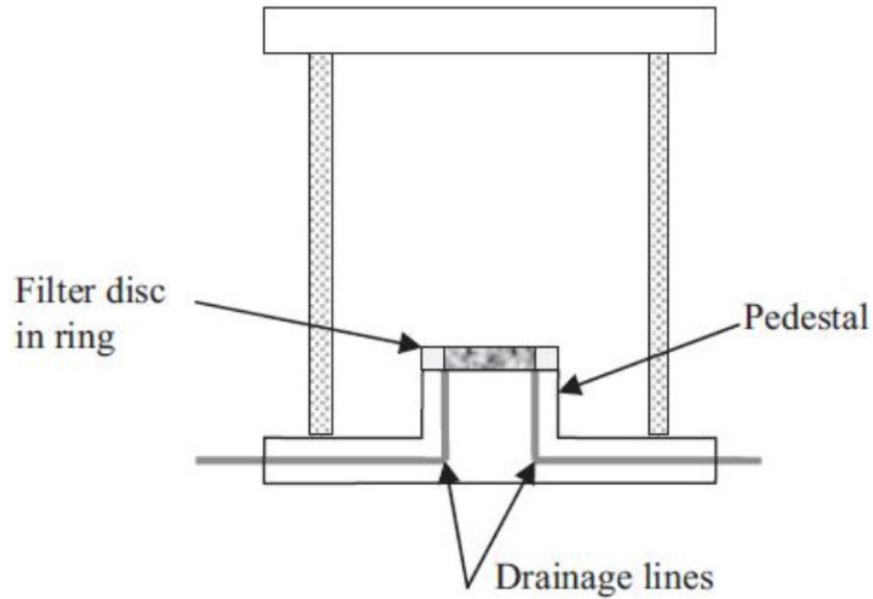


Figure 2.13 Chamber to saturate a ceramic filter disc (Murray and Sivakumar 2010)

Another approach for saturating the HAEV ceramic disc was presented by other researchers (Bishop and Henkel 1962; Fredlund 1973; Hoyos 1998). The ceramic disc having an AEV of 500 kPa was installed in the test cell, as shown in Figure 2.14. The drainage lines were saturated and the connection below the ceramic disc was flushed to eliminate any air bubbles trapped beneath the HAE disc. Next, the triaxial assembly was set up and de-aired water was filled till 25 mm (approximately 1 inch) above the top surface of the ceramic disc. Air pressurized to 600 kPa was applied from the top onto the surface of the water, which indirectly pressurized the water. One of the drainage valves, connected to the base of the ceramic disc was opened and the rise of water level in the attached burette was recorded. The high pressure dissolved the air into the water and the HAE disc became saturated. Subsequently, the air pressure was gradually released to prevent any dissolved air from diffusing into the ceramic disk. A similar approach was used by other researchers (Banerjee 2017).

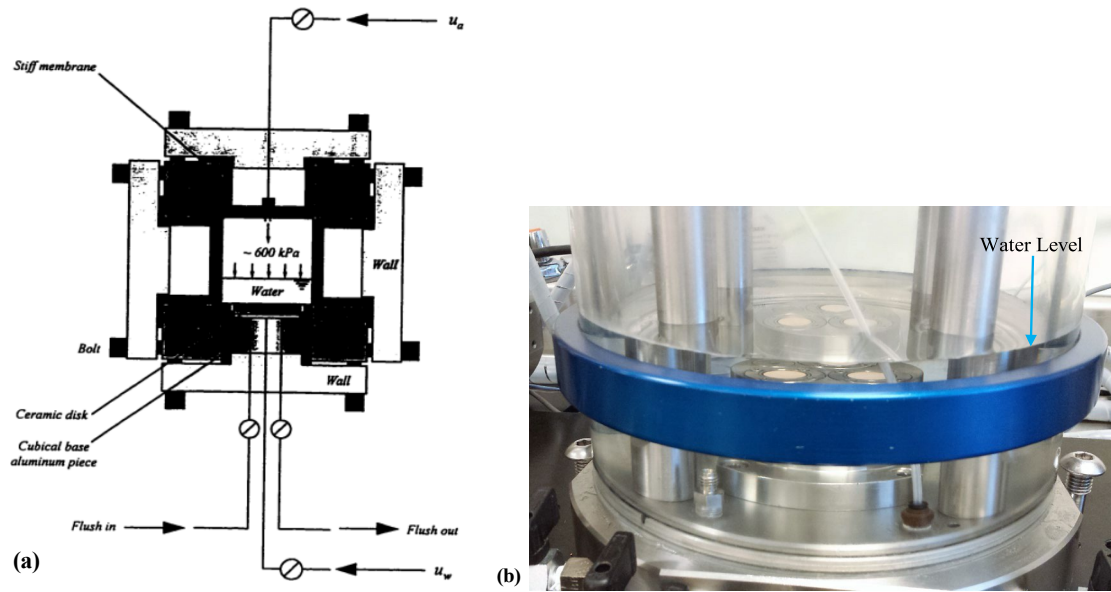


Figure 2.14 Saturation of HAEV ceramic disc in a test cell by (a) Hoyos (1998) and (b) Banerjee (2017)

2.9.1.3 Limitations of Axis-Translation Technique

Olson and Langfelder (1965) reasoned that by increasing the air pressure acting on the soil specimen, the soil solids and the pore water become compressed isotropically. However, as these are practically incompressible, the air pressure increase resulted in an insignificant alteration in the curvature of contractile skin. Therefore, the value of matric suction ($u_a - u_w$) would have remained almost constant. Henceforth, they concluded that the axis-translation technique would be suitable for soils having only a continuous air-water interface. Later, Bocking and Fredlund (1980) had similar observations and it was concluded that based on the rate of increase of air pressure, the actual value of matric suction might momentarily increase beyond its applied value. It was concluded that if the specimen contains occluded pore air, which makes it highly compressible, the actual matric suction might be overestimated. In addition, the diffusion of air through the ceramic disc is a major limitation for the duration of each test. The dissolved air above the ceramic disc might diffuse through the HAE ceramic disc into the base chamber, where it enlarges and accumulates due to relatively lower pressure. This might obstruct the flow of water through the ceramic disc. Therefore, the axis-translation technique ideally works for soils when they have continuous phases of pore water and pore air.

2.9.2 Osmotic Suction Technique

The osmotic suction method achieves control of matric suction by allowing the pore water to equilibrate with a salt solution of known osmotic potential, and the soil specimen is separated from the salt solution by a semi-permeable membrane. The semi-permeable membrane is permeable to water molecules but impermeable to salt molecules. The experimental setup by Cui and Delage (1996), demonstrating the procedure of inducing suction using osmosis is shown in Figure 2.15. The osmotic suction technique was initially adopted by researchers from biological sciences for controlling the osmotic pressure of plant nutrient solutions by using Polyethylene Glycol, commonly referred to by its acronym, PEG. Later, suction control by means of the osmotic suction technique was adopted in the field of soil sciences. In geotechnical engineering, this technique was also adopted to control suction in triaxial setups and suction-controlled tests in oedometer (Cui and Delage 1996; Ng et al. 2007). The main benefit of this technique is that cavitation is prevented while maintaining a negative pore water pressure within the soil. The disadvantages, include the

long duration of each test may not be feasible, as the semi-permeable membrane is delicate. The migration of soil salts, which are dissolved in pore water in the soil, into the salt solution may affect the soil water chemistry and soil properties (Murray and Sivakumar 2010).

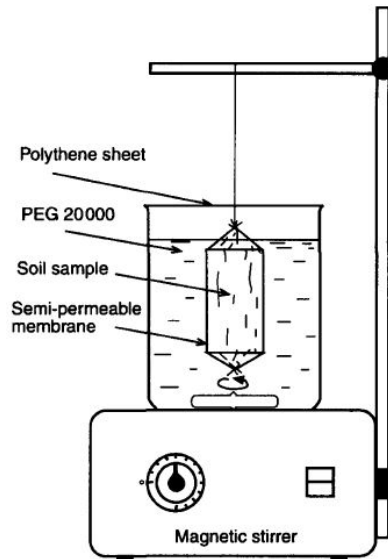


Figure 2.15 Osmotic suction technique to impose suction in soil specimen (Cui and Delage 1996)

2.9.3 Vapor Equilibrium Technique

The vapor equilibrium technique was introduced by researchers for application in soil sciences. This technique controls the soil suction by controlling the relative humidity, which could be achieved by two methods: (i) isopiestic method, and (ii) two-pressure method. The isopiestic or “same pressure” method depends on achieving the vapor pressure equilibrium for salt or acid solutions in a closed thermodynamic environment (Lu and Likos, 2004). The “two-pressure” method relies on the control of relative humidity by changing the pressure or temperature; or by mixing vapor-saturated gas with a dry gas (Lu and Likos, 2004). The control of soil suction in unsaturated soil testing using the vapor pressure technique was conducted by (Banerjee et al. 2020a; Blatz and Graham 2000; Likos and Lu 2003; Patil et al. 2016a; Tang et al. 2002). In this approach, the soil specimen is placed in a thermodynamically sealed system controlled by the air flowing through a desiccator where an aqueous solution results in a controlled partial vapor pressure generated by the salt solution of known concentration. The suction is maintained by regulating the flow of moist or dry air through the soil specimen till the target relative humidity is achieved when the soil suction is in equilibrium with the partial vapor pressure. The “two-pressure” humidity control method was used by (Likos and Lu 2003) to develop a system that could be modified to be used along with a triaxial device to test specimens under high suction states (Figure 2.16). A similar system was used by other researchers (Banerjee et al. 2020c; a; Patil et al. 2016a).

The vapor equilibrium technique has similar advantages to the osmotic suction technique, with the added advantage that this technique could be used for very high suction states like 4 to 600 MPa (Murray and Sivakumar, 2010). However, the lower suction levels (less than 4 MPa) cannot be applied using this technique. Also, the suction equilibration time is very high, and it takes up to 1 – 2 months to attain equilibrium for standard triaxial specimens.

2.10 Modified Unsaturated Soil Triaxial Testing System

The conventional triaxial testing device has been altered to incorporate unsaturated soil testing by many researchers. The modifications introduced include the precise measurement of the volume changes in soil, the volume of water flowing into or out of the soil specimen, and the volume of air inflow or outflow to control the required suction. The modifications also comprise the independent control and measurement of pore air and pore water pressures over a wider range, minimizing the errors due to the expansion of the triaxial cell with an increase in pressure, and flushing devices to remove air from the base of the high air-entry ceramic disk during a test. The advent of computer technology, sensors, and mechanical devices has enabled these modifications to be incorporated into soil testing. Some of these modified triaxial devices and the tests conducted have been discussed in the next section.

2.10.1 Independent Pore Water and Pore Air Pressures Control and Measurement

The triaxial tests on unsaturated soils were performed by Bishop and Donald (1961) using a modified version of the conventional triaxial setup, where the pore air and pore water pressures were individually controlled or measured. The tests confirmed that the pore water pressure could be measured through a saturated ceramic disk, which was attached and sealed to the base pedestal. However, the pore water pressure measurement was restricted to less than 90 kPa below atmospheric pressure, to prevent cavitation. The pore air pressure was applied through a porous stone at the top of the soil specimen.

Bishop and Blight (1963) verified the application of the axis translation technique to induce matric suction in the testing of unsaturated soil. The matric suction induced was more than 1 atm, which was till then the maximum induced matric suction. Gulhati and Satija (1981) performed a series of consolidated drained (CD) and constant water (CW) triaxial tests, where the pore air and pore-water pressures were controlled or measured throughout the tests. A similar set of CD triaxial tests was performed by Escario and Sáez (1986), which employed the axis translation technique. Later, many researchers conducted triaxial tests with independent control of pore air and pore water pressures. The primary modifications required for unsaturated soil testing were presented by Fredlund and Rahardjo (1993), which included the HEA disk and independent control of pore air and pore water pressures (Figure 2.18). A similar test setup was used by Rahardjo et al. (2004) to perform a series of CD and CW triaxial tests on compacted sandy clay specimens. They concluded that the specimens exhibited characteristics of overconsolidated soil with post-peak softening and dilatancy at higher suction levels. They observed that the matric suction reduces with the shearing of specimens in CW tests.

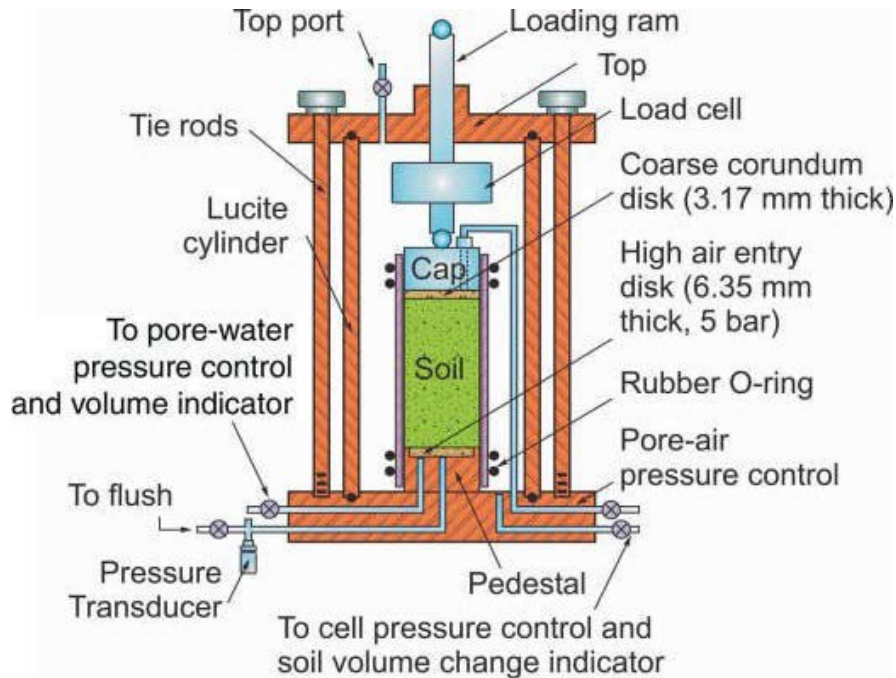


Figure 2.18 Modified triaxial setup for unsaturated soil testing (Fredlund and Rahardjo 1993)

Meanwhile, Sharma (1998) used a porous stone to apply air pressure at one end of the specimen but used an HAEV disk at both ends of the specimen to apply pore water pressure. This technique aided in reducing equilibration time but exposed the tests to the possibility of air bubbles being entrapped in the center of the soil specimen, owing to the movement of the waterfront from both ends of the specimen. A similar approach was adopted by researchers such as Rojas et al. (2008) where the pore air and pore water pressures were applied from both ends of the specimens by installing a HAEV ceramic disk at the core of the base pedestal, with an annular ring of porous stone (as shown in Figure 2.19).

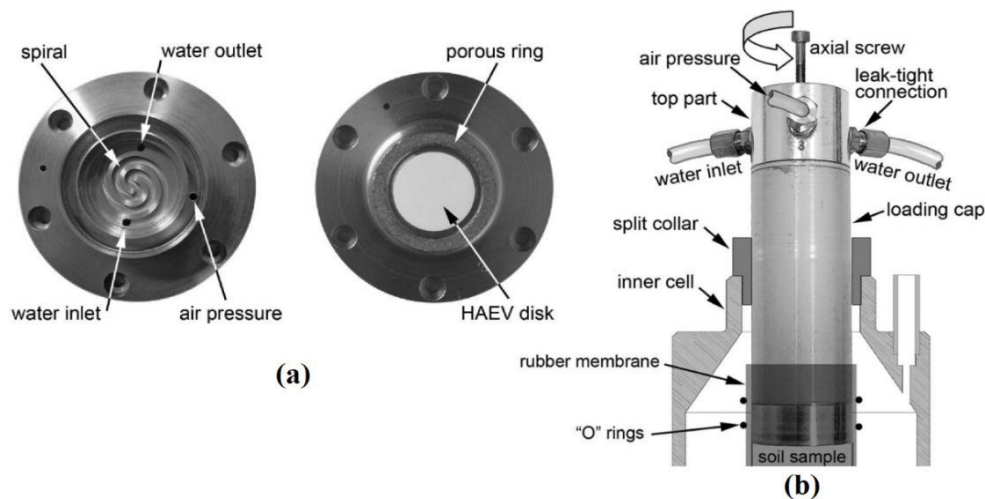


Figure 2.19 Modifications to (a) base platen, and (b) top cap assembly (Rojas et al. 2008)

Rampino et al. (1999, 2000) developed a new setup to perform suction-controlled triaxial tests by adopting the axis translation technique. Various compacted specimens of silty sands were tested at suction levels varying from 0 to 400 kPa. The deviator stress and the volumetric strain response demonstrated post-peak softening and dilation after initial compaction, which showed that the specimen behaved as dense sand.

Ishikawa et al. (2014) performed tests on a piece of medium-sized triaxial equipment (as shown in Figure 2.20) to study the mechanical behavior of unsaturated subbase course materials using the pressure membrane method with hydrophilic microporous filters, instead of HAE ceramic discs. The main motive for using pressure membranes and installing a water supply on both ends of the soil specimen was to reduce the testing time by developing double drainage, as was confirmed by (Ishikawa et al. 2010; Nishiumura et al. 2012). The pore air and pore water pressure applied to the specimen from the top cap and the bottom pedestal, respectively, were controlled independently. Additional tests were performed on the same setup by Zhang et al. (2014) to study the strength characteristics of subbase course material subjected to the variation in the degree of saturation and the loading strain rate. The soil selected was a subbase course material, comprising of natural crusher-run made from angular, crushed, hard andesite stone. The consolidated drained triaxial tests on the compacted specimens showed initial compression (up to less than 1%) and subsequent dilation for all specimens. Similarly, the deviator stress response showed post-peak softening behavior. Also, the strain rate for shearing demonstrated that the higher strain rates resulted in higher peak deviator stress, and the dilation initiated at a lower axial strain, with a higher dilation angle.

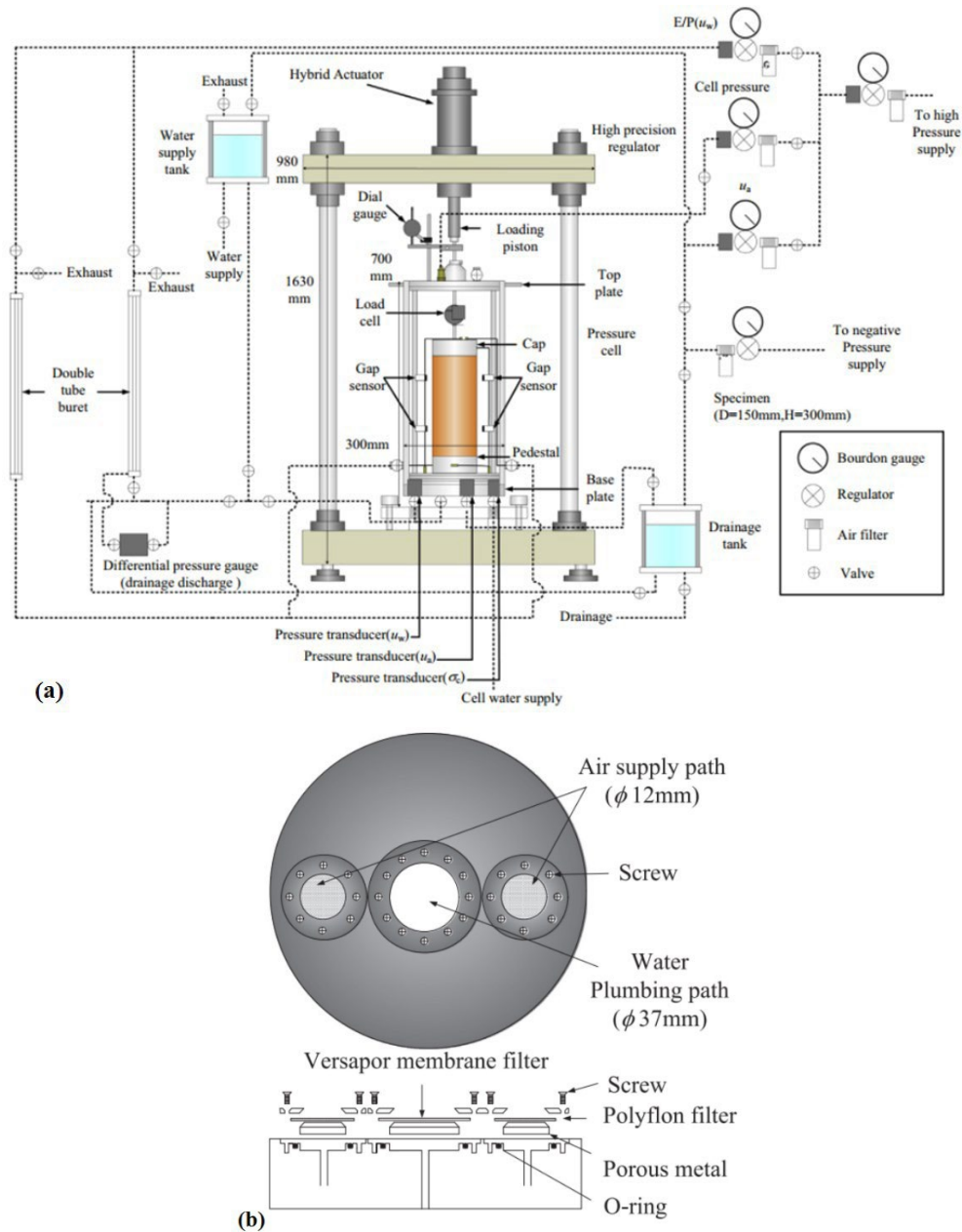


Figure 2.20 (a) General setup of medium-sized triaxial apparatus and (b) Structure of top cap and base pedestal (Ishikawa et al., 2014)

Rosone et al. (2016) conducted a series of suction-controlled drained triaxial tests on unsaturated specimens of scaly clay on a modified triaxial device using an axis translation technique. The independent control of air pressure from the top cap and water pressure through the combination of two HAE ceramic discs (AEV of 500 kPa and 1500 kPa) at the base pedestal enabled the control of matric suction. The experimental program was defined based on a two-independent stress state variable approach by Fredlund and Morgenstern (1977). The matric suction induced on the specimens varied from 50 to 500 kPa. All the specimens, except for the 500 kPa suction specimens, were dynamically compacted on the dry side of optimum (2% drier than optimum moisture content) and subjected to net mean stress of 50 kPa and matric suction of 50 kPa before the required suction was induced. Due to the excessive time required to

equilibrate specimens from a matric suction of 50 kPa to 500 kPa, the specimens to be tested at a matric suction of 500 kPa were directly subjected to a suction of 500 kPa and net mean stress of 50 kPa. The response of the compacted specimens to shearing showed an increase in deviator stress to its peak value with a corresponding increase in axial strain when suction was less than 500 kPa. However, for specimens subjected to 500 kPa, slight post-peak softening was observed. Elaborate analyses of the test results were performed, and yield curves were estimated using the isotropic consolidation data. The shear strength envelope at saturated and unsaturated conditions was generated using the two-independent stress state variable approach by Fredlund and Morgenstern (1977). Additionally, the apparent cohesion was estimated for the soil over a wide range of suction states by using the macropore degree of saturation as Bishop's effective stress parameter, χ . It was observed that at high suction (greater than 9 MPa), the use of macropore degree of saturation as χ predicted that the apparent cohesion decreased to zero, due to excessive desaturation (Rosone et al. 2016). Moreover, apparent cohesion was also predicted over the suction range considered in the study (0 - 500 kPa) by using the hyperbolic envelope. Using this approach, it was detected that the rate of increase of apparent cohesion gradually decreased after matric suction of 100 kPa, which was near the AEV of the soil (Rosone et al. 2016).

New setups were developed by other researchers in the recent past where the axis translation technique was used to apply suction in the soil up to 750 kPa on sandy soils (Patil 2014; Patil et al. 2016b) and silty soils ((Banerjee 2017; Banerjee et al. 2020b, 2021).

2.10.2 Volume Measurement

The various volume measurements required to be measured accurately include (i) the volume of the soil specimen, (ii) the volume of water flowing into or out of the specimen through the HAE disc, and (iii) the volume of air flowing in or out of the specimen to maintain the required soil suction. Researchers have attempted to capture the volume changes in the soil and volume of air and water supply to maintain suction accurately, by various methods which have been discussed in this section.

Initial problems regarding the expansion of triaxial cells with an increase in cell pressure were addressed by (Bishop and Donald 1961), where the use of double-walled triaxial cells was suggested. Mercury was used as an internal cell fluid, while water was utilized as the external cell fluid. The application of equal pressures to both cells prevented any expansion of the inner cell. The schematic plot of the modified triaxial setup is shown in Figure 2.21.

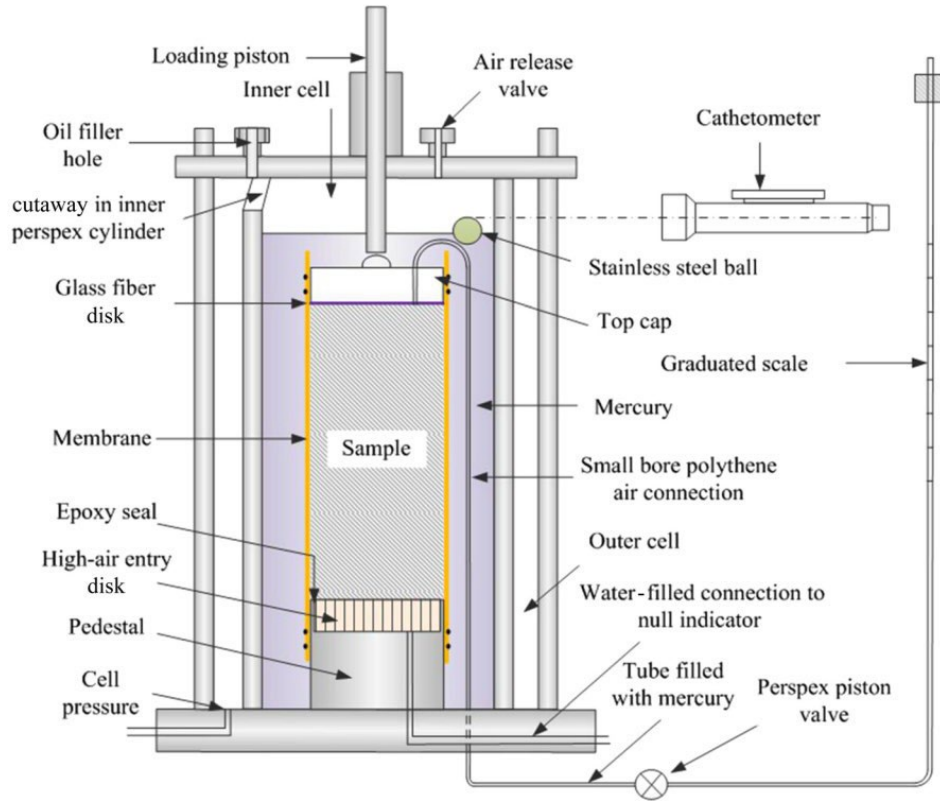


Figure 2.21 Schematic plot of triaxial setup for unsaturated soils (modified from Bishop and Donald, 1961; adopted from Li and Zhang, 2015)

Ng et al. (2002) developed a simple triaxial device by installing a highly accurate differential pressure transducer in a Bishop and Wesley (1975) type triaxial cell. The differential pressure transducer measured the alterations in the volume of soil by measuring the pressure difference between the water inside the inner cell and that in a reference tube. The schematic representation of the setup is shown in Figure 2.22.

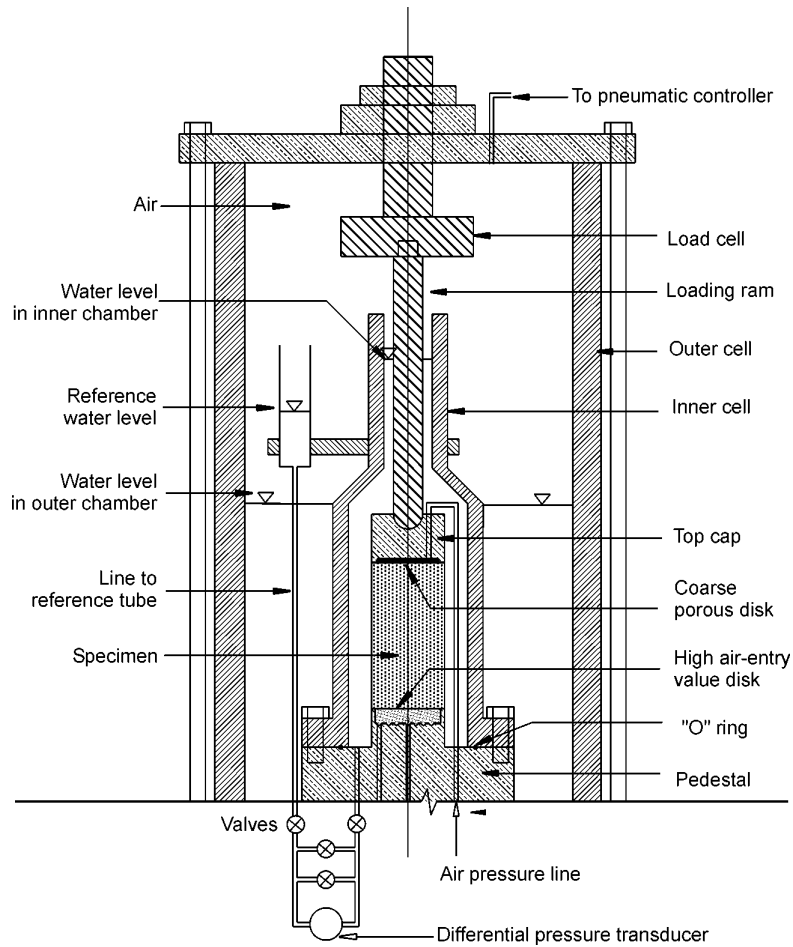


Figure 2.22 Schematic of new triaxial setup to measure the volume change of the specimen (Ng et al. 2002)

Kayadelen et al. (2007) attempted to evaluate the critical state parameters with respect to matric suction for highly plastic clayey soils, for which a series of triaxial tests were conducted on modified triaxial equipment (Figure 2.23). The axis-translation technique was adopted to control suction and prevent cavitation. The pore air and pore water pressures were independently controlled and measured (Kayadelen et al. 2007). It was assumed by the authors that the difference between overall soil and pore water volume changes causes the air volume to change. However, this assumption has major limitations as the expansion of the triaxial cell and the pipes connecting the pressure lines were neglected and their effect was included in the air volume change. The volume change transducer connected to the pore water line measured the volume of water flowing in or out of the soil specimen. An additional volume change transducer was attached to the constant pressure device and inlet for the triaxial cell, which recorded the volume change of the soil specimen. To prevent the diffusion of air through the rubber (or latex) membrane into the cell water, the soil specimen was enclosed within two latex membranes with two slotted aluminum sheets separated by silicone grease. A similar approach was recommended by Alonso et al. (1990) to prevent air diffusion from the specimen to the confining liquid in the cell. The triaxial tests were conducted on specimens with induced matric suction up to 400 kPa, which was at a degree of saturation of approximately 75%. The consolidated drained tests conducted on the residual clayey soil specimens showed a compressive behavior.



Figure 2.23 Modified triaxial testing equipment (Kayadelen et al. 2007)

Houston et al. (2008) performed a series of consolidated drained (CD) triaxial tests on four types of compacted soil specimens such as sandy silty clay, lean clay, silty sand, and poorly graded sand to study the unsaturated soil properties using a modified triaxial device. The errors in volume change measurement due to the expansion of the triaxial cell with higher pressure were addressed by using a double-walled triaxial cell. The volume change of the soil specimen was measured by measuring the volume of water flowing into the inner cell which applied the confining pressure. Since the inner cell experienced the same pressure on the inside and outside, it did not deform, thereby the errors due to cell expansion were minimized. The authors also suggested the equilibration of the soil specimen outside the triaxial cell to minimize the time required to attain equilibrium in unsaturated soils. The tests conducted mostly showed initial compression and then dilation for sandy silty clay, silty sand, and poorly graded sand, while only compression was observed for lean clay.

Many researchers have resorted to alternative ways of determining volume change using strain gauges (Thom et al. 2008), radial strain belts, and submersible displacement transducers (Cabarkapa and Cuccovillo 2006). Other researchers attempted to develop a cost-effective modified triaxial device to test unsaturated specimens, by using calibration charts to determine the errors introduced due to cell expansion in a single triaxial cell and other components (Burrage et al. 2012).

Li et al. (2015) and Li and Zhang (2015) proposed modifications to a conventional triaxial testing device to make unsaturated soil testing affordable. It was suggested that in lieu of controlling suction, the use of high suction tensiometers would record the changes in matric suction during constant water triaxial tests. Furthermore, the volume measurements were done using photogrammetry-based methods. The triaxial setup used for this purpose is shown in Figure 2.24a. The schematic diagram shows the location of targets (as shown in Figure 2.24b), which were high-contrast observation points, which could be automatically detected by the photogrammetry software. The images taken during testing enabled the authors to recreate a three-dimensional model of the soil specimen. The soil selected for the test comprised a combination of Fairbanks silt and Kaolin in the ratio of 85:15. Constant Water (CW) triaxial tests were conducted on compacted specimens having initial suction up to 500 kPa. The deviator stress response showed post-peak

softening for all specimens subjected to a low net confining pressure of 5 kPa and for all specimens having initial suction greater than 150 kPa for all net confining pressures. However, for specimens subjected to a net confining pressure of 200 kPa with initial suction less than 150 kPa, an increase in deviator stress was observed with a corresponding increase in axial strain. The rate of decrease of deviator stress with respect to axial strain increased drastically with an increase in initial suction and a decrease in net confining pressure. The volume change behavior was observed to be initially compressive (up to an axial strain of 1%), and then dilatant behavior was observed for all specimens when subject to a net confining pressure of 5 kPa (Li and Zhang 2015). Whereas only when the specimens were subjected to a net confining pressure of 200 kPa and sheared, the specimens having an initial suction of more than 150 kPa, demonstrated dilatancy, after initial compression. The remaining specimens (initial suction less than 150 kPa) showed only compression during shearing. It was also noted that the matric suction reduced gradually with an increase in net mean stress, during isotropic consolidation, and the decrease was more noticeable for specimens having higher initial suction.

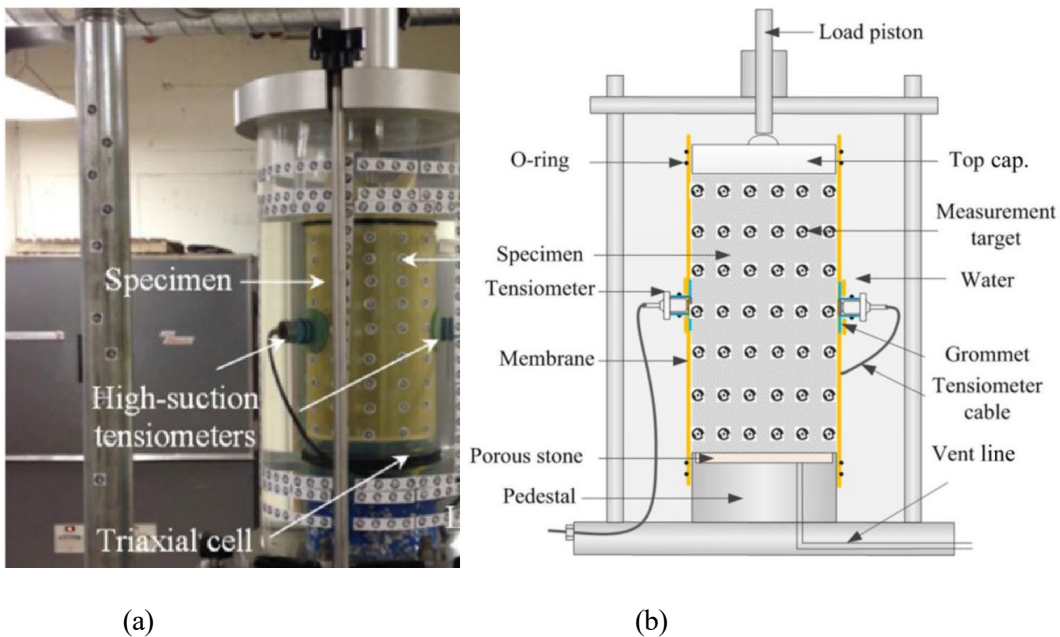


Figure 2.24 Proposed triaxial testing system: (a) photograph of the setup; (b) schematic plot (after (Li and Zhang 2015))

Ma et al. (2016) performed a series of consolidated drained triaxial tests on unsaturated silty soil using a suction-controlled double-cell triaxial apparatus. The pore air pressure was applied from the top cap, while the pore water was applied from the base pedestal. The volumetric strains during shearing were computed using a differential pressure transducer, which measured the difference in pressure due to varying levels of water between the inner cell and the reference tube. A similar approach was used earlier by Ng et al. (2002). The axial deformation was computed using a strain gauge. The radial deformation was determined from the axial and volumetric deformations. The tests were conducted on various specimens having low suction, from 15 to 90 kPa. The stress-strain response during shearing demonstrated post-peak softening. The volume change response showed initial compression till the axial strain reached 5%, and then dilation. It was noted that the dilation angle increased with an increase in induced suction and net confining pressure. However, the increase in net confining pressure decreased the tendency of the specimen to dilate.

Numerous studies were conducted to determine the volume changes in unsaturated soils during triaxial testing, however, the mechanism to measure the volume changes remained the same or similar.

2.11 Summary

This chapter describes various topics from literature related to the determination of the shear strength of unsaturated soils. First, the difference between saturated and unsaturated soils by considering the mechanics involved in governing the behavior of unsaturated soils is described. The importance of surface tension, capillarity, and soil suction in unsaturated soils are presented. The influence of the soil water characteristic curve, air-entry value, residual soil suction, and hydraulic hysteresis on the response of unsaturated soils are discussed.

The concept of shear strength of unsaturated soil is introduced and the methods to determine the shear strength are described. An elaborate discussion on the determination of shear strength using triaxial tests is presented. The various techniques to apply, control, and measure soil suction are described in brief. A review of the past and recent advances in triaxial test equipment for the determination of the hydromechanical response of unsaturated soils is presented in detail.

3. ADVANCED TRIAXIAL TESTING TO DETERMINE THE SHEAR STRENGTH OF UNSATURATED SOILS

The conventional triaxial device needed a few additional features to efficiently perform suction-controlled triaxial tests. These include the modifications to the base pedestal to incorporate ceramic disks, an arrangement to apply air pressure, a double-walled triaxial cell, a volume change device, and a flushing device. The fully automated double-walled triaxial test setup used throughout this research is shown in Figure 3.1a. The setup for determining the resilient modulus of soils is shown in Figure 3.1b. A schematic diagram of the triaxial setup is shown in Figure 3.2. Figure 3.3 shows a closer view of the triaxial assembly.

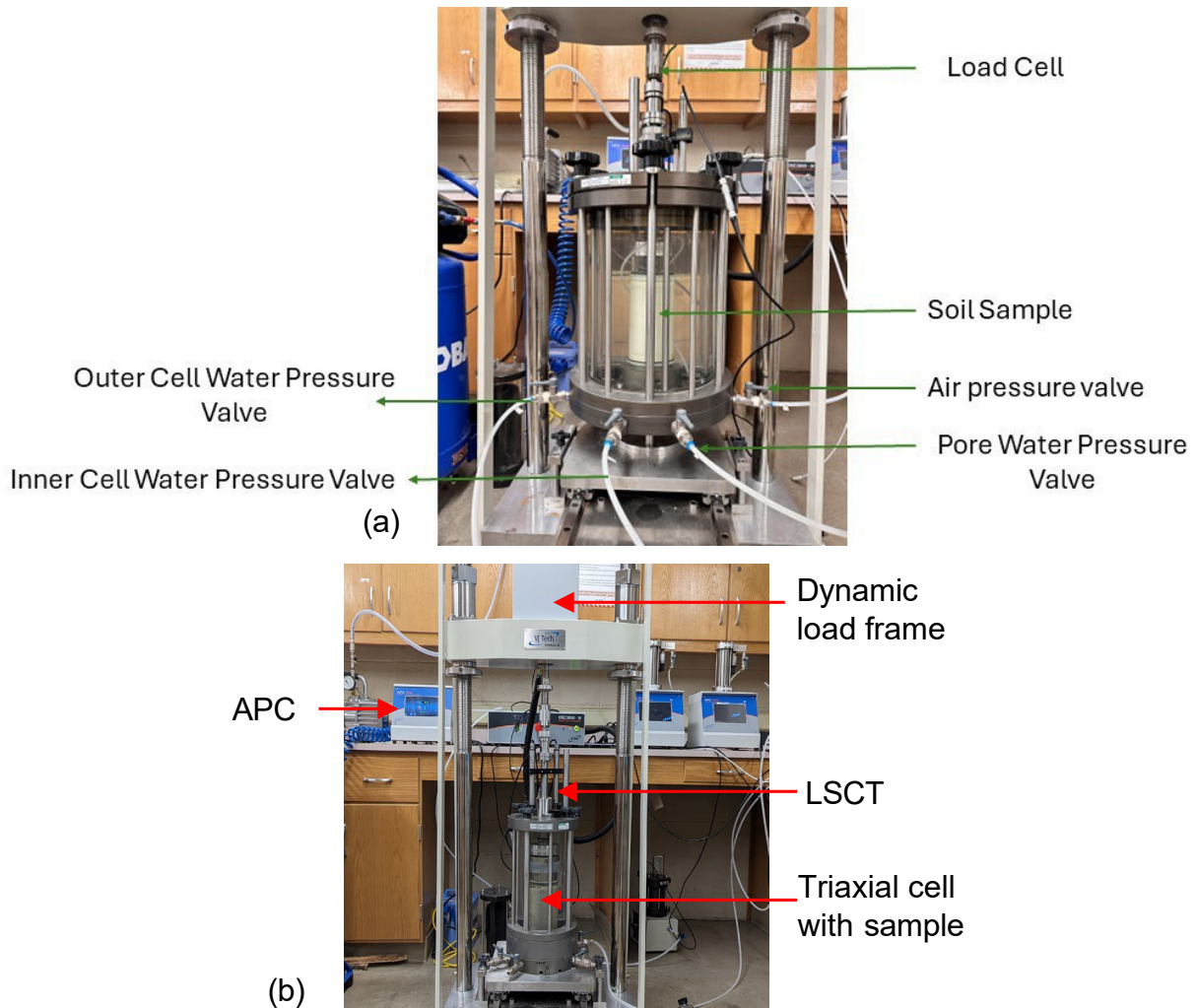


Figure 3.1 Panoramic view of the (a) fully automated double-walled triaxial test setup and (b) repeated load triaxial setup

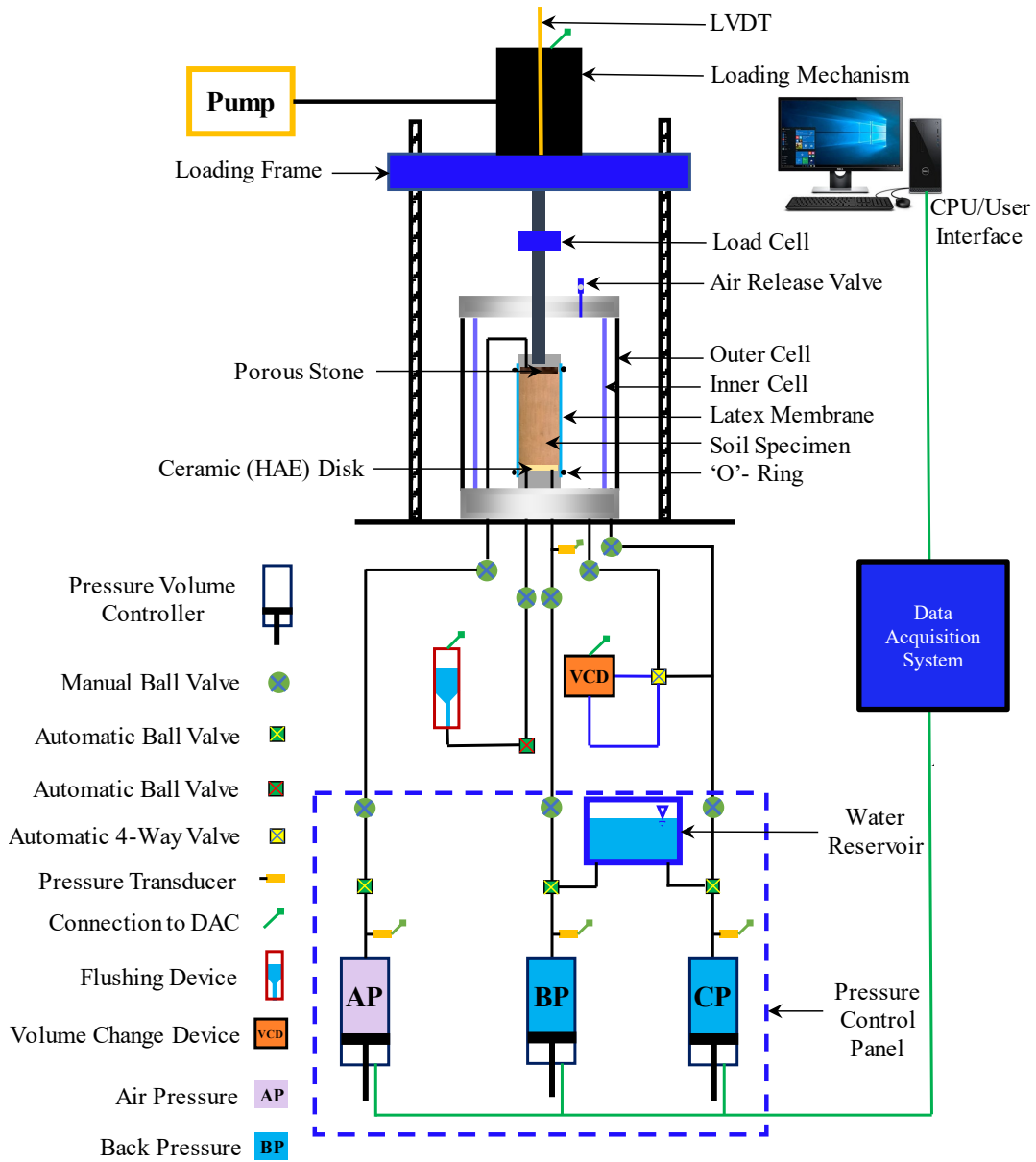


Figure 3.2 A schematic diagram of the fully automated double-walled triaxial setup



Figure 3.3 A closer view of the experimental setup and soil sample (a) before and (b) after the completion of a test

3.1 Modifications to the base pedestal to implement the axis-translation technique

The major limitation of traditional triaxial equipment to perform tests on unsaturated specimens is the control and measurement of suction having a magnitude greater than 100 kPa (1 atm). Since cavitation occurs when pore water pressure falls below absolute zero (or -100 kPa), the axis translation technique (Hilf, 1956) is used to allow the modified triaxial equipment to control suction in excess of 100 kPa in magnitude. In the axis-translation technique, the air pressure is increased beyond atmospheric pressure, and pore water pressure is kept at or near the atmospheric pressure.

However, porous stones would allow the passage of air through them to the saturated pore water pressure lines, which would result in an erroneous measurement of pore water pressure. To prevent such a problem, an artificially manufactured High Air Entry (HAE) disk was used in this research to separate the soil specimen and the pore water pressure line. The base pedestal was fitted with three HAE ceramic disks of higher air entry value than the matric suction to be applied. Whereas the top cap was fitted with a traditional porous stone to allow the passage of air to the soil specimen. The different pressure units are shown in Figure 3.4. The independent control of these pressures controls the soil condition and simulates the overburden pressure and matric suction applied to the soil sample.

Automatic Pressure Controllers are used for controlling and measuring the pressure (and volume where applicable) inside a Triaxial Cell. They are controlled by either:

- De-aired water via a water distribution panel (Figure 3.4 a and c) or
- Air from a compressed air supply (Figure 3.4 b)

The system features a single channel equipped with precise Pressure and Volume control capabilities, enhanced by feedback mechanisms for optimal performance. It can effortlessly generate pressures reaching up to 1000 kPa (10 bar) while maintaining exceptional control within a narrow margin of ± 0.1 kPa. The controllers have the flexibility to ramp up or down pressure at a specified rate, expressed in kPa per hour, facilitating gradual adjustments tailored to operational requirements.

Additionally, the system offers versatility in setting and sustaining either pressure in kPa or volume in cc, ensuring compatibility with varied experimental or operational parameters. With a volumetric capacity of 200 cc, accurate readings down to 0.001 cc provide meticulous control over fluid volumes, crucial for precision applications in research, industrial processes, or other specialized fields.



Figure 3.4 The different pressure units for independent control of overburden pressure and matric suction within a soil sample

The HAE ceramic disks were attached to steel rings using epoxy to prevent any leakage at the interface of the two materials (Figure 3.5). The stainless-steel ring was fitted with ‘O’-rings and these HAE disks encased in the ring were fitted securely into the base pedestal.

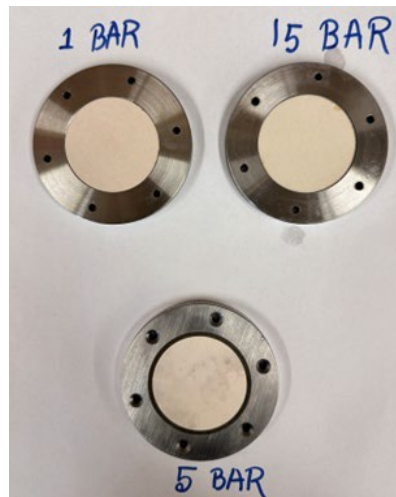


Figure 3.5 The ceramic disks used to maintain matric suction via the axis translation technique

3.1.1 Double-walled triaxial cell

Generally, the single-walled cell is used to perform triaxial tests on both saturated and unsaturated specimens. However, the difference in pressure on either side of the cell results in the expansion of the cell during testing. The volume change in the soil specimen is generally computed from the measurement of water flowing towards or away from the cell. The expansion of the cell with an increase in pressure results in water flowing into the cell to maintain the target confining pressure. This causes an error in the measurement of the change of soil volume during testing if proper corrections are not applied, which requires an elaborate calibration at regular intervals. To mitigate this problem, the double-walled cell was used in this research (Figure 3.1a).

The double-walled cell comprised of an inner and outer cell, which were connected via pipes. Any pressure that was applied to the outer cell automatically was applied to the inner cell. Hence, the inner cell was subjected to the same external and internal pressures, thereby preventing differential pressures, cell expansion, and leakage of water; and reducing system compliance errors. An automatic volume change device was used to accurately measure the volume of water entering the inner cell. These features enabled accurate measurement, control, and data collection of pressures and changes in specimen volume throughout the test.

3.1.2 Automatic volume change device

One of the greatest difficulties in triaxial testing of unsaturated soils is the determination of the sample volume. The difficulty comes from the fact that the voids of the specimen are partially filled with water and partially filled with air. When the volume of the specimen changes, there is a decrease or increase in the voids. If the voids were completely filled with water or in other words the sample is saturated, this change in the volume of voids would result in the same amount of water moving in or out of the sample. In an unsaturated specimen, though, that is not the case since there is also air in the voids which can be compressed. It is, therefore, essential to measure the actual volume change of the sample by other means.

A volume change device is used to determine the actual volume change of a triaxial sample. This is installed between the inner and outer compartments of an unsaturated triaxial cell in order to read the volume of the water that is moving in and out of the inner cell. The volume change device incorporates a hydraulic mechanism that moves a piston either upwards or downwards, depending on the direction of flow, when water is passing through it. The movement of the piston is proportional to the volume of the moving water; therefore, after correlating the movement of the piston to the water volume, through calibration, the device can accurately measure the volume of the water that moves in or out of the inner cell. After applying some necessary corrections, this reading will correspond to the change in the volume of the sample during the test. A volume change device used in the triaxial setup is shown in Figure 3.6.

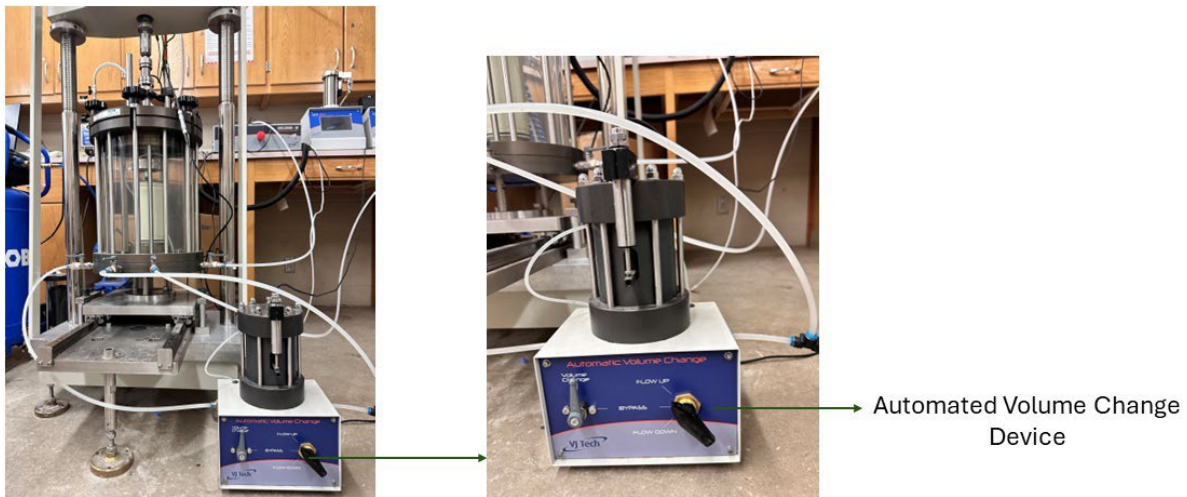


Figure 3.6 Automated volume change device

3.1.3 Saturation of Ceramic Disc

The saturation of the ceramic disk prior to the commencement of the triaxial test is pivotal. The ceramic disks were fitted to the base pedestal of the triaxial setup and after placing the triaxial cell, the chamber was sealed. The cell was filled with de-aired water. One end of the pore water pressure line, which was connected in parallel to the pore pressure transducer, was connected to the volume change device to

enable accurate measurement of the volume of water flowing through the ceramic disks. While the other end was closed using the manual valve. The connection from the other end of the volume change device was connected to a burette as a supplementary volume measurement system.

The air pressure line from the pressure control panel was connected to the air release valve on top of the triaxial cell and gradually the air pressure was increased to a value greater than the air-entry value of the ceramic disk. The water gradually flows through the ceramic disk and its rate is recorded. The rate of water flow was compared with the applied air pressure and the permeability of the ceramic disk was estimated, to ensure that there was no leakage in the base pedestal assembly and ceramic disks had no cracks. Once the rate of water flow was consistent with the expected values, the air pressure was maintained for more than 4 hours to ensure complete saturation of all the ceramic disks.

Consequently, the air pressure gradually decreased to atmospheric pressure, and the water from the triaxial was drained out. The connections to the pore water pressure line were changed from the volume change device to the back pressure control panel and the ceramic disk was flushed. Thereafter, a pore water pressure of 10 kPa was applied to the ceramic disk, to ensure that while placing the soil sample, the ceramic disk remained saturated. Similar approaches have been used by Hoyos (1998) and Banerjee (2017).

3.2 Saturated Soil Triaxial Testing

3.2.1 General

A series of independent tests at the same net confining pressure were performed at varying shearing rates to determine the suitable shearing rate for all triaxial tests on saturated specimens. The most appropriate axial shearing rate was determined to be 0.05%/min. Three consolidated drained (CD) triaxial tests were performed following the conventional triaxial compression (CTC) stress path for saturated specimens. The compacted specimens were weighed, and the height was measured in orthogonal directions. The diameter was measured in orthogonal directions at three equally spaced locations along the longitudinal axis of the compacted specimen and the average of these readings was recorded.

The base pedestal fitted with a saturated porous stone was attached to the base plate of the triaxial setup and the pore pressure lines (or pipes) were saturated using manual control. A moist filter paper was placed on the previously saturated porous stone to prevent the migration of fine particles into the pore pressure line. Additionally, the filter paper prevented the clogging of the porous stone. The compacted specimen was mounted on the base pedestal with the porous stone. Another filter paper was placed on the top of the specimen. The top cap fitted with another porous stone was carefully placed on the compacted specimen. The entire assembly of the base pedestal, compacted soil specimen, and the top cap was enclosed using a latex membrane and three 'O'-rings at both ends of the assembly. The double-walled cells were placed, and the entire chamber was sealed. Initially, the outer cell and later the inner cell were filled with de-aired water by applying a 15 kPa pressure from the pressure control panel. Since the air release valve was open, the soil specimen did not experience any significant confining pressure. Once the inner cell was almost filled, the pressure was reduced to 5 kPa and after it was filled, the air release valve was closed. Subsequently, the cell pressure was increased to 15 kPa and a back pressure of 5 kPa was introduced. Thus, an effective confining pressure of 10 kPa was maintained. Seating stress of 5 kPa was applied to the axial actuator to maintain proper contact with the top surface of the specimen.

3.2.2 Saturation of the specimen

The first stage of a saturated triaxial test is the process of saturation, where the soil is gradually saturated while maintaining positive effective confining pressure throughout the process. This procedure was

conducted as per the guidelines of ASTM D7181-11. After the water-front reached the top of the specimen, the applied suction was removed. When the water came out through the top porous stone, due to the back pressure of 5 kPa, the valve to the top cap was closed.

Subsequently, the specimen was saturated using a back pressure approach. The specimen was saturated by either dissolving the pore air into the pore water or by collapsing the air bubbles due to the introduction of high back pressure. According to ASTM D7181-11, the specimen is considered to be fully saturated when Skempton's pore-water parameter, B , is greater than 0.95. The B -value is the ratio of an increase in pore water pressure (Δu) due to an increase in cell pressure ($\Delta\sigma_3$) and is defined using the following expression:

$$BB - \text{value} = \frac{\Delta u}{\Delta\sigma_3} \quad (3.1)$$

To check the B -value, the drainage valve connected to the base of the specimen was closed, and the cell pressure was increased by 15 kPa. The generation of excess pore water pressure (Δu) due to incremental cell pressure ($\Delta\sigma_3$) was recorded after the stabilization of the pore water pressure. The B -value was calculated using Equation 3.3.

In this research, the criterion for complete saturation was set at a B -value of 0.96. The B -value was checked after both the cell and pore pressure had stabilized. If the criterion for full saturation was not met, the drainage valve was opened, and both the cell pressure and the back pressure were gradually increased by an equal increment of 15 kPa/h. The pressures were increased gradually to allow proper pore pressure equalization throughout the specimen. It was observed that the final value of the back pressure required for complete saturation was in excess of 600 kPa.

3.2.3 Isotropic Consolidation of the specimen

The consolidation stage involves the dissipation of excess pore water pressure generated due to the application of the target effective pressure at which the shearing would be conducted. During consolidation, the volume of the soil specimen undergoes changes due to the dissipation of excess pore water pressure. The target consolidation stress was achieved by ramping up the cell pressure while maintaining constant back pressure. The target cell pressure was reached in 30 seconds and the change of volume of soil specimen and the volume of water flowing out of the specimen was recorded and plotted.

Subsequently, when both the volumes reached a constant value and the volume of water flowing out of the specimen was the same as the change in volume of the soil specimen, the consolidation was assumed to be completed. This was generally observed after 10 hours. To ensure that the primary consolidation was practically completed for all tests, 24 hours of consolidation was implemented. A similar procedure was used to consolidate the specimens to effective confining pressures of 100, 200, and 400 kPa. These samples were then tested to study the behavior of the compacted soil during shearing at varying effective confining pressures.

3.2.4 Shearing under Drained conditions

After consolidation, the specimen was sheared monotonically following the Conventional Triaxial Compression (CTC) stress path in drained conditions. For the consolidated drained (CD) test following the CTC stress path, both the cell pressure and the back pressure were maintained at a constant value, while the specimen was loaded axially under constant axial strain rate (strain-controlled test) or under constant axial stress rate (stress-controlled test). The post-peak response could only be obtained from a

strain-controlled test, since in stress-controlled tests, the test gets terminated after reaching peak stress. Therefore, in this research, strain-controlled tests were conducted on all the specimens.

The determination of the appropriate strain rate is essential for consolidated drained tests. Since the shearing rate influences the peak deviator stress and the volume change response of soil specimens, an independent study was conducted to study the influence of axial strain rate on the mechanical behavior of compacted specimens of silty soil. The most appropriate strain rate for a saturated specimen was determined to be 0.05%/min, which was obtained by determining the fastest strain rate which practically had a negligible effect on the mechanical response of the soil during shearing. This shearing rate was selected since it allowed proper dissipation of excess pore water pressure throughout the specimen.

Three saturated specimens were sheared at varying effective confining pressures of 100, 200, and 400 kPa at a constant axial strain rate of 0.01%/min to study the mechanical response of the soil under drained conditions. The deviator stress response was carefully analyzed to determine the strength of the saturated soil at the peak stress state and the critical state. The deviator stress responses of saturated specimens to shearing at the effective confining pressures of 100, 200, and 400 kPa are shown in Figure 3.7. In these tests, it was also observed that the specimens failed, without any distinct shear planes, by bulging at the center.

The shear strength parameters were obtained by plotting the Mohr Circle at peak stress (Figure 3.8). The effective cohesion was obtained as 30 kPa and the effective angle of internal friction was 26.9° . The slope of the critical state line was determined to be 1.047 and the slope of the individual p' - q stress path was calculated to be 3:1, which has been shown later.

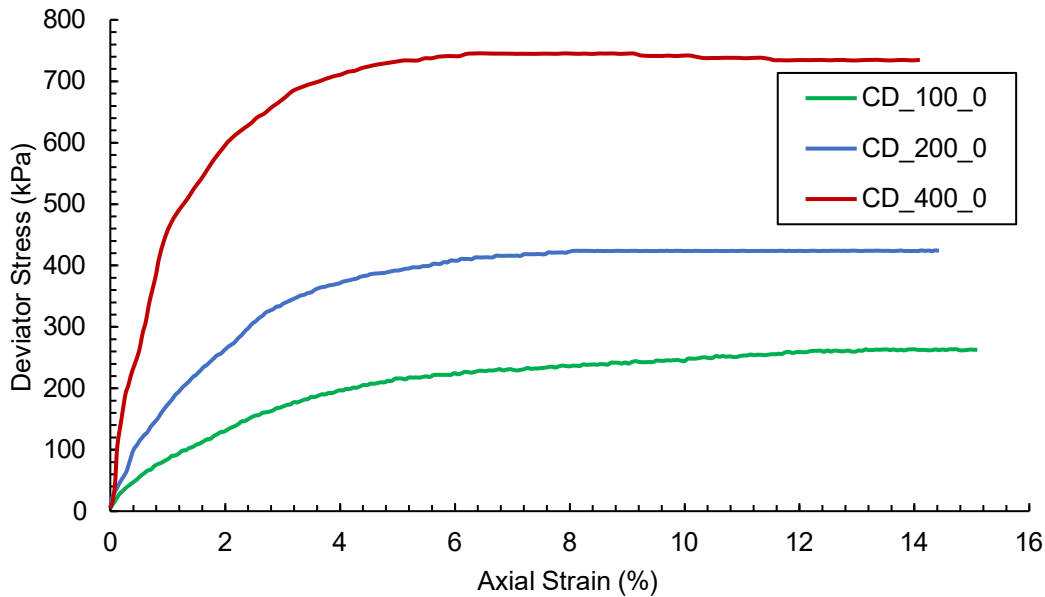


Figure 3.7 Deviator stress response of saturated silt for varying effective confining pressure

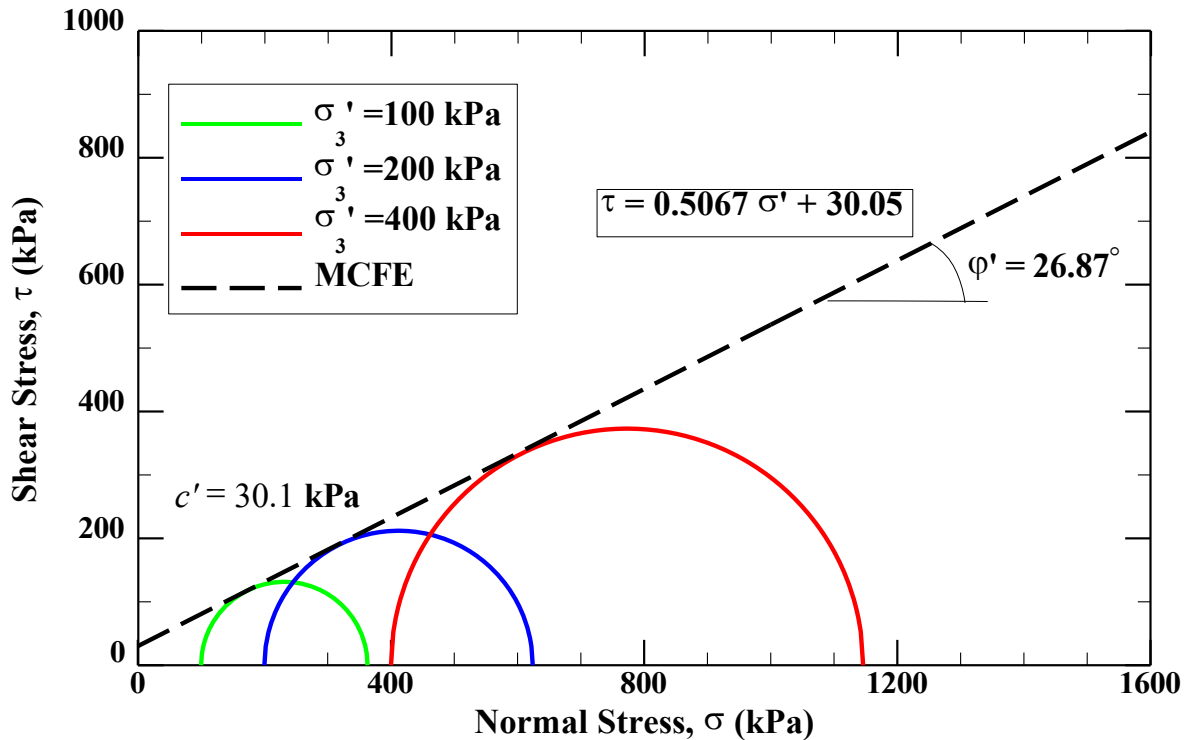


Figure 3.8 Determination of peak shear strength parameters for saturated silt specimen using Mohr-Coulomb failure criterion

3.3 Unsaturated Soil Triaxial Testing

3.3.1 General

The modifications to the triaxial device enabled the testing of unsaturated specimens. The optimum axial strain rate for shearing was determined to be 0.003%/min, which had been selected based on the response of deviator stress and volumetric strain during shearing and the consideration of an appropriate practical duration for the completion of an unsaturated triaxial test. A series of suction-controlled triaxial tests under drained conditions following the conventional triaxial compression (CTC) stress path were performed and matric suction was induced within the soil specimen using the principle of axis-translation technique.

3.3.2 Stress Variables and Shear Strength of Unsaturated Soils

The identification of the appropriate stress variables that control the behavior of unsaturated soil is essential prior to testing of unsaturated soils. The independent two-stress state variable approach by (Fredlund and Morgenstern 1977) has been one of the most widely accepted theories for the determination of effective stress acting on an unsaturated soil. The stress state variables, i.e., net normal stress ($\sigma - u_a$), and matric suction ($u_a - u_w$), were considered independent parameters that primarily controlled the behavior of unsaturated soils.

The independent two-stress state variable approach can be integrated with the Mohr-Coulomb failure criterion, and the shear strength at failure, τ_f of unsaturated soil can be estimated using the following relation:

$$\tau_f = c' + (\sigma - u_a)_f \tan \phi' + (u_a - u_w)_f \tan \phi^b \quad (3.2)$$

where, c' and ϕ' are effective cohesion and effective angle of internal friction of the saturated soil, respectively, and ϕ^b is the friction angle, which is due to the contribution of the matric suction on the shear strength of the soil. Alternatively, the parameters net mean stress, p' , deviator stress, q , and the matric suction, s are used to study the behavior of unsaturated soils, which are expressed as follows:

$$p = \frac{\sigma_1 + 2\sigma_3}{3} - u_a \quad (3.1)$$

$$q = \sigma_1 - \sigma_3 \quad (3.2)$$

$$s = u_a - u_w \quad (3.3)$$

where, σ_1 and σ_3 are the major and minor principal stresses, which are assumed to be the axial and radial stresses acting on the specimen. The parameters, u_a and u_w are the pore air and pore water pressure, respectively.

3.3.3 Testing Procedure

The axis translation technique was used to apply and control the matric suction inside the specimen during the tests. Independent control of pore air and pore water pressures facilitated the application of matric suction, following the axis translation technique (Hilf 1956). The following stages are performed to determine the shear strength and volume change behavior of unsaturated specimens.

3.3.3.1 Stage 1: Suction equalization

The compacted soil sample was initially saturated and then brought to the required matric suction to mitigate the effect of SWCC hysteresis. Once the desired matric suction was approximately achieved, the mass and dimensions were carefully measured, and the specimen was mounted on the base pedestal fitted with a saturated HAE ceramic disk in the triaxial cell. Previously, the pore water pressure lines were filled with de-aired water and the base pedestal was flushed thoroughly. The double-walled cell was placed, and the chamber was sealed. The inner and outer triaxial cells were also filled with de-aired water and a cell pressure of 30 kPa was applied with a pore water pressure of 10 kPa maintained through the bottom pedestal and an initial pore air pressure of 20 kPa applied at the top of the specimen via porous stone. Therefore, the initial net confining pressure, $(\sigma_3 - u_a)$ being applied was 10 kPa.

The cell pressure and pore air pressure were gradually increased, at a constant rate of 10 kPa/hr, to attain the desired matric suction. Hence, the matric suction was imposed using the axis-translation technique. The suction equilibration was completed when the water content change was less than 0.04%/day or 0.5 cm³/day, which was followed by Banerjee (2017) and Ng et al. (2013). In this research, the suction was considered to be equilibrated when the change in water content was less than 0.04%/day. It generally required 5-7 days to achieve equilibration for the required matric suction, since the specimens were pre-equilibrated at a nearby suction level. The suction equalization process was facilitated by using different types of ceramic disks during testing. The 5-bar HAE ceramic disk was used for performing tests on specimens having a matric suction of 250 kPa.

3.3.3.2 Stage 2: Isotropic Consolidation

Once the required matric suction was achieved, the isotropic consolidation stage commenced. In the case of the axis translation technique, the matric suction was maintained by controlling the pore air pressure and pore water pressure at a constant value, while the cell pressure was gradually increased at the rate of 10 kPa/h to its required value to attain the requisite net confining pressures. Each specimen was consolidated for more than 24 hours to ensure complete dissipation of pore air and water pressure. During this stage, the volume change of the specimen is recorded carefully.

3.3.3.3 Stage 3: Shearing

After isotropic consolidation, the specimen was sheared monotonically by axially loading at a constant axial strain rate (strain-controlled test) of 0.003%/min, while a constant net confining pressure and matric suction was maintained throughout the test. The conventional triaxial compression (CTC) stress path under drained conditions was followed during the shearing stage.

A schematic representation of the sequences involved in the unsaturated triaxial test is shown in Figure 3.9. In this case, the test was performed at a matric suction of 250 kPa at a net confining pressure of 200 kPa. It also shows the values of axial and radial stresses, pore air pressure, pore water pressure, net confining pressure, and the matric suction acting on the specimen at the end of each stage of unsaturated soil testing.

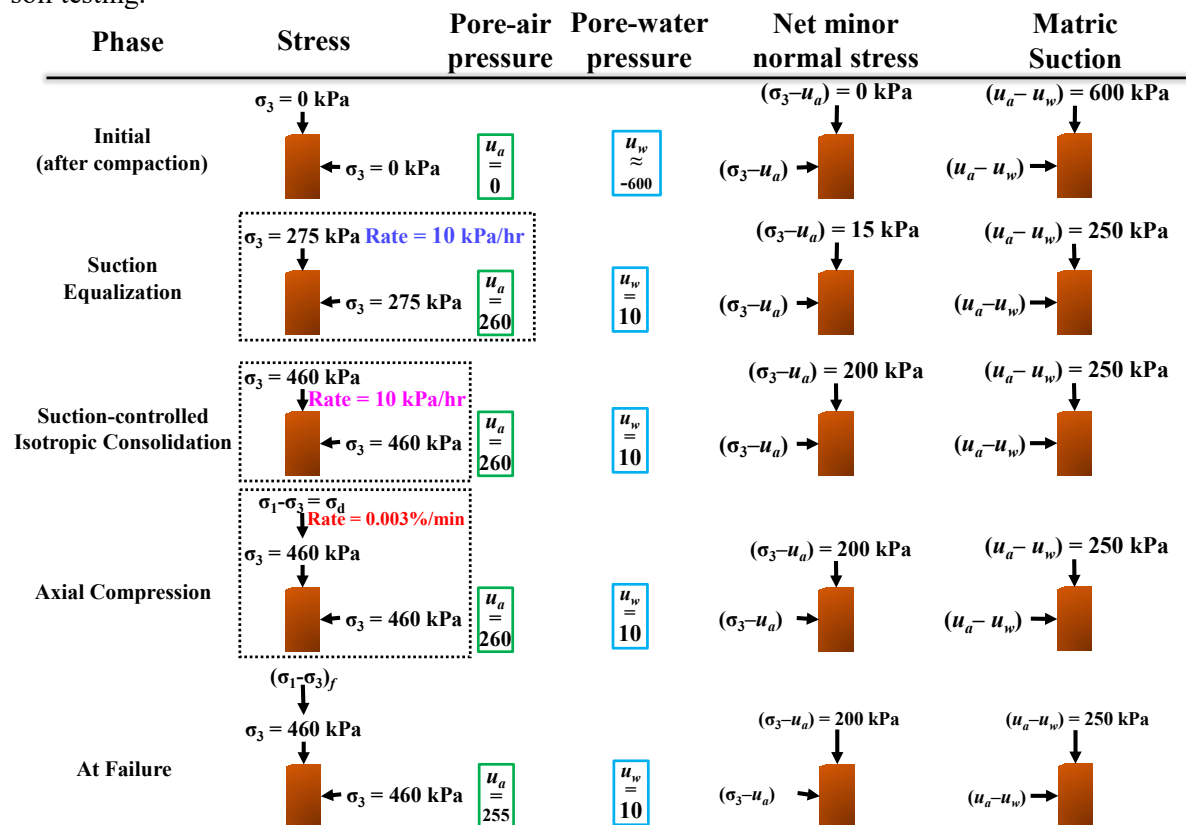


Figure 3.9 Schematic of procedure to perform an unsaturated triaxial test at a net confining pressure of 200 kPa and matric suction of 250 kPa under drained conditions.

3.3.4 Test Program

A small series of triaxial tests were performed to investigate the effect of the increase of net confining pressure and matric suction on the mechanical response of soil when subjected to the loading in the form of hydrostatic compression (HC) and conventional triaxial compression (CTC). The following values of stress variables were considered during the series of single-stage monotonic triaxial tests:

Net confining pressure, $(\sigma_3 - u_a)$: 100, 200 and 400 kPa

Matric suction, $(u_a - u_w)$: 0 (saturated) and 250 kPa

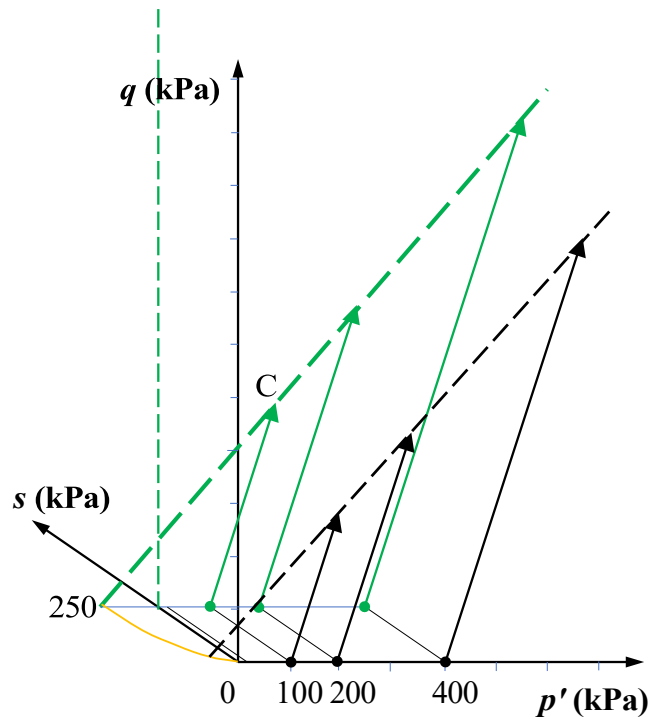


Figure 3.10 Saturated and suction-controlled CTC stress paths in $p':q:s$ space

3.4 Mechanical Response under Suction-controlled Shearing

The results of the shearing stage for all the unsaturated specimens have been discussed in this section. The compression of soil is represented as a positive volumetric strain, while, the dilation is represented by a negative sign, which is the general sign convention followed for soils. Additionally, the nomenclature followed to represent each test is “CD_x_y”, where, CD denotes the Consolidated Drained test; x and y represent the net confining pressure $(\sigma_3 - u_a)$ and the matric suction $(u_a - u_w)$ applied in kPa during the test, respectively.

The deviatoric stress response of the unsaturated specimens during shearing in drained conditions at constant induced matric suction of 250 has been shown in Figure 3.11. It can be observed that the strength of the specimen increases with an increase in confining pressure. The response of deviator stress in unsaturated soil showed that the increase in net confining pressure resulted in an increase in the initial stiffness of the specimen. The stiffness of the soil increases with increased confining pressure as evidenced by the increased slope of the initial portion of the stress versus strain curve.

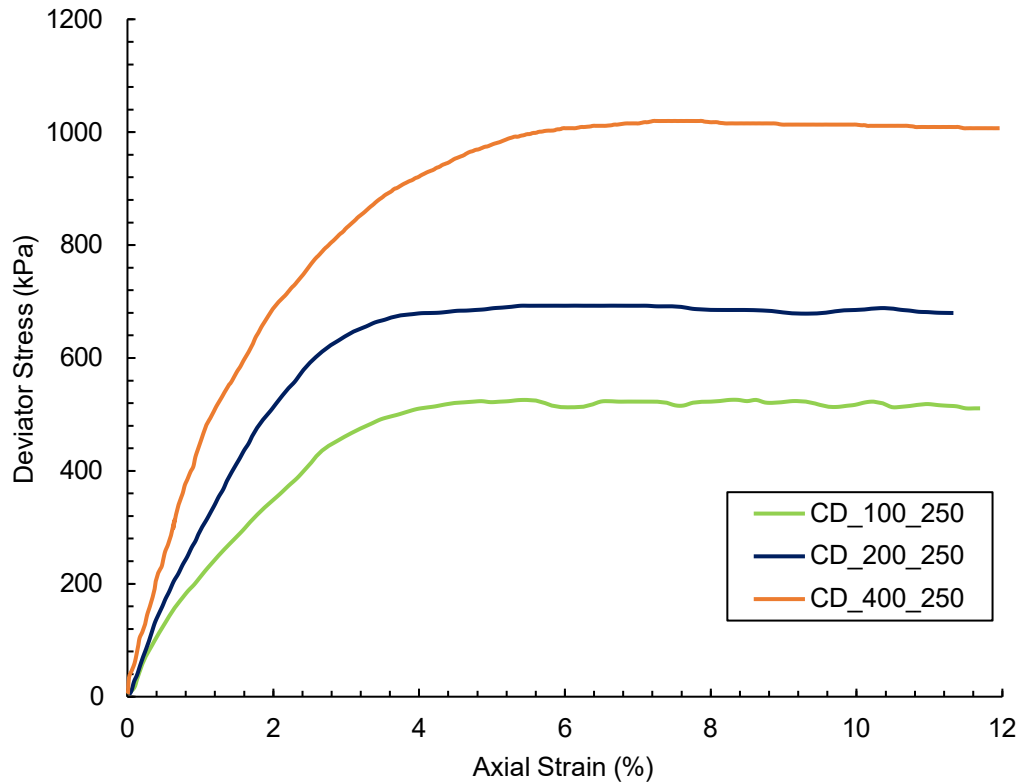


Figure 3.11 Deviatoric stress response of consolidated specimen at induced matric suction of 200 kPa under drained condition

The peak values of the deviator stress response were used to generate the corresponding Mohr's circle of stress at failure for each net mean stress. The modified linear failure envelope was developed based on Equation 2.14 and shown in Figure 3.12. The total cohesion, which is the sum of effective cohesion in saturated soil and the apparent cohesion due to matric suction was observed to be 115 kPa at a suction of 250 kPa, while the effective friction angle (26.7°) was observed to be nearly the same as that for saturated soil. Similarly, the critical state line (CSL) for saturated soil and unsaturated soil at a suction of 250 kPa was determined and shown in Figure 3.13. At nearly 1.05, the slope of CSL of the saturated soil was similar to that for unsaturated soil. However, the contribution of suction to the increased strength of the soil is evident from the higher apparent strength of the soil in an unsaturated state. This increased strength and higher position of CSL in p-q space mean that the stiffness of the soil is generally higher, and higher stresses are needed to fail the specimens in an unsaturated state.

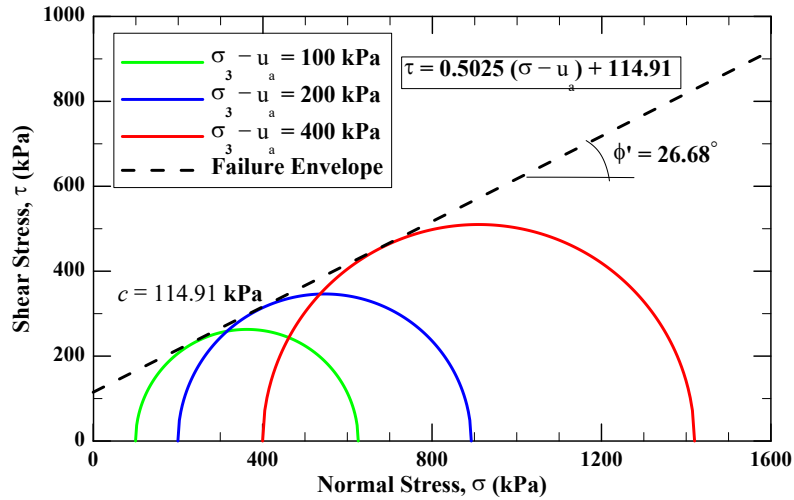


Figure 3.12 Determination of peak shear strength parameters for unsaturated silt specimen using modified Mohr-Coulomb failure criterion

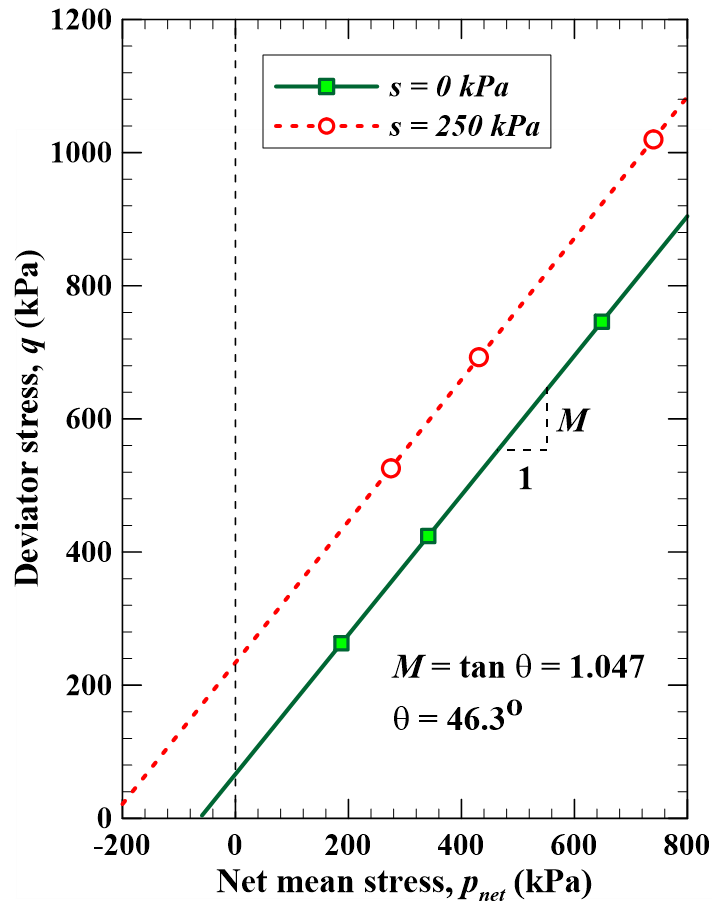


Figure 3.13 Critical state lines in p-q space for saturated and unsaturated soils

However, wetting-induced collapse may occur in some of these soils. For high plasticity clayey soils, suction-controlled testing is limited due to the limitations of current technology to apply higher pressures to induce higher suction through axis translation techniques. There is a need for the identification of safer

ways of replicating higher suction values to study the response of clayey soils. The desiccation-induced cracks in clayey soils occur at much higher suction levels, especially for high plasticity clays like bentonite and their response needs to be considered to efficiently predict the behavior of such soils.

3.5 Summary

The role of advancement in triaxial testing devices to study the response of unsaturated soil has been discussed in this chapter. The installation of an advanced triaxial testing device that can control matric suction in soils has been demonstrated through a series of triaxial tests under consolidated drained conditions. The increase in strength in unsaturated soil has been determined through a time-consuming process as discussed in this chapter. The limitations of testing unsaturated high plasticity clays have also been discussed where there is a need to develop simpler and safer testing protocols that would not need the high mechanical stresses to induce or measure suction in clayey soils. Due to the extreme weather conditions that might induce significant values of matric suction subsequent chapters discuss the effects of extreme weather and resulting intense and prolonged droughts on the stability of embankments in different regions of the nation. Overall, the importance of considering the unsaturated behavior of soils has been highlighted in Chapters 2 and 3.

4. IMPACT OF EXTREME WEATHER ON EXPANSIVE SOIL

4.1 Introduction

Expansive soils are prevalent in arid and semiarid regions worldwide, including Australia, Canada, China, India, South Africa, and the United States. These soils generally display a moderate to high ability to be molded, a low to moderate level of strength, and a high tendency to swell and shrink in volume (Alonso et al. 2003; Sherwood 1962). The weathering by-products of limestone material and alluvial deposits in the North Central Texas region result in moderate- to high-plasticity clayey soils. In this region, the montmorillonite-rich Eagle Ford Shale clay from the upper Cretaceous period is expansive in nature (Puppala et al. 2006). To mitigate the adverse effects of these soils, different rehabilitation strategies have been employed in the region (He et al. 2018; Jang et al. 2022; Talluri et al. 2020). Untreated forms of expansive soils typically undergo high swell–shrink characteristics with a variation in the moisture regime. Desiccation cracking occurs within the plastic fill materials as a result of repeated drying and wetting cycles (Acharya et al. 2017). The most important deformation phenomenon of unsaturated soils, and especially expansive soils, is swelling and shrinking (Banerjee 2017). The engineering properties of collapsible, residual, compacted, and expansive soils, which are usually in an unsaturated state, can be better understood by considering the impact of matric suction (Fredlund 2000). Expansive soils have high values of swelling and compression indices and are subject to frequent changes in matric suction ($u_a - u_w$), which causes additional volume changes. A structure constructed on expansive soil is subject to heave or settlement depending on moisture suction fluctuations (Fredlund 2000). Hence, it is crucial to consider the influence of matric suction when evaluating slope stability. Figure 4.1 illustrates the change in suction in the soil profile with climatic condition changes.

Embankments and levees are critical infrastructures that are often impacted by storms and hurricanes. Earthen embankments are used primarily as a means of transportation networks and flood defenses. These act as lifelines for mankind as transportation facilities and river training structures and are often the last form of defense against flooding. The failure of such structures due to extreme climatic events can cause societal and economic disruption (Vardon 2015). Recently, a levee failed on the Pajaro River in central California that had experienced prolonged periods of drought followed by incessant precipitation. This resulted in mass evacuations and flooding, which highlights the need to study the effects of extreme weather on critical civil infrastructure.

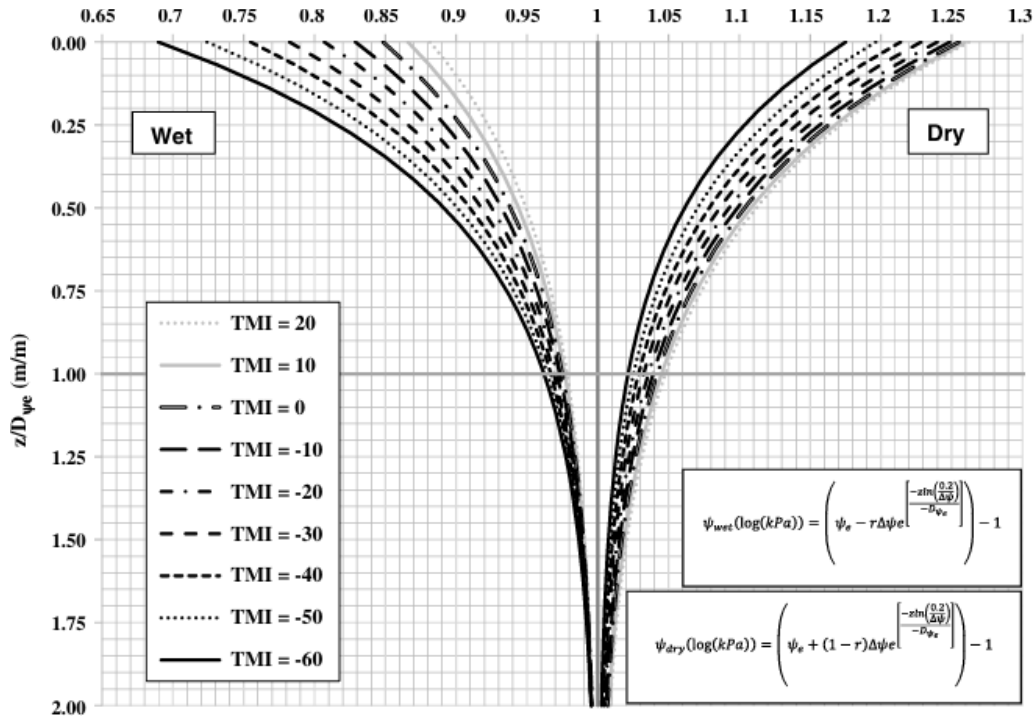


Figure 4.1 Normalized plot of suction (in kPa) with depth for dry and wet conditions (adopted from Vann and Houston 2021)

Several factors such as surface erosion, softening of the soil, tensile cracking, soil desiccation, and seismicity can contribute to the failure of a slope (Leshchinsky et al. 2015). Researchers have illustrated that, for soil slopes, the behavior of the deeper layers is governed by the changing water table, while the surface layers are governed by atmospheric conditions (Alonso et al. 2003). Extreme weather can cause a negative effect or even a calamitous effect on the stability of the slope as the slopes are continuously exposed to extreme climatic conditions (Fredlund et al. 2012). It was illustrated that the critical parameters for slope stability are the hydraulic properties, including permeability and water retention, which are highly influenced by environmental factors (Fredlund et al. 2012).

Desiccation cracks develop when the soil can no longer withstand the tensile stresses caused by shrinkage (Fredlund 1987). During precipitation, water infiltrates the soil through these cracks. Infiltration elevates the pore water pressure, leading to a subsequent decrease in the shear strength of the soil, which causes failure to occur (Cho and Lee 2002; Rahardjo et al. 1995). After prolonged exposure to environmental factors like the wetting–drying cycle, fully softened shear strength eventually develops in clays (Saleh and Wright 1997). Surficial failures may occur abruptly and without warning. At times, they may be accompanied by fissures or other indications of impending failures. A slope demonstrates greater strength in the dry season due to the soil being in an unsaturated state with negative pore water pressure and higher values of matric suction. This can also lead to an overestimation of the factor of safety (McCleskey et al. 2008). Numerous slopes at the desiccated state fail when subjected to intense rainfall due to a decrease in matric suction and an increase in pore water pressure (Figure 4.2).

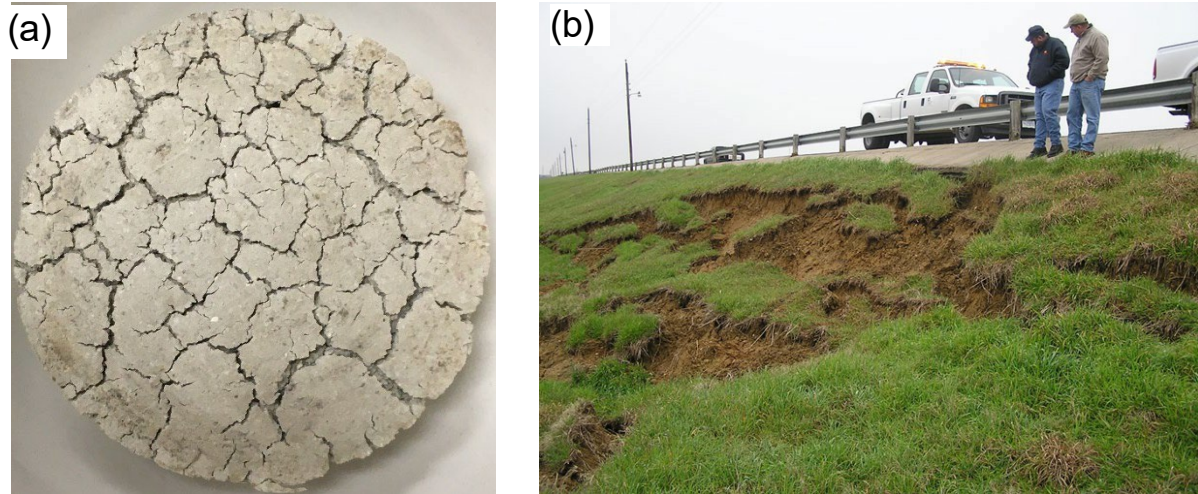


Figure 4.2 (a) Desiccation crack formation of expansive soil, (b) surficial failure of expansive soil embankment (Banerjee 2017)

The impact of extreme weather may increase the severity and frequency of these issues, which may be modeled by incorporating the climate prediction models in the slope stability analysis. The soil–water characteristic curve establishes the relationship between the volumetric water content of the soil and the matric suction, which, in turn, determines the failure mechanism. The phenomenon is influenced by the flux boundary conditions, specifically rainfall infiltration, evaporation, and evapotranspiration at the interface between the soil and the atmosphere (Rahardjo et al. 2007). The increased rainfall can cause failure in earthen structures (Robinson and Vahedifard 2016; Vahedifard et al. 2020). In addition to the intensity of rainfall, other factors such as the characteristics of rainfall, previous precipitation, soil properties, and topography also play a role in the failure of a slope (Church and Miles 1987). This issue becomes amplified when we consider the distress in expansive soils caused by drought-like conditions (Banerjee et al. 2020c, 2021). Any drought-like condition followed by intense precipitation can cause severe damage to earthen structures, which are anticipated to be negatively impacted by extreme weather (Banerjee et al. 2020a, 2021; Kumar et al. 2021). Figure 4.3 shows the interaction between climatic conditions and expansive slope and the subsequent formation of desiccation cracks due to shrinkage–swelling, which ultimately leads to surficial failure. Extreme weather may also affect agricultural productivity through higher soil erosion, which may occur due to higher-intensity storms, floods, and the exposure of deeper layers due to the formation of desiccation cracks in expansive soils during prolonged periods of drought. Therefore, there is an urgent need to study the behavior of embankments when subjected to stresses caused by extreme weather.

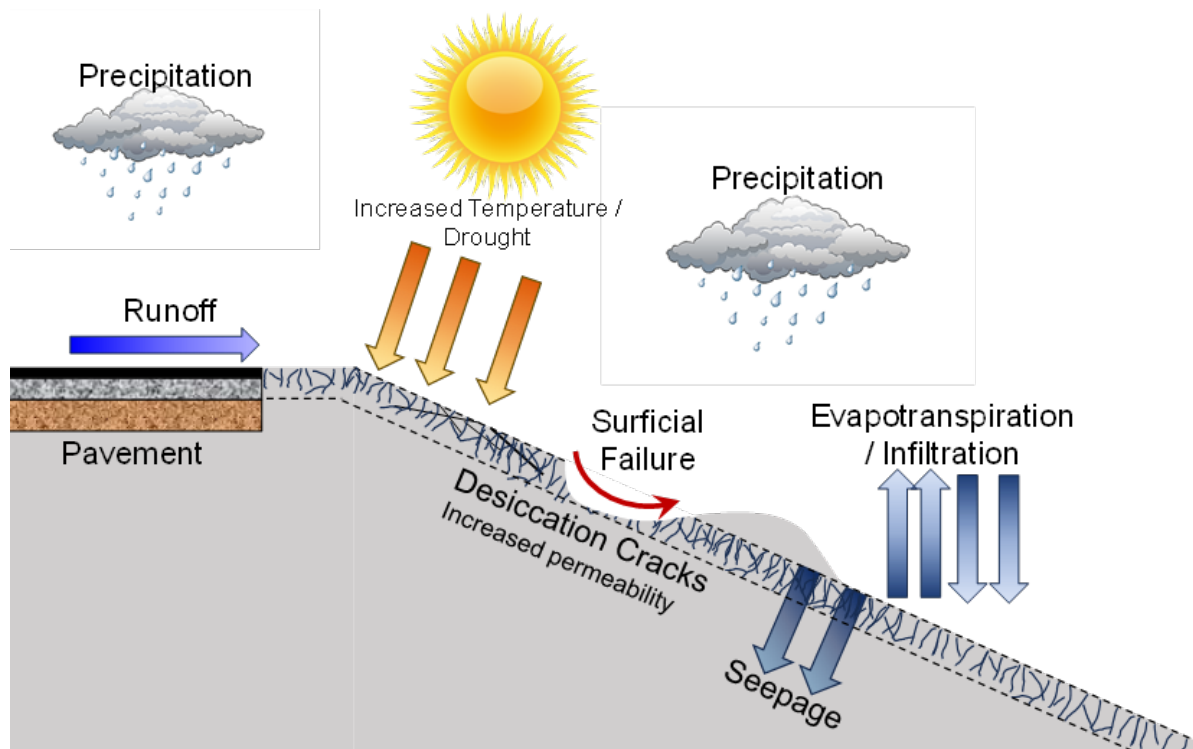


Figure 4.3 Schematic of climatic interactions with slope and surficial failure

4.2 Incorporating Extreme Weather Data in Geotechnical Engineering

The advancement in climate and geotechnical modeling has enabled the measurement of the effects of extreme weather on geotechnical infrastructures. Assessing the impact of extreme weather on the stability of slopes and embankments involves analyzing three intricate processes: (a) forecasting more detailed future climate data, (b) calculating pore water pressures (PWP) in slopes caused by changes in variables due to climate conditions, and (c) estimating the factor of the safety of slopes based on the calculated PWP.

Coupled hydro-mechanical finite element analysis can be used for the slope stability analysis of expansive clay embankments and to consider the effect of extreme weather-induced instability. Researchers have used this method to consider the characteristics of expansive clay and the presence of desiccation cracks and found an increase in the saturated coefficient of permeability for the surface layer (Qi and Vanapalli 2016, 2015).

There are several climate models available to predict future climate scenarios. The CMIP6 (Coupled Model Intercomparison Project Phase 6) presents new global climate model data. CMIP6 utilizes shared socioeconomic pathways (SSPs) to simulate different socioeconomic scenarios that may be affected by urbanization, population growth, changes in gross domestic product in different nations, and greenhouse gas (GHG) emissions (O'Neill et al. 2014). Figure 4.4 demonstrates the predictions for global mean temperature change in the future based on different scenarios considered in SSPs.

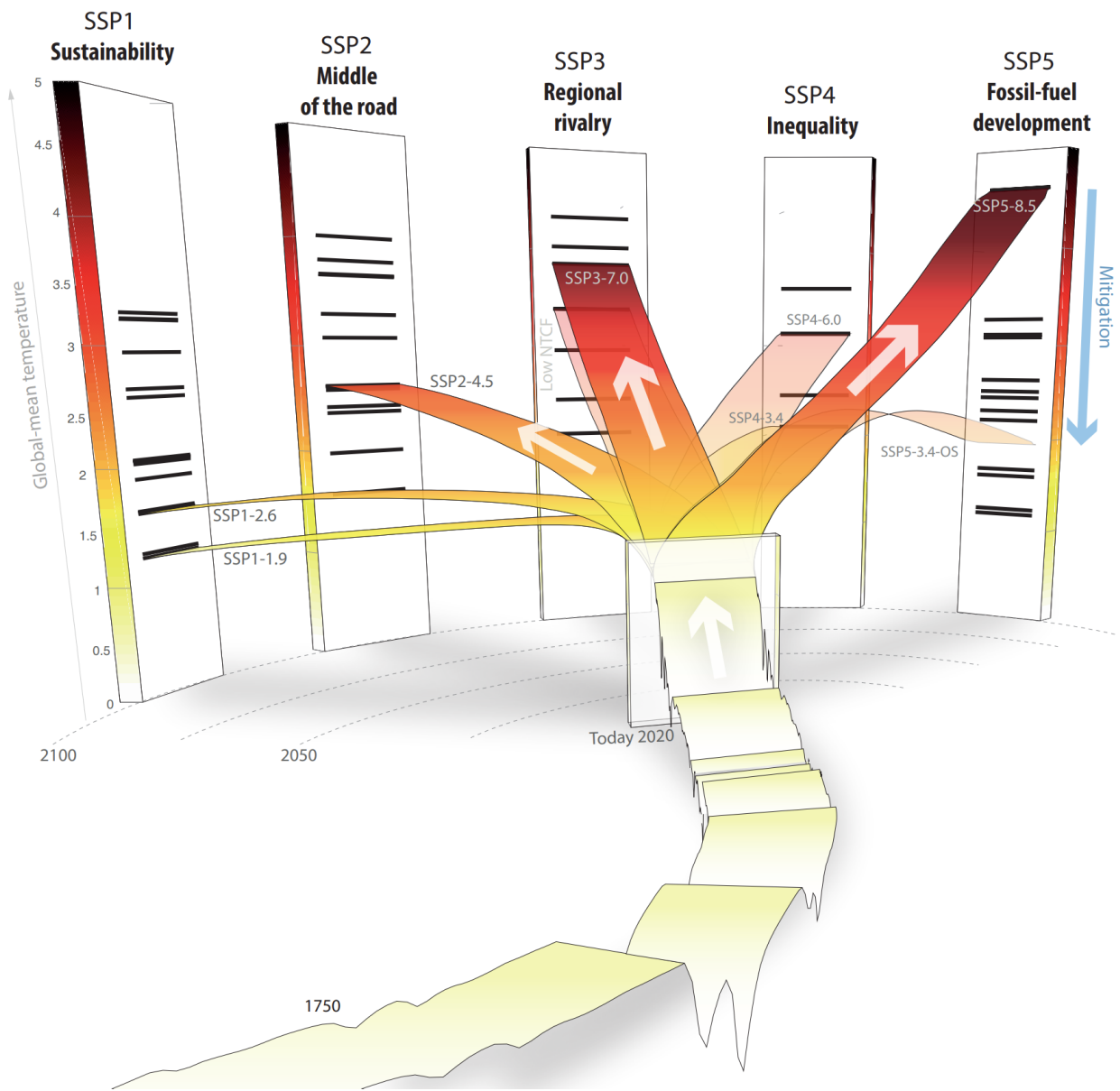


Figure 4.4 SSP scenarios and their five SSP families (Meinshausen et al. 2020)

The CMIP6 models reveal an approximately 6°C temperature increase and an increase of 10–30% precipitation over the US under the high emission scenario of SSP5–8.5 by the end of the century, which is considered the extreme scenario (Almazroui et al. 2021). The consideration of the increased intensity and frequency of extreme precipitation due to extreme weather is an important aspect of the design of future infrastructure as well as the stability analysis of existing infrastructure.

Robinson et al. (2017) conducted a study to examine how future excessive precipitation will affect landslides in a region close to Seattle, Washington, in the United States. The CMIP5 climate dataset was utilized to generate a collection of current and future intensity–duration–frequency (IDF) curves. Though the analysis focused on a specific emission scenario and intensity duration, the findings of their research suggest that the projected climate conditions in the future may have detrimental consequences for future landslides. Additionally, relying solely on historical climate data in design could result in underestimating the potential risks involved (Robinson et al. 2017). Researchers have examined the impact of extreme weather on the stability of embankments. The previous work was conducted using the CMIP5 climate dataset, and the climate data were updated to incorporate the introduced shared socioeconomic pathways in CMIP6.

The impact of increased mean precipitation and extreme precipitation events due to extreme weather on the slope stability of an expansive clay embankment in North Central Texas is presented to develop the framework. Four general circulation models (GCMs) were compared to the climate normals from the National Oceanic and Atmospheric Administration’s National Center for Environmental Information (NOAA NCEI) database to consider the effect of extreme weather. Historical and future precipitation data for 30 years of the location were considered in the study for the climate ensemble. A combination of finite-element-based software, SEEP/W, and limit-equilibrium-approach-based software, SLOPE/W, was used to quantify the stability of the slope in terms of the factor of safety. The FOS of the embankment slope under baseline and future precipitation were analyzed and compared. The impact of fissures and cracks was assessed by utilizing the soil water characteristic curve (SWCC) and hydraulic conductivity function, which incorporates an elevated saturated coefficient of permeability to accurately simulate the surface layer conditions in the in-situ condition. The study presents a framework to effectively quantify the effect of increased precipitation due to extreme weather on the existing embankment infrastructure. This study also presents a pioneering study of climatic impact on the short-term failure of embankments of expansive soils using the CMIP6 climate dataset, as most of the assessments of the impact of extreme weather on existing infrastructure were conducted using the previous CMIP5 dataset.

4.3 Climate Data

4.3.1 Historical Climate Data

Baseline climate (BC) is considered the datum for the extreme weather impact assessment for this study. Historical precipitation was used to establish climate model prediction suitable for the location. The 30 years of precipitation data between 1981-2010 was considered in the study as the baseline precipitation. The baseline data for the comparison with four General Circulation Models (GCMs) are collected from NASA Earth Exchange Global Daily Downscaled Projections (NEX–GDDP) data repository. The observed climate normal data was collected from the NOAA NCEI database for the nearest meteorological station of the study location. The rainfall and mean air temperature data with the daily temporal resolution are shown in Figure 4.5. The comparison of average daily rainfall for each month with the observed climate normals was conducted as shown in Table 4.1. Root Mean Square Error (RMSE) is a metric used to evaluate the precision of predicted values in relation to the true value. Regression analysis is a statistical technique used to effectively summarize observed data. The coefficient of determination, also known as the R^2 -value, quantifies the degree of correlation between two variables. From Table 4.1, it can be interpreted that some of the GCMs are better suited for some parameters used for comparison. Though the R^2 -value of the data from GFDL ESM4 is not the lowest, it has the lowest root mean square error (RMSE) and low average annual precipitation error. The CESM2 dataset has a very high percentage of annual precipitation error. Chai and Draxler (2014) showed the use of RMSE for the comparison of climate models. The data from the Geophysical Fluid Dynamics Laboratory (GFDL), USA was selected to predict the future climate data. From Figure 4.5, it can be observed that the average annual precipitation has been 903.8 mm for over 30 years. Daily precipitation of 40 mm or higher is

considered a heavy precipitation event in this study. As shown in Figure 4.5, over 30 years, there have been 48 days with 40 mm or more daily precipitation. In September 1999, 74.6 mm of precipitation per day was the highest amount ever recorded in the period.

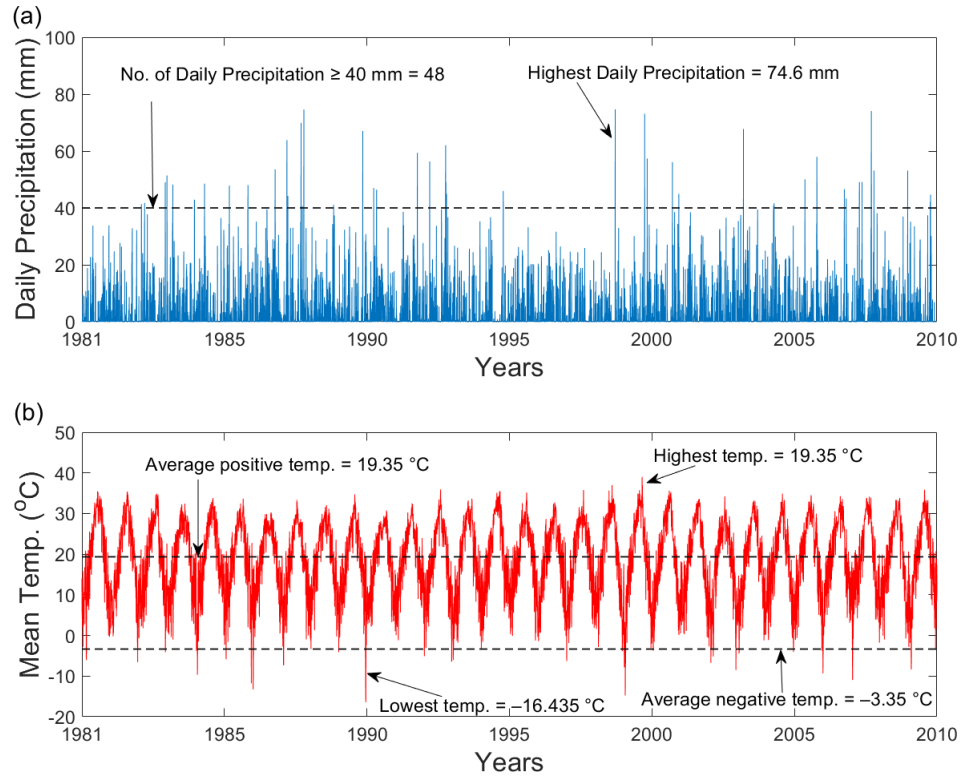


Figure 4.5 Baseline climatic conditions between 1981 and 2010: (a) daily precipitation, (b) daily mean temperature

Table 4.1 Comparison of different GCMs in relation to baseline climate

GCM	Modeling Center	RMSE (mm) *	R ²	Percentage Error (Annual)
CESM2	National Center for Atmospheric Research, USA	14.81	0.83	15.26
ACCESS CM2	Australian Community Climate and Earth System Simulator, Australia	13.51	0.73	9.21
GFDL ESM4	Geophysical Fluid Dynamics Laboratory (GFDL), USA	12.68	0.77	8.50
CanESM5	Canadian Centre for Climate Modelling and Analysis, Canada	13.63	0.64	7.69

* RMSE—root-mean-square error.

4.3.2 Future Climate Dataset

The future climate (FC) data for the site location in Texas was collected from the NASA NEX-GDDP (Thrasher et al. 2022). Considering the inherent constraints of extreme weather models, it is crucial to implement bias adjustment when applying them at the local level. These models, which work at large

scales, often fail to accurately capture local climatic variations, leading to systematic inaccuracies or biases. Improving model accuracy by aligning model outputs with observed local climate data through bias correction is essential for making well-informed decisions. Nevertheless, the implementation of this method necessitates prudence in order to prevent the introduction of additional errors. Although bias correction enhances the accuracy of local climate model estimates, it is unable to entirely eradicate all forms of uncertainty (Giorgi and Gao 2018). Downscaling techniques are utilized to tackle the low spatial resolution data obtained from Global Climate Models. The NEX GDDP dataset includes downscaled, bias-corrected climate scenarios from the General Circulation Models (GCMs) in $0.25^\circ \times 0.25^\circ$ resolution (Thrasher et al. 2022). The data from the GFDL ESM4 model was collected for two socio-economic pathways (SSPs), SSP2-4.5, and SSP5-8.5, and two different periods, 2031-2060 and 2071-2100. The daily precipitation data for these SSPs and periods are shown in Figure 4.6. Shared Socioeconomic Pathways (SSPs) are a collection of scenarios created to illustrate possible future changes in human society. These transformations may be influenced by factors such as population expansion, economic progress, technological breakthroughs, and other similar factors. SSPs play a crucial role in predicting future levels of greenhouse gas emissions and their effects on extreme weather. The Earth's energy budget imbalance resulting from variations in greenhouse gas concentrations in the atmosphere is categorized into five specific levels of radiative forcing. In SSP2, Environmental systems undergo degradation, although with some improvements, and overall witness a decrease in the intensity of resource and energy utilization. The SSP5-8.5 scenario predicts that there will be high levels of greenhouse gas emissions and insufficient efforts to mitigate extreme weather. This will lead to a global temperature increase of 4–6 °C above pre-industrial levels by the end of the century. The scenario also predicts a peak radiative forcing of 8.5 W/m² before a subsequent decrease (Richter and Tokinaga 2020). It can be observed from Figure 4.6 a & b that for SSP2-4.5 the number of extreme precipitation events does not increase with time.

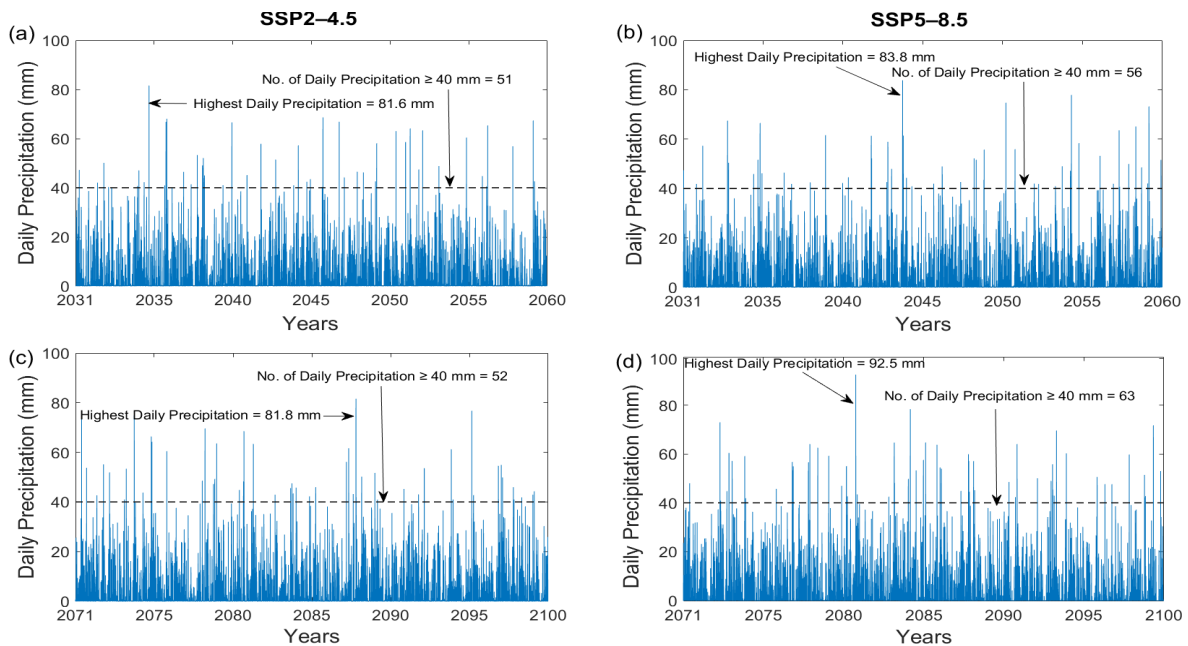


Figure 4.6 Modeled future daily precipitation from GFDL ESM4 dataset: (a) SSP2-4.5 2031–2060, (b) SSP5-8.5 2031–2060, (c) SSP2-4.5 2071–2100, and (d) SSP5-8.5 2071–2100

4.3.3 Extreme Events

For most of the climate data repository, the data are often limited to daily resolution, but the intensity of precipitation can fluctuate from minutes to hours. The precipitation data resolution for NEX GDDP was daily. The historical extreme precipitation events were compared to the DDF curves to address the effects

of the temporal resolution of precipitation and more plausible resolutions were chosen. An intensity–duration–frequency curve was converted to a DDF curve for a selected period. The DDF curve for the embankment location is shown in Figure 4.7 and was obtained from the National Oceanic and Atmospheric Administration (NOAA) Atlas 14. As the 30-year climatic ensemble is considered for the study, the return period of the extreme precipitation for the highest rainfall is considered to be 30 years and the duration of the event is estimated using the DDF curve.

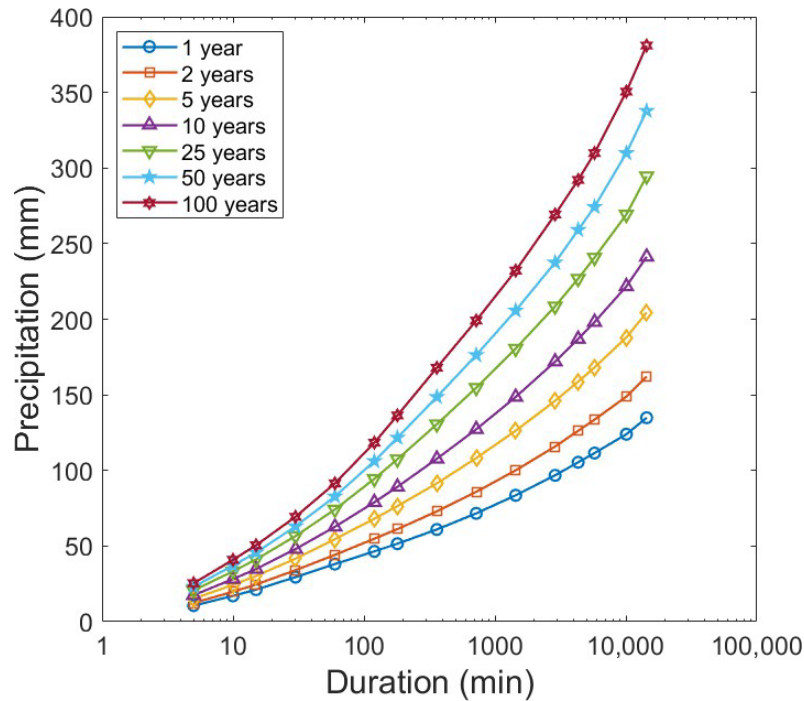


Figure 4.7 Depth–duration–frequency curves for the site

4.4 Numerical Modeling and Analysis

4.4.1 Soil Properties

Most of the soil data was obtained from various experiments and studies conducted by the authors and their research groups. The SWCC data of the soil are presented in Figure 4.8. The SWCC was determined using the filter paper method and a chilled mirror hygrometer. The closed-form solution proposed by the Fredlund–Xing (FX) (1994) model was used as shown below to fit the experimental data into the SWCC curve (Fredlund and Xing 1994). The hydraulic conductivity and volumetric water content in unsaturated soils are dependent on matric suction. The air entry value (AEV) is the critical suction at which soil starts to lose moisture with increasing desaturation. AEV is dependent on the pore spaces and pore structure within the soil. The AEV of this soil at its maximum dry density was determined to be 10 kPa. The saturated volumetric water content and residual volumetric water content were computed to be 0.441 and 0.08, respectively. The unsaturated hydraulic conductivity of the soil was determined based on experimental studies conducted on a modified suction-controlled permeability setup. The soil sample was maintained at a specific suction state, while the hydraulic conductivity was measured after equilibration. The steps were repeated for different suction levels, and the HCF of the soil used in this study is shown in Figure 4.9. Table 4.2 shows the soil properties used in the study. For compacted core soil, shear strength parameters were measured using a direct shear test, and a torsional ring shear test was used for the strength parameters of the surface layer.

$$\theta_w = C(\psi)\theta_s \left[\frac{1}{\ln \left\{ e + \left(\frac{\psi}{a} \right)^n \right\}} \right]^m \quad (4.1)$$

where θ_w , θ_s , and θ_r are natural, saturated, and residual volumetric water content, respectively, ψ is matric suction, and a , n , and m are the curve fitting parameters. The hydraulic conductivity function from the data in Figure 4.8 was fitted using the van Genuchten (1980) model, as shown below (van Genuchten 1980).

$$K(h) = K_s S_e^l [1 - (1 - S_e^{l/m})^m]^2 \quad (4.2)$$

where K_s is saturated hydraulic conductivity, l is the pore conductivity parameter, S_e is effective saturation, and m represents the curve fitting parameter. Some of the material properties for this study were collected from experiments conducted in several studies (Acharya et al. 2017; Dronamraju 2008; McCleskey et al. 2008).

Table 4.2 Soil properties used in the study

Region	Soil Property	Value
Compacted fill / Surface layer	Dry unit weight (kN/m ³)	16.5
Compacted fill soil	Saturated Coefficient of Permeability, k_s (m/s)	8.1×10^{-8}
	Cohesion, c (kPa)	38
	Angle of internal friction, ϕ (°)	17
Surface layer (desiccated soil)	Saturated Coefficient of Permeability, k_s (m/s)	8×10^{-5}
	Cohesion, c (kPa)	0
	Angle of internal friction, ϕ (°)	27

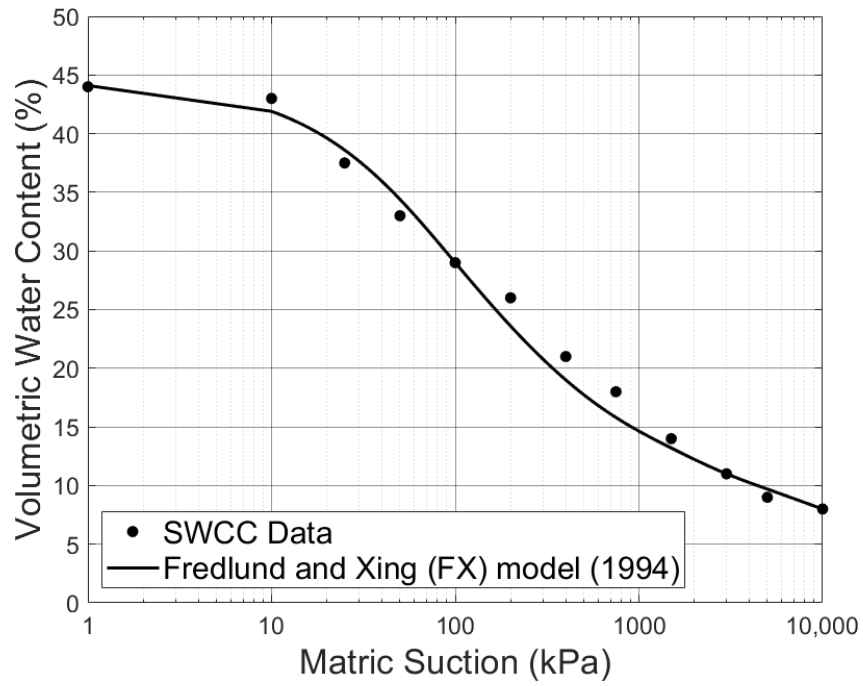


Figure 4.8 Soil-water characteristics curve of the soil plotted using the FX model (Fredlund and Xing 1994).

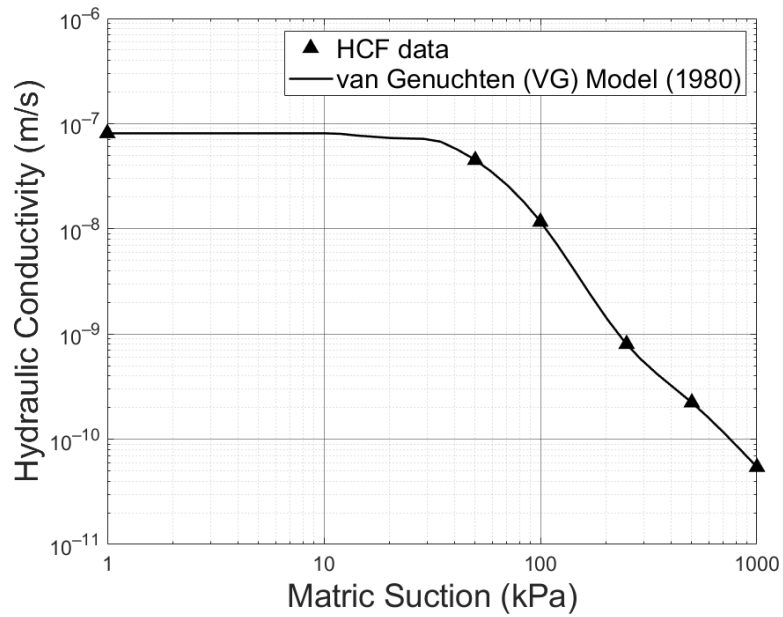


Figure 4.9 Hydraulic conductivity function of soil plotted using VG model (van Genuchten 1980)

4.4.2 Geometry of the Section

In this study, the steepest part of an embankment of expansive soil was considered for analysis. The cross-section of the slope with a steepness of 2.5 H:1 V is shown in Figure 4.10. The embankment has two parts: compacted fill soil and surface layer. The surface layer thickness of the slope is 1.1 m (3.6 ft). The slope has a height of 8.54 m (28 ft), and the ground water table is situated at 8 m on the right side and 4 m on the left side above the base of the embankment. A mesh convergence study was conducted on the embankment section with a non-fissured surface layer to obtain an optimum mesh size suitable for the study. The change in the factor of safety (FOS) with mesh size was considered. Based on the mesh convergence study, a mesh size of 0.8 m was considered for the analysis. The mesh structure of the embankment is illustrated in Figure 4.10. For better modeling of the fissured surface layer and estimation of flow through the surface layer, the surface layer of 1.1 m is modeled with four layers of finer mesh. The finite element analysis (FEA) model is scaled up in both the horizontal and vertical dimensions to prevent the influence of boundary conditions. The bottom boundary is considered to be rigid with no permissible movement in either direction, while the two lateral boundaries are free to move only vertically. The desiccated layer is considered for the 3 m wide shoulder provided at the top of the embankment.

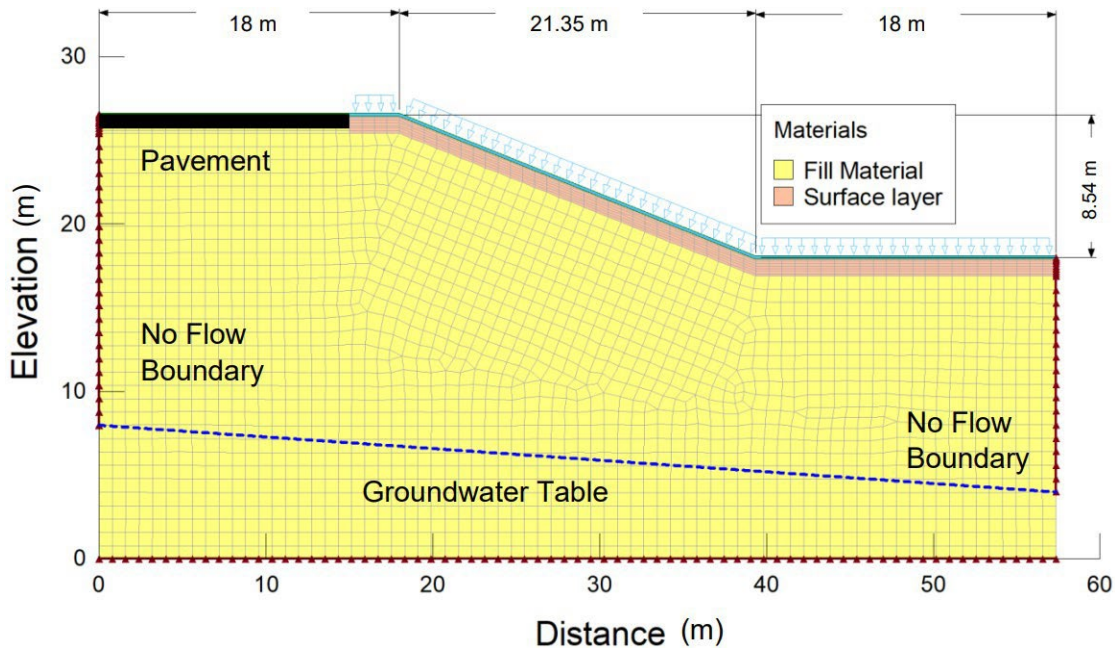


Figure 4.10 Profile and mesh structure of the embankment

4.4.3 Numerical Modeling of Unsaturated Soil

A finite element transient variably saturated seepage analysis was performed using SEEP/W software to model the temporal and spatial distribution of pore water pressures within the embankments. The soil material model was considered to be in a saturated or unsaturated state to account for all types of soil characteristics. The flow through the soil in both saturated and unsaturated conditions was simulated in Geo-slope GeoStudio SEEP/W 2023.1.1 using Darcy's law. In unsaturated conditions, the changing hydraulic conductivity with matric suction or degree of saturation was considered by using the HCF curve from Figure 4.9. The partial differential equation that governs the calculation of flux for 2D transient flow is shown below:

$$\frac{\partial}{\partial x} \left(k_x \frac{\partial H}{\partial x} \right) + \frac{\partial}{\partial y} \left(k_y \frac{\partial H}{\partial y} \right) + Q = m_w \gamma_w \frac{\partial H}{\partial t} \quad (4.3)$$

where H is the total hydraulic head, k_x and k_y are the coefficient of permeability in the x (horizontal) and y (vertical) direction, respectively, Q is the boundary flux, and m_w is the storage curve slope.

In SEEP/W, Richard's (1931) equation was employed to accurately estimate the effect of unsaturated flow. The equation for 2D flow through pores can be written as follows (Richards 1931):

$$K \frac{\partial \theta}{\partial t} = \frac{\partial}{\partial x_i} \left[K \left(K_{ij}^A \frac{\partial h}{\partial x_i} + K_{iz}^A \right) \right] - S \quad (4.4)$$

where h is the pressure head in the soil, θ is the volumetric water content, S represents the sink term, x_i are the coordinates, K_{ij}^A is the anisotropy tensor, and K is the hydraulic conductivity function.

The boundary conditions are illustrated in Figure 4.10. The flux boundary was used to simulate the intensity of rainfall and duration and applied on the slope. The top portion of the slope is impermeable considering the presence of the pavement. No flow boundaries were considered on either the right or left side above the groundwater table and the base of the profile was considered the no-flow boundary. The flux boundary for the precipitation was considered to be in a non-ponding condition; this prevented the accumulation of rainfall on the slope of the embankment.

At each time step of 0.5 h, SEEP/W simulated the seepage conditions, and that pore water pressure was used for the limit-equilibrium-based software, SLOPE/W 2023.1.1 analysis, which uses the Morgenstern–Price (1965) method to determine the factor of safety (FOS) of the slope (Morgenstern and Price 1965). The seepage conditions were imported from SEEP/W using a similar grid technique. The unsaturated shear strength was determined using the GeoStudio SLOPE/W program, which utilizes the extended Mohr-Coulomb failure model. This model provides two methods to incorporate the influence of matric suction on the shear strength of the soil. The unsaturated shear strength is determined using two independent stress variables: the net normal stress and the matric suction. The method proposed was used to consider the unsaturated shear strength (Vanapalli et al. 1996). This method can be expressed as:

$$\tau = c' + (\sigma_n - u_a) \tan \phi' + (u_a - u_w) \left[\left(\frac{\theta_w - \theta_r}{\theta_s - \theta_r} \right) \tan \phi' \right] \quad (4.5)$$

where τ represents the unsaturated shear strength, c' is the effective cohesion, σ_n represents the total stress, ϕ' is the effective angle of internal friction, $(\sigma_n - u_a)$ is the net normal stress, and $(u_a - u_w)$ is the matric suction. The strength due to suction was incorporated into the limit equilibrium (LE) method employed by SLOPE/W. The factor of safety from the coupled hydro-geotechnical model obtained through the integration of the FE and LE methods was used as the indicator of the stability of the slope.

4.4.4 Results and Discussion

The impact of the changing climate on the embankment was evaluated with a variation of FOS from slope stability analysis conducted by coupled hydro-geotechnical modeling. Precipitation, among all other climatic parameters, has the most short-term destabilizing effect. As the embankment was built with expansive soil, due to swelling–shrinkage properties, desiccation cracks were found to occur. From the field data collected from the literature, the depth of the desiccated layer was 1.1 m. Considering the extreme events and the effect of drought, the coefficient of permeability was considered to be significantly higher by magnitude, as shown in Table 4.2. Due to rainfall infiltration, the desiccated zone

parallel to the slope became saturated. For all cases, the slope was considered to have a desiccated surface.

The FOS results from SLOPE/W for the embankment for historical precipitation are shown in Figure 4.11. Figures 4.12 and 4.13 illustrate FOS with pore water pressure distribution for SSP2-4.5 and SSP5-8.5, respectively. The reduction in FOS can be seen in FC scenarios compared to the historical climate data. Due to the increased precipitation intensity and coefficient of permeability of the surface layer, the FOS decreased further for extreme events. The FOS continuously decreased with the increasing intensity of precipitation, which was due to the reduction in the matric suction. In the “middle of the road” scenario, SSP2, the maximum rainfall intensity and the number of extreme precipitations does not increase significantly from the middle of the century to the end of the century. Thus, the change in FOS for the scenario with time is much less. However, for the higher gas emission scenario, SSP5–8.5, the decrease is significant at the end of the century as the number of extreme precipitation events and maximum daily precipitation both increase, which also increases the duration of future design storms significantly. The reduction in FOS for SSP5–8.5 compared to the historical climate was found to be 19.5%. Figure 4.11 also shows the variation in PWP in the surface layer of the slope for historical precipitation. The higher PWP in the desiccated layer can be observed for extreme precipitation events. From the pore water pressure distributions for extreme events, the accumulation of percolated water between the desiccated layer and the non-desiccated layer can be observed. The intense precipitation and the difference between the coefficient of permeability may be the reason behind this accumulation. From Figures 4.11 to 4.13, it can be observed that with an increase in the intensity of precipitation and duration of the event, the accumulation of percolated water between the desiccated layer and the non-desiccated layer increased. This may have facilitated the continued surficial failure.

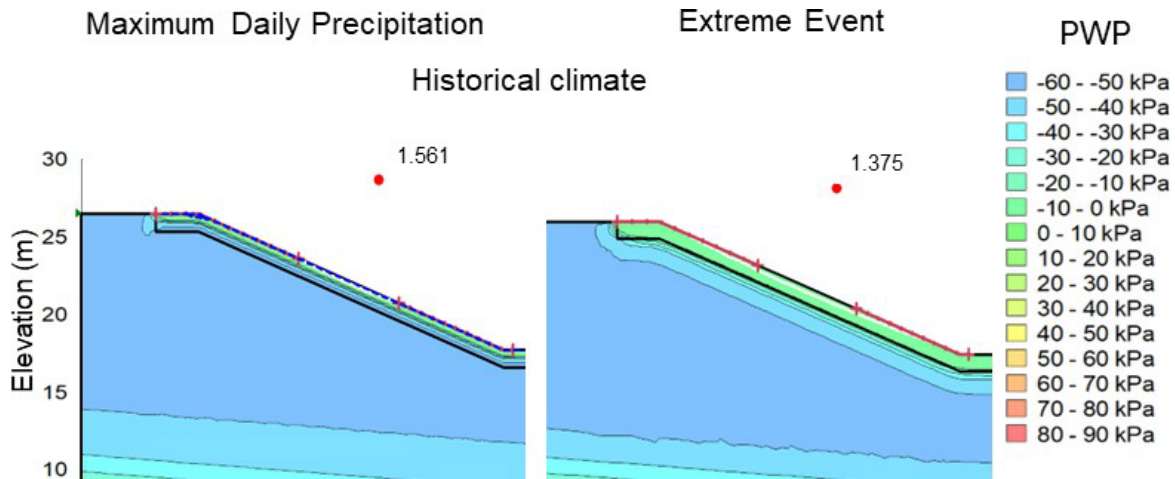


Figure 4.11 FOS with PWP distribution at the end of the precipitation event for the different scenarios for historical data

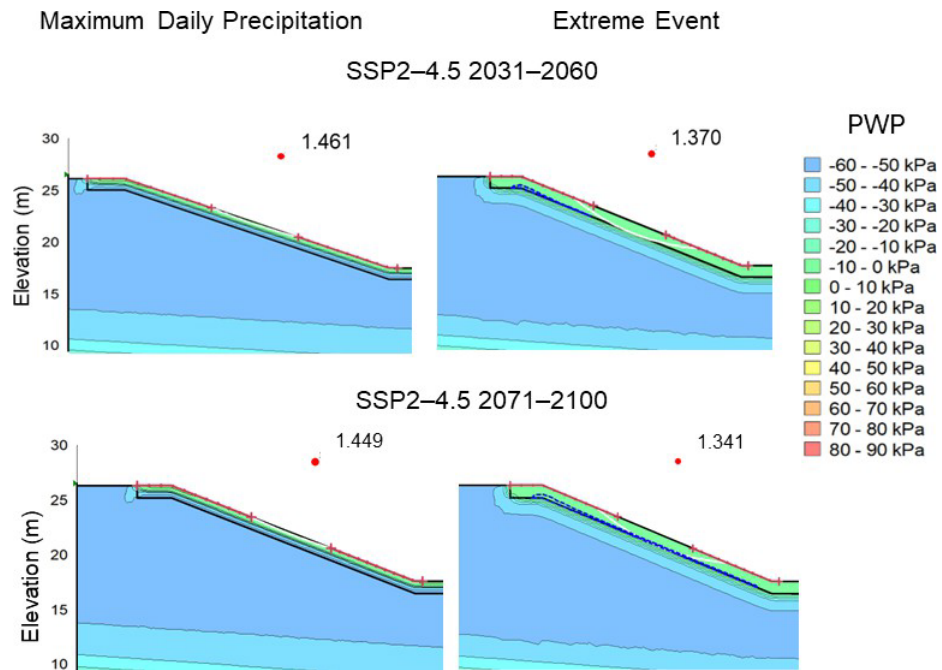


Figure 4.12 FOS with PWP distribution at the end of the precipitation event for the different scenarios in the future for SSP2-4.5

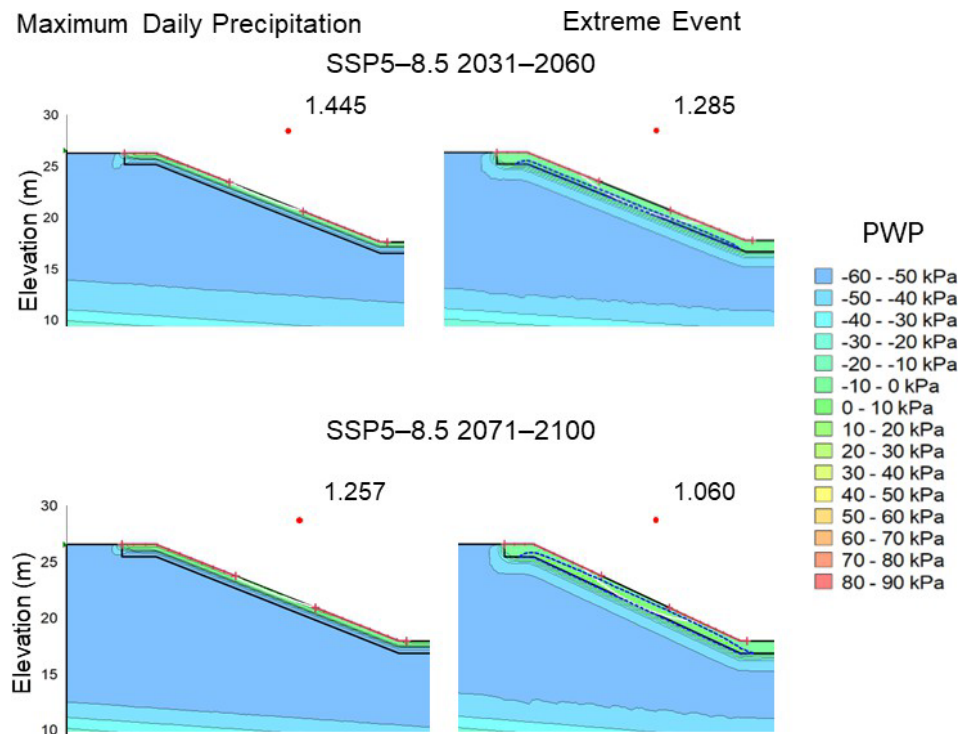


Figure 4.13 FOS with PWP distribution at the end of the precipitation event for the different scenarios in the future for SSP5-8.5

The effect of extreme weather was estimated using transient seepage and slope stability analysis. The

factor of safety of the slope was determined for each step with an interval of 30 min for a 24-hour precipitation event. The degradation of FOS with time is shown in Figure 4.14. The reduction in the matric suction of the soil due to rainfall could have been attributed to the reduction in the stability of the slope.

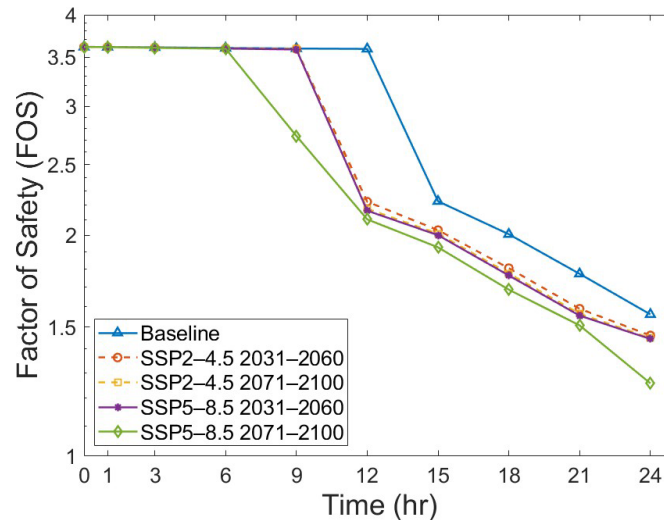


Figure 4.14 Change in FOS with temporal variations for 24 h precipitation for the baseline and future climate

It can be observed that, initially, the FOS was more than 3.5 and the value was stable for the initial hours for every scenario. With time, rainwater permeated further inside the embankment and reduced the matric suction, which eventually decreased the unsaturated shear strength. The intense rainfall generated high pore water pressure early in the surface layer. The infiltration of rainfall in the desiccated layer caused the rapid degradation of FOS with time, mostly after 12 hours of rainfall. The accumulation of water between the two layers discussed earlier could be the reason behind this rapid degradation of the stability of the slope.

4.5 Summary

In this study, the impact of changing climate on the stability of earth embankments built with expansive soil was numerically analyzed. The focus of the study was to investigate the effect of the change in precipitation imparted due to extreme weather and the formation of desiccated layers due to the swell–shrink characteristics of the soil. The important observations of the study are as follows:

- Slopes built with expansive soil tend to form desiccation cracks due to swelling and shrinkage with climatic interactions. In the study, the stability of the slope was found to be reduced due to the formation of the desiccated surface layer.
- A 23% increase in the maximum daily precipitation and a 31.25% increase in the number of extreme precipitation events for SSP5 at the end of the century compared to historical precipitation between 1981 and 2010 was observed. In the future, the intensity of precipitation is predicted to be higher, with shorter intervals between the occurrence of extreme precipitation events.
- The stability analysis of the slope was conducted for two different SSPs: one with moderate greenhouse gas emissions and the other one with extreme GHG emissions with no emission control. The stability of the slope was predicted to be dependent on the greenhouse gas emission scenarios as it directly impacts the number of extreme precipitation events and the amount of daily precipitation.

- For both scenarios, two 30-year periods from the middle and end of the century were considered. With progress in the future, the FOS of the slope was predicted to be lower, and this reduction was significant for the extreme GHG emission scenario. The possibility of surficial failure was predicted to increase significantly for extreme events.

The influence of SSP5, which is an extreme scenario, on the precipitation intensity may be significant enough to induce the surficial surface of slopes with a desiccated top layer for other earthen embankments as well. Additional studies need to be conducted to understand the impact of other parameters such as temperature and solar radiation for different scenarios of extreme weather to quantify the potential impact of extreme weather on the resilience of earthen structures in different regions. Subsequently, sustainable measures need to be investigated and implemented to mitigate such issues by the end of the century. The incorporation of thermal and environmental stresses caused by extreme weather should be considered in the design of new structures, as such change is expected to have a negative impact on earthen infrastructures like dams, levees, and pavements throughout their lifespan.

5. NUMERICAL ANALYSIS OF THE IMPACT OF EXTREME WEATHER ON EXPANSIVE SOIL EMBANKMENT IN SOUTH DAKOTA

5.1 Location of Interest

An embankment section from Central South Dakota is considered in the study of the impact of increased precipitation induced by extreme weather. The embankment is considered to be built on highly plastic clay (CH) soil.

5.2 Soil Properties

The soil properties used to model the embankment were tested. The SWCC data of the soil is presented in Figure 5.1. The SWCC in the drying curve was determined using Hyprop 2 and a chilled mirror hygrometer as shown in Figure 5.2. The Hyprop was used for suction between 0 – 1500 kPa and high suction at the dry side was determined using WP4C, chilled mirror hygrometer. The closed-form solution proposed by the Fredlund–Xing (FX) (1994) model was used as shown below to fit the experimental data into the SWCC curve (Fredlund and Xing 1994). The hydraulic conductivity and volumetric water content in unsaturated soils are dependent on matric suction. The air entry value (AEV) is the critical suction at which soil starts to lose moisture with increasing desaturation. The AEV of this soil at its maximum dry density was determined to be 9 kPa. The saturated volumetric water content and residual volumetric water content were computed to be 0.585 and 0.1, respectively. The unsaturated hydraulic conductivity of the soil was determined based on experimental studies conducted on the Hyprop 2 setup shown in Figure 5.3. The soil sample was maintained at a specific suction state, while the hydraulic conductivity was measured after equilibration. The steps were repeated for different suction levels, and the HCF of the soil used in this study is shown in Figure 5.3. Table 5.1 shows the soil properties used in the study. For compacted core soil, shear strength parameters were measured using a direct shear test, and the fully softened shear strength characteristics were used for the strength parameters of the surface layer.

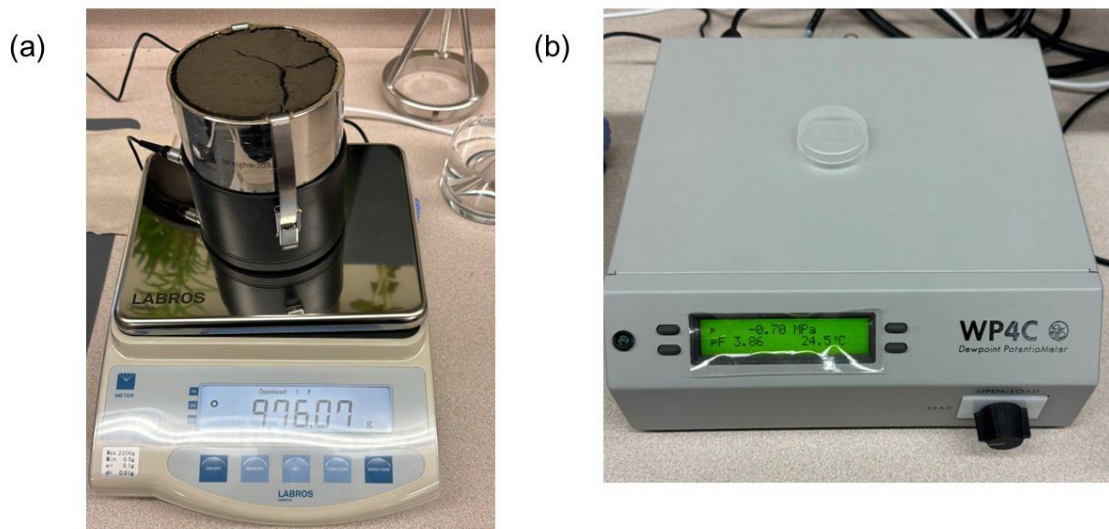


Figure 5.1 (a) Hyprop, (b) WP4C setup for SWCC and HCF determination

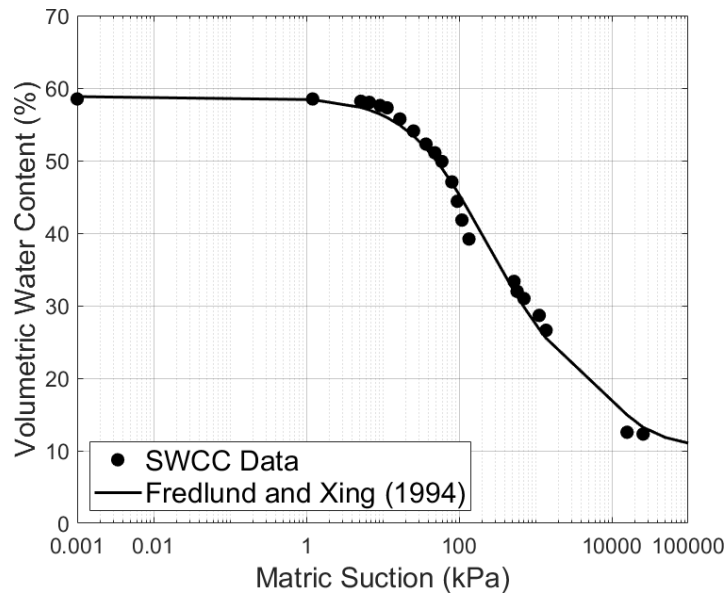


Figure 5.2 Soil-Water Characteristics Curve of soil collected from Jones County

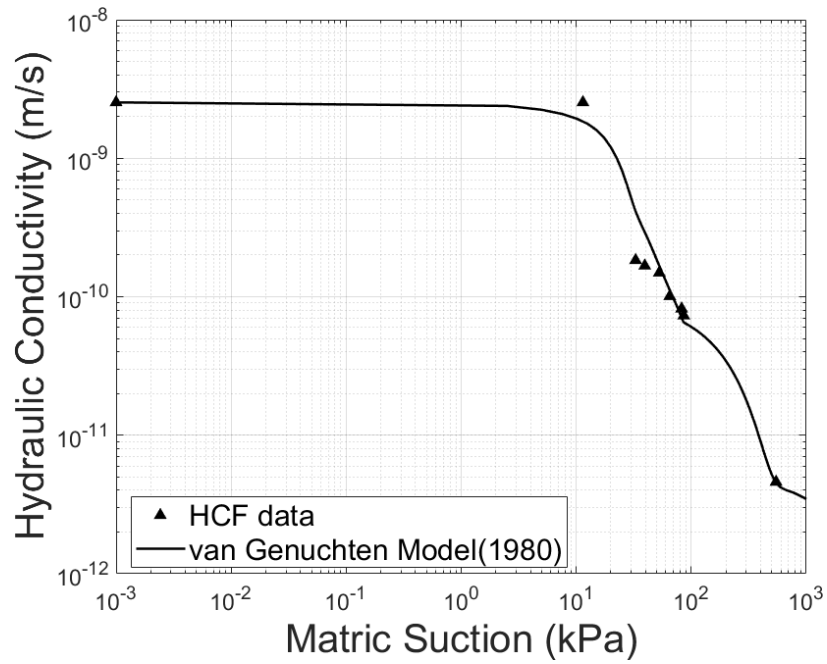


Figure 5.3 Hydraulic Conductivity Function Curve of soil collected from Jones County

Table 5.1 Soil properties used for the numerical study

Region	Soil Property	Value
Compacted fill / Surface layer	Dry unit weight (kN/m ³)	14.8
Compacted fill soil	Saturated Coefficient of Permeability, k_s (m/s)	2.53×10^{-9}
	Cohesion, c (kPa)	39.7
	Angle of internal friction, ϕ (°)	9.6
Surface layer (desiccated soil)	Saturated Coefficient of Permeability, k_s (m/s)	2.5×10^{-6}
	Cohesion, c (kPa)	0
	Angle of internal friction, ϕ (°)	20.4

5.3 Geometry of the Slope

In this study, a part of an embankment slope of expansive soil in central South Dakota was considered for analysis. The cross-section of the slope with a steepness of 2.4 H:1 V is shown in Figure 5.4. The embankment has two parts: compacted fill soil and surface layer. The surface layer thickness of the slope is 1.1 m (3.6 ft). The groundwater table (GWT) was considered to be high as the precipitation pattern has consecutive rainfall events. A mesh size of 0.75 m was considered for the analysis. The mesh structure of the embankment is illustrated in Figure 5.4. For better modeling of the fissured surface layer and estimation of flow through the surface layer, the surface layer of 1.1 m is modeled with four layers of finer mesh. The finite element analysis (FEA) model is scaled up in both the horizontal and vertical dimensions to prevent the influence of boundary conditions. The bottom boundary is considered to be rigid with no permissible movement in either direction, while the two lateral boundaries are free to move only vertically. The desiccated layer is considered for the 3 m wide shoulder provided at the top of the embankment.

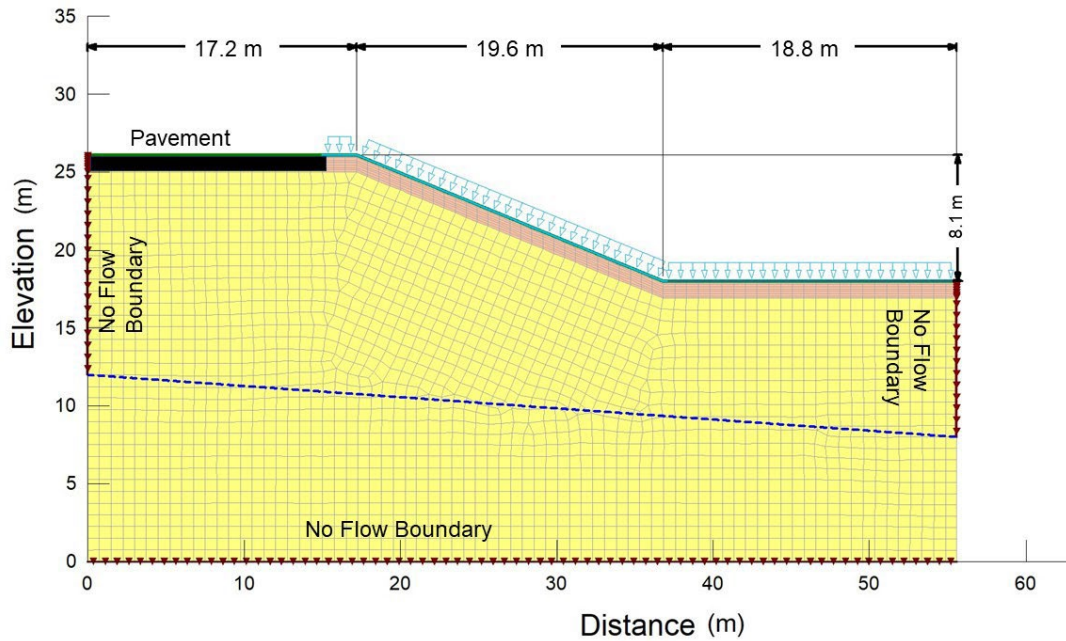


Figure 5.4 Mesh structure of the slope for the study

5.4 Climate Dataset

5.4.1 Baseline Climate

The 30 years of precipitation data between 1981-2010 was considered as baseline precipitation to study the effect of extreme weather. The baseline data for the comparison with five General Circulation Models (GCMs) were collected from NEX-GDDP data respiratory and the observed climate normal data was collected from the NOAA NCEI database for the nearest meteorological station of the study location. The comparison of average daily rainfall for each month with the observed monthly climate normals was conducted as shown in Table 5.2. The data from the Community Earth System Model version 2 (CESM2), USA was selected to predict the future climate data as it was found to have better R^2 , RMSE, and least error in annual precipitation. The annual precipitation was found to be 500.8 mm. In this study, heavy precipitation was considered for the daily precipitation of 40 mm or higher. As shown in Figure 5.5, over 30 years, there have been 6 days with 40 mm or more daily precipitation. In September 2004, 45.86 mm of daily precipitation was the highest amount ever recorded in the period. The daily precipitation and mean air temperature are shown in Figure 5.5.

Table 5.2 Comparison of GCMs and NOAA climate normals

GCM	Modeling Center	RMSE (mm) *	R ²	Percentage Error (Annual)
CESM2	National Center for Atmospheric Research, USA	2.96	0.98	1.45
ACCESS CM2	Australian Community Climate and Earth System Simulator, Australia	4.22	0.97	4.65
GFDL ESM4	Geophysical Fluid Dynamics Laboratory (GFDL), USA	5.22	0.96	4.60
CanESM5	Canadian Centre for Climate Modelling and Analysis, Canada	4.60	0.97	4.42
GISS-E2-1-G	NASA Goddard Institute for Space Studies, USA	4.42	0.96	5.41

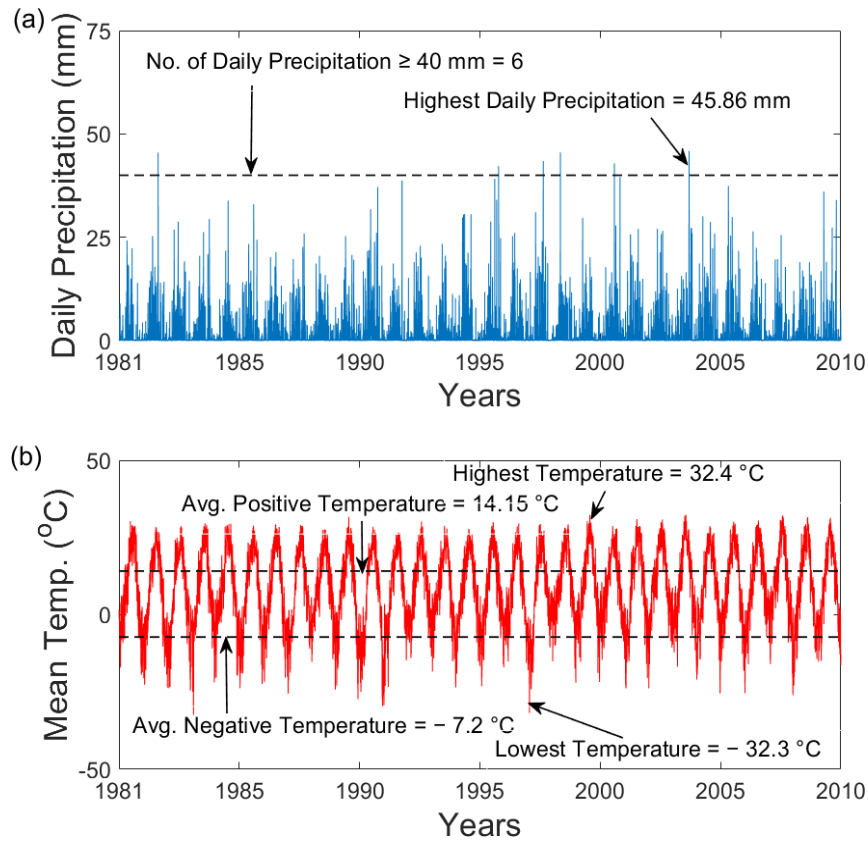


Figure 5.5 Baseline climate data for study location in central South Dakota

5.4.2 Future Precipitation

The downscaled future precipitation dataset was collected from the NEX GDDP for the CESM2 GCM in $0.25^\circ \times 0.25^\circ$ resolution. The data from the CESM2 model was collected for two socio-economic pathways (SSPs), SSP2-4.5, and SSP5-8.5, and two different periods, 2031-2060 and 2071-2100. The daily precipitation data for these SSPs and periods are shown in Figure 5.6. Though the number of extreme precipitation events is less in South Dakota, the number of extreme precipitation events more than doubled for the SSP5-8.5 at the end of the century. The highest daily precipitation also increased by approximately 33% for the condition compared to baseline precipitation.

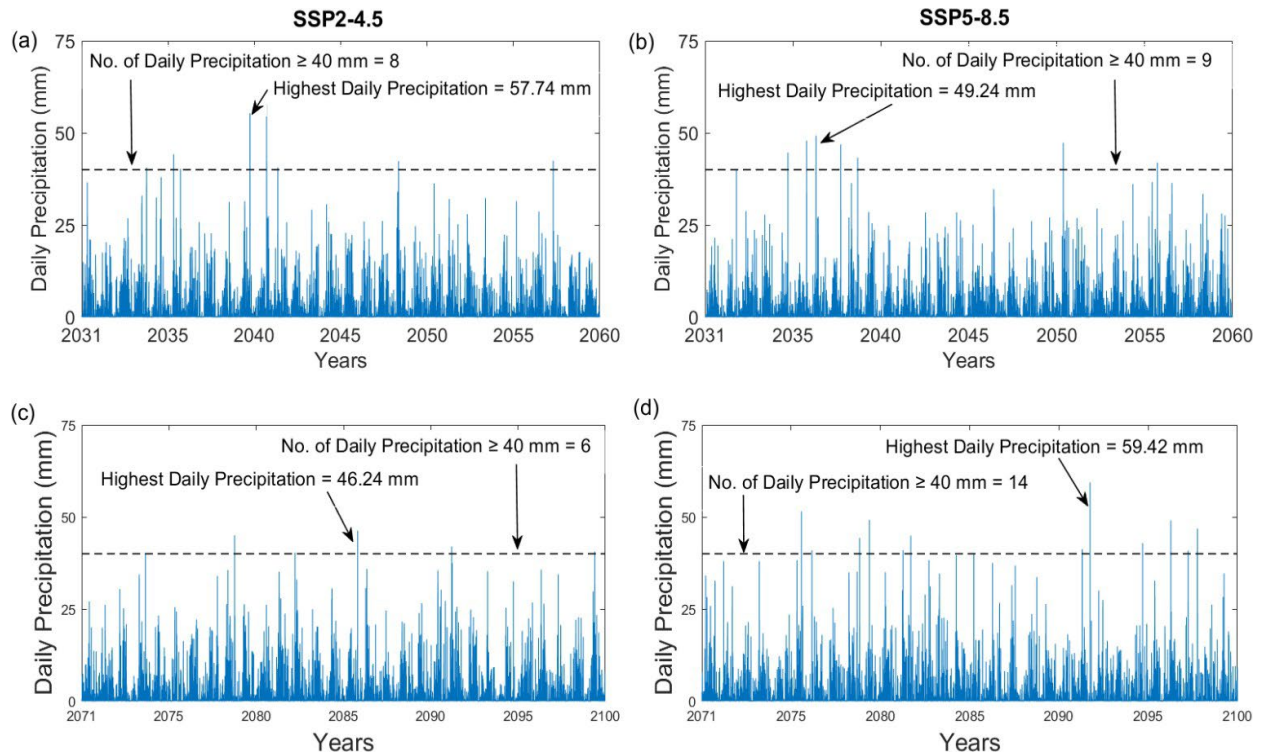


Figure 5.6 Predicted future daily precipitation from CESM2 dataset of the study location in South Dakota: (a) SSP2–4.5 2031–2060, (b) SSP5–8.5 2031–2060, (c) SSP2–4.5 2071–2100, and (d) SSP5–8.5 2071–2100

5.4.3 Extreme Events

The precipitation data resolution collected from NEX GDDP was daily. The historical extreme precipitation events were compared to the depth-duration-frequency curves to address the effects of the temporal resolution of precipitation and more plausible resolutions were chosen. The DDF curve used for baseline and future precipitation was obtained from the National Oceanic and Atmospheric Administration (NOAA) Atlas 14. The 30-year climatic ensemble is considered for the study, the return period of the extreme precipitation for the highest rainfall is considered to be 30 years and the duration of the event is estimated using the DDF curve. The DDF curves for the central South Dakota location are shown in Figure 5.7.

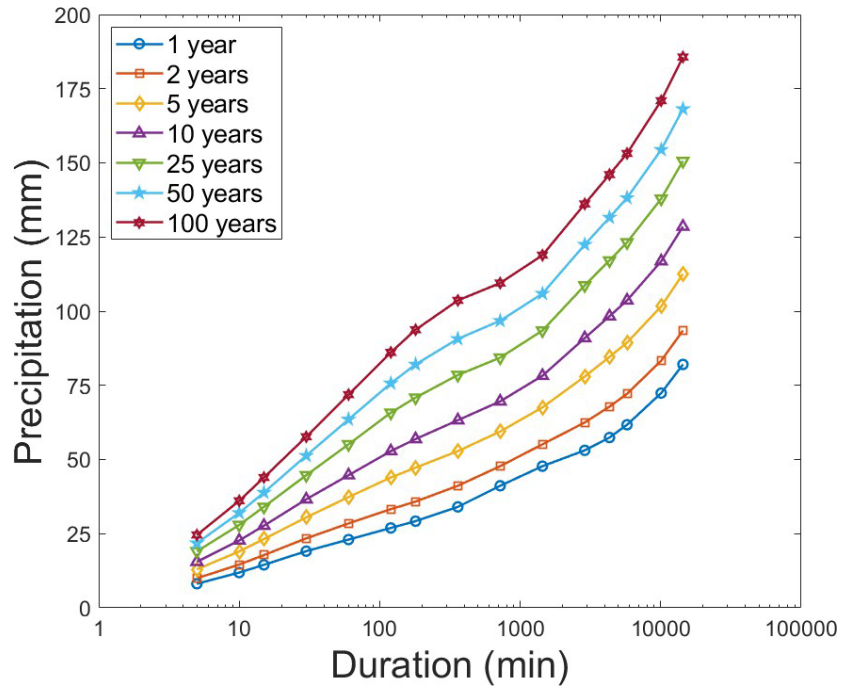


Figure 5.7 Depth–duration–frequency curves for location in South Dakota

5.5 Results and Discussion

The effect of extreme weather on the embankment was evaluated with a variation of FOS from slope stability analysis conducted by coupled hydro-geotechnical modeling. Climatic parameters like precipitation have the most short-term destabilizing effect. As the embankment was built with expansive soil, due to swelling–shrinkage properties, desiccation cracks were found to occur. From the field data collected from the literature, the depth of the desiccated layer was 1.1 m. The desiccated zone parallel to the slope became saturated and caused surficial failure.

The FOS results from SLOPE/W for the embankment for historical precipitation, SSP2, and SSP5 are presented in Table 5.3. The reduction in FOS can be seen in FC scenarios compared to the historical climate. Due to the increased precipitation intensity and coefficient of permeability of the surface layer, the FOS decreased further for extreme events. The FOS continuously decreased with the increasing intensity of precipitation, which was due to the reduction in the matric suction. In SSP2, the maximum rainfall intensity and the number of extreme precipitations decrease from the middle of the century to the end of the century. Thus, the change in FOS for the scenario is less. However, for the higher gas emission scenario, SSP5–8.5, the decrease is significant at the end of the century as the number of extreme precipitation events and maximum daily precipitation both increase, which also increases the duration of future design storms significantly. As the duration of extreme precipitation events for historical and the end-of-century scenarios of SSP2–4.5 are much less, the FOS for extreme events decreased compared to a daily precipitation event. This may have facilitated the continued surficial failure. Figure 5.8 shows the PWP distribution for daily precipitation in the SSP5–8.5 end-of-century scenario.

Table 5.3 Comparison of factor of safety (FOS) for different scenarios

Parameter	Maximum Daily Precipitation	Extreme Event
	Baseline/Historical Precipitation	
Duration of Precipitation	1 day	28 min
FOS	2.54	2.69
SSP2-4.5 2031-2060		
Duration of Precipitation	1 day	85 min
FOS	2.33	1.96
SSP2-4.5 2071-2100		
Duration of Precipitation	1 day	30 min
FOS	2.50	2.54
SSP5-8.5 2031-2060		
Duration of Precipitation	1 day	40 min
FOS	2.47	2.22
SSP5-8.5 2071-2100		
Duration of Precipitation	1 day	90 min
FOS	2.28	1.89

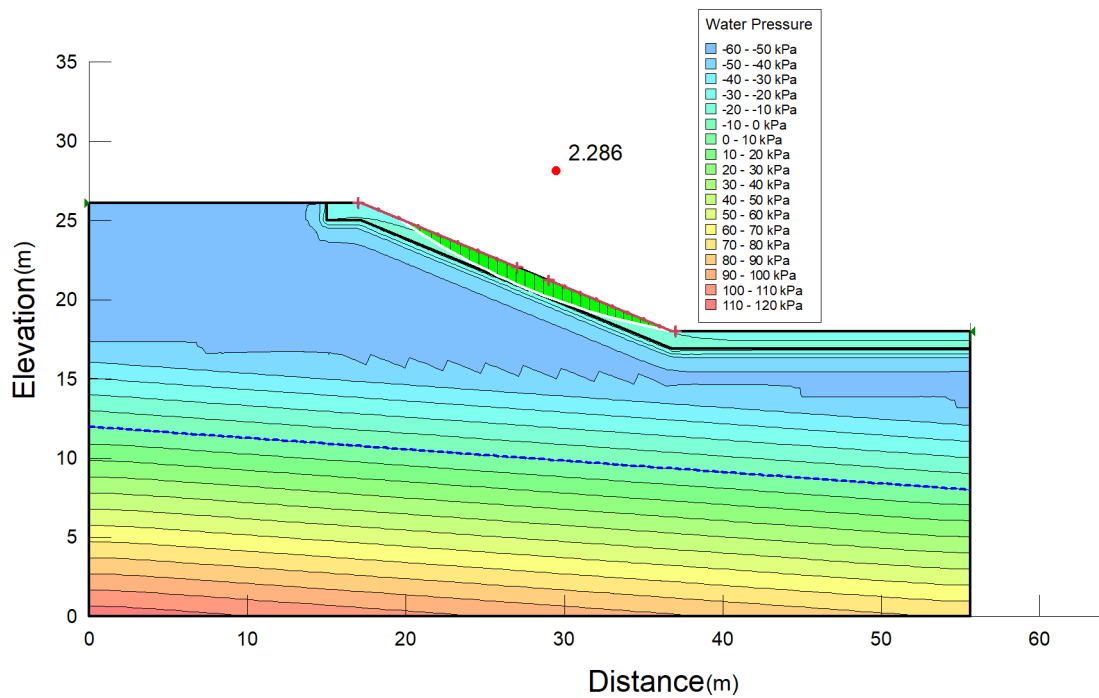


Figure 5.8 PWP distribution of slope under SSP5-8.5 2071-2100 daily precipitation event

5.6 Conclusions

In this study, the effect of change in precipitation due to extreme weather on the slope stability of embankments built with expansive soil in central South Dakota was numerically analyzed. The main focus of the study was to investigate the effect of the change in precipitation on the formation of desiccated layers due to the swell–shrink characteristics of the native soil. The important observations of the study are as follows:

- The stability analysis of the slope was conducted for two different SSPs: one with moderate greenhouse gas emissions (SSP2-4.5) and the other one with extreme GHG emissions with no emission control (SSP5-8.5). The stability of the slope was dependent on the number of extreme precipitation events and the amount of daily precipitation. For SSP2-4.5, rainfall intensity and the number of extreme events were reduced for the end-of-century scenario.
- Due to the exponential increase in the number of extreme events for SSP5-8.5, the FOS was reduced by approximately 30% and the duration of the event increased 3 times compared to baseline climate.

6. PERFORMANCE OF CEMENT- AND BIOPOLYMER-TREATED SULFATE-RICH EXPANSIVE SOIL

6.1 Introduction

The damage caused by volume changes induced by moisture fluctuations in expansive soils have been discussed in Chapter 1. Due to the presence of expansive soils, the parts of the western and southern United States and the Northern Great Plains have faced a multitude of problems involving the civil and transportation infrastructure (Nelson and Miller 1997; Taher et al. 2020). Stabilization of sulfate-rich soils using traditional calcium-based stabilizers like cement and lime leads to sulfate-induced heave due to the formation of an expansive mineral, ettringite. While ordinary Portland cement has many benefits as a soil stabilizer, it also has some disadvantages, especially in terms of its impact on the environment. The biggest concerns are related to CO₂ and NO_x (nitrogen oxides) emissions as well as the production of airborne particulate matter (Chang et al. 2015). Cement used for soil treatment stays in place for a long time because cement mixtures degrade slowly. The presence of cement in the soil has the potential to disturb the ecosystem, resulting in problems like increased pH levels and deterioration of the soil which can lead to desertification (Ayeldeen and Kitazume 2017). Cement stabilization also has other drawbacks, which include brittle failures and susceptibility to low-temperature cracking (Puppala et al. 2003). To address the limitations of traditional stabilizers, bio-geoengineered technologies like microbial-induced calcium precipitation (MICP) and enzyme-induced calcite precipitation (EICP) have emerged as viable alternatives that are gaining attention. However, the efficacy of MICP and EICP relies on the microbial population's abundance and is best suited for cohesionless soils (Ivanov and Chu 2008).

Recent studies have proposed using biopolymers directly in the field to improve the engineering qualities of problematic soils (Acharya et al. 2017; Chang et al. 2020). Biopolymers interact with clay minerals in a complex mechanism. The interaction and bonding between biopolymers and clay particles depends on the chemical composition of the clay minerals. Soils treated with biopolymers have improved soil strengthening, lower hydraulic conductivity, improved soil dynamic characteristics, and higher resistance to soil erosion in geotechnical engineering (Bouazza et al. 2009; Chang and Cho 2019; Im et al. 2017). Guar gum, a commonly used biopolymer in food preparation, acts as a thickening and binding agent. It has distinct chemical bonding capabilities that induce viscosity and colloidal thixotropic dispersion, permitting the creation of strong cohesive gels (Sharma et al. 2018). Researchers have studied the use of guar gum to increase the slope stability of highly plastic soil from an embankment (Acharya et al. 2017; Ghosh et al. 2025). It has been observed that the addition of guar gum in soils has led to an increase in the unconfined compressive strength of treated soil (Sujatha and Saisree 2019). Their study investigated the potential of modifying the geotechnical properties of the soil favorably by using the gelling and bonding characteristics of biopolymers like guar gum.

Expansive soils are subjected to seasonal drying-wetting cycles and freezing-thawing cycles in seasonally frozen regions. Ice lens development involves the constant migration and accumulation of water, resulting in changes in hydrothermal characteristics and microstructure. This process leads to a complex transfer of mass and energy. Due to freezing-thawing cycles, the clayey soil accumulates plastic volume change (Nishimura 2021). Repeated freezing-thawing develops cracks in expansive soils, which leads to mechanical degradation of subgrade soil (Lu et al. 2019). The compacted subgrade soil shows dilation due to freeze-thaw cycles. A small number of freeze-thaw cycles lead to rapid degradation of the resilient modulus of clayey soil (Ghosh and Banerjee 2025; Qi et al. 2006). Only a limited number of studies have been conducted to investigate the effect of freeze-thaw cycles on mechanical degradation and the long-term performance of cement- and biopolymer-treated expansive soil (Liu et al. 2023; Lu et al. 2020; Solanki et al. 2013). Therefore, a detailed study is needed to investigate the effect of the addition of biopolymer as co-additive to the cement to stabilize expansive soil.

In this study, an experimental program was formulated to investigate the engineering properties of sulfate-rich expansive soils treated with cement and biopolymer to bridge the existing research gaps. The sulfate-rich expansive soil native to regions of South Dakota was treated with cement and biopolymer for a comparative analysis between the traditional and the biopolymer stabilization of soil. A series of laboratory tests of engineering properties encompassing 1D-swell, linear shrinkage, unconfined compressive strength (UCS), repeated load triaxial (RLT), and chemical tests such as change in pH were conducted on the untreated and stabilized soils to understand the macroscopic changes during stabilization. Subsequently, a series of freezing-thawing (F-T) laboratory tests were carried out to evaluate the impact on moisture loss, volume change, and mechanical performance on both untreated and treated soils. Field Emission Scanning Electron Microscopy (FE-SEM) studies were performed on control soil, cement-treated, and biopolymer-treated specimens to examine the morphological changes due to stabilization. The objective of this study was to investigate the effectiveness of biopolymer as a co-additive to cement to stabilize the subgrade soil in colder regions and potentially reduce the carbon footprint of traditional soil stabilization techniques. A limited number of recent studies have undertaken repeated load triaxial (RLT) tests on treated soils following freeze-thaw (F-T) cycles to assess the degradation of resilient modulus (M_R). This study represents one of the pioneering research efforts to employ a series of RLT tests for the assessment of resilient modulus (M_R) degradation in cement-treated soil due to F-T cycles. Before this investigation, no other documented research endeavors had explored the utilization of biopolymers as co-additives with cement in the treatment of expansive soil. The reduction of the use of cement can result in a subsequent reduction in the formation of ettringite and the overall detrimental effect of cement on the environment.

6.2 Materials

The soil and stabilizers used for this study have been discussed in this section of the chapter.

6.2.1 Expansive Soil

The soil used for the experimental study was collected from the project site in Jones County, South Dakota. Initially, a series of geotechnical tests were conducted on the collected soil following the American Society for Testing and Materials (ASTM) and the Texas Department of Transportation (TxDOT). Table 6.1 presents the fundamental properties of the soil. Figure 6.1 illustrates the particle size distribution of the collected soil. The soil was classified as a highly plastic clay (CH) in accordance with the Unified Soil Classification System (USCS) based on the test results shown in Table 6.1.

Table 6.1 Basic geotechnical properties of the soil used in this study

Properties	Standards	Value
Specific Gravity, G_s	ASTM D854	2.75
Liquid limit, LL (%)	ASTM D4318	65.6
Plasticity Index, PI (%)	ASTM D4318	38.7
Sand content (4.75 mm - 75 μ) (%)	ASTM D7928	21.3
Silt content (75 μ - 2 μ) (%)	ASTM D7928	37.1
Clay content (< 2 μ) (%)	ASTM D7928	41.6
USCS Classification	ASTM D2487	CH
Optimum moisture content, OMC (%) (Standard Proctor)	ASTM D698	31.5
Maximum dry density, MDD (g/cm ³) (Standard Proctor)	ASTM D698	1.437
Optimum moisture content, OMC (%) (Harvard Proctor)	USBR GR-84-14	27.6
Maximum dry density, MDD (g/cm ³) (Harvard Miniature Proctor)	USBR GR-84-14	1.455

Note:

ASTM: American Society for Testing and Materials

USBR: United States Bureau of Reclamation (Scavuzzo 1984)

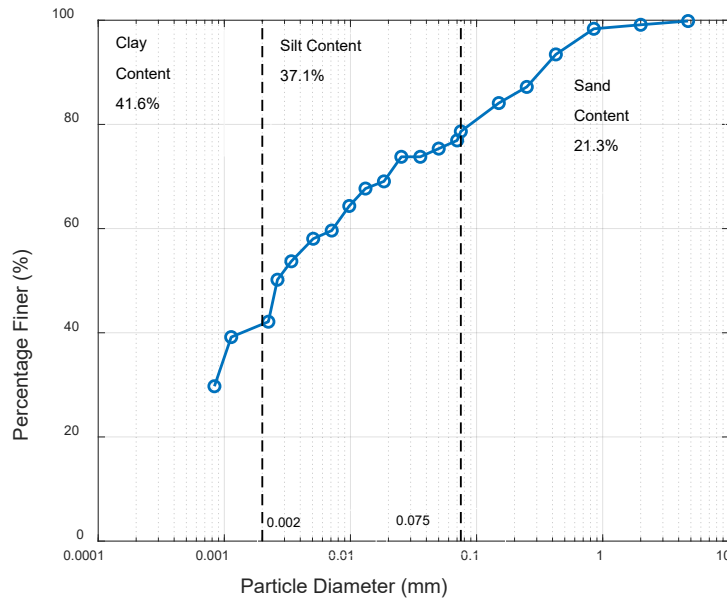


Figure 6.1 Particle Size Distribution of the native soil

To assess the expansive characteristics of the soil, one-dimensional free swell strain (in accordance with ASTM D4546) and linear shrinkage (following Tex-107-E) were measured. The soluble sulfate content and pH of the soil were measured as per Tex-145-E and Tex-128-E, respectively, and the results of these tests are tabulated in Table 6.2. The vertical swell (1-D) test and linear shrinkage strain test for the

untreated soil used in the study provided results of 5.2% and 17.6%, respectively. The soil may be considered as high swell-shrink soils. Such soils need to be treated efficiently to minimize distress to civil infrastructure due to volume changes with changes in moisture regime. The measured soluble sulfate content of the collected native soil was found to be 10,800 ppm as per Tex-145-E. The soil was classified as a high sulfate soil (sulfate content > 8,000 ppm) by TxDOT guidelines.

Table 6.2 Expansive and Chemical properties of the soil used in the study

Properties	Standards	Value
Vertical free swell strain (%)	ASTM D4546	5.23
Linear shrinkage strain (%)	Tex-107-E	17.59
Soil pH	Tex-128-E	7.70
Soluble sulfate content (ppm)	Tex-145-E	10,800

6.2.2 Additives

In this study, two different types of chemicals, Type-I cement (ordinary Portland cement) and Guar Gum as biopolymer (BP), were employed to stabilize the expansive soil. Additionally, a combination of Type-I cement and biopolymers was used as coadditives to enhance the engineering properties of the expansive soil.

6.2.3 Cement

Type-I cement (as per ASTM C150) was considered one of the two stabilizing agents used on the expansive soil in the study. The three major components of the cement were lime (CaO), silica (SiO₂), and alumina (Al₂O₃). The dosage of the cement for the cement-stabilized subgrade soil was selected from the recommendations of PCA guidelines (Gross and Adaska 2020). As per PCA guidelines, treatment dosages for cement-stabilized subgrade should be between 3% - 6%. The minimum and maximum limits of the recommendation, 3%, and 6% dosages were selected in this study, respectively.

6.2.4 Biopolymer

Biopolymers can directly interact with clay particles due to the presence of electrical charges (Fatehi et al. 2021). The chemical bonds between biopolymer and clay particles can be generated through various electrostatic interactions, hydrogen bonding, ionic bonds, or van der Waals forces. The mechanism of biopolymer-treated interaction is determined by several elements, including the electrical charges of the biopolymer, the presence of natural cations inside the clay, and the level of charge on the surfaces of the clay mineral sheets (Chang et al. 2015; Latifi et al. 2017). Expansive soil has a high content of montmorillonite clay which has higher negative charges compared to other clay minerals. The higher negative charges increase the absorption of the biopolymer solution (Latifi et al. 2017). The biopolymer hydrogel establishes direct interaction with the soil by covering the soil particles and creating robust chemical bonds upon addition to the soil mass and subsequent drying. This results in the creation of a network composed of soil particles and biopolymers. These networks significantly increase the interparticle bonding between particles (Fatehi et al. 2021).

Several studies were conducted for different biopolymer uses in geotechnical applications, such as encapsulating biological materials, constructing compacted covers, and stabilizing soil and mine tailings, among other applications. Biopolymers like agar gum, xanthan gum, guar gum, gellan gum, and chitosan have been previously used for biopolymer-based soil treatment (Chang et al. 2020). Guar gum was used for soil strengthening, erosion resistance by increasing moisture retention capacity, and stabilization of mine tailings (Sujatha and Saisree 2019). Guar gums illustrate hydrophilic polysaccharides, exhibiting a

rod-like polymeric structure wherein galactose side chains are attached to the mannose backbone with an average molecular ratio of 1:2 (Figure 6.2). The D-mannose units are connected by β (1-4) glycoside linkage in straight chains, while the D-galactose units are linked alternately through (1-6) glycoside linkage (Sharma et al. 2018). Guar gum has distinct physical properties. Hydrocarbons, fats, alcohols, esters, and ketones are typically insoluble in it. However, it has a high solubility in water. The galactose units on the mannose units interact with water molecules in a water environment, resulting in intermolecular chain entanglement. This phenomenon contributes to the thickening and increased viscosity of the solution (Pathania et al. 2016). The abundance of hydroxyl ions in guar gum allows for the formation of hydrogen bonds with hydrated minerals and organic surfaces, resulting in a higher degree of linking. Furthermore, cross-linking guar hydrogels with Ca^{2+} ions improves aggregation (Reddy et al. 2018). It was observed in the literature that biopolymer dosage varied between 0.5 to 2.5% for stabilization (Bouazza et al. 2009; Chang et al. 2015; Sujatha and Saisree 2019).

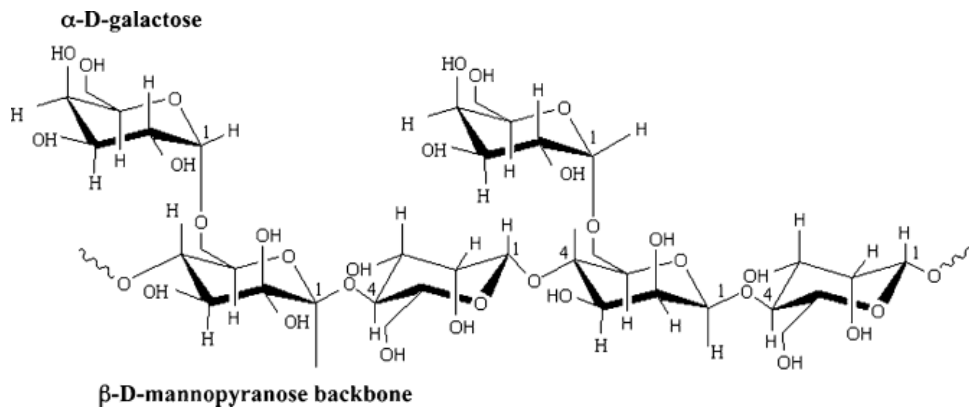


Figure 6.2 Molecular structure of guar gum (adapted from Mudgil et al. 2014)

6.3 Specimen Preparation

The collected soil was air-dried and sieved through a 4.75 mm sieve (US sieve #4). The preliminary properties of the soil and grain size distribution are discussed and shown in Table 6.1 and Figure 6.1. The moisture content-dry density relationships for each treatment were established using two compaction methods: the Harvard miniature compaction apparatus (according to USBR GR-84-14) and the standard proctor compaction apparatus (as per ASTM D698). The Harvard miniature compaction apparatus allows for a quicker determination of moisture content-dry density relationships with smaller soil quantities (Scavuzzo 1984). Each specimen for the unconfined compression test was compacted in three equivalent lifts using the undercompaction technique as recommended by Ladd (1978) and Samuel (2019) at its optimum moisture content (OMC), achieving 95% of its respective maximum dry density (MDD) from the Harvard miniature compaction test. To reduce errors caused by end effects, the height-to-diameter ratio of the specimens was between 2 to 2.5 (ASTM D2166-16). The specimen for UCS tests was prepared in a diameter of 33 ± 1 mm (~ 1.3 in.), and a height of 71 ± 2 mm (~ 2.8 in.). The stiffness properties of the untreated soil and treated soil at low strain levels were measured using the repeated load triaxial (RLT) test to determine the resilient modulus of the soil specimens. The specimens with a diameter of 71 ± 1 mm (~ 2.8 in.) and height of 141 ± 2 mm (~ 5.6 in.) were compacted statically in a split mold in five layers using the undercompaction technique (Banerjee 2017; Ladd 1978; Pereira dos Santos et al. 2022). The OMC and MDD were considered from the standard proctor tests for different additives (as per ASTM D698). The prepared specimens were cured for a period of 7 and 28 days at 98 ± 2 % RH for cement-treated soil and the biopolymer-treated soil specimens were wrapped in plastic for 7 and 28 days at constant humidity and temperature conditions.

6.4 Experimental Program

The study aimed to examine the impact of adding cement and biopolymer, specifically guar gum, on controlling the expansive nature of the soil and enhancing the mechanical qualities of sulfate-rich expansive soil. In addition, a combination of cement and biopolymer was utilized to examine their coupling effect. In order to assess the durability of the soil that was treated, we analyzed the strength and stiffness characteristics of both the untreated and treated soil. This analysis was conducted both before and after subjecting the soil to many freeze-thaw cycles, which will be addressed in a subsequent section. The study includes the testing of unsaturated characteristics of the expansive soil. The different types of equipment used for this study are shown in Figure 6.3.

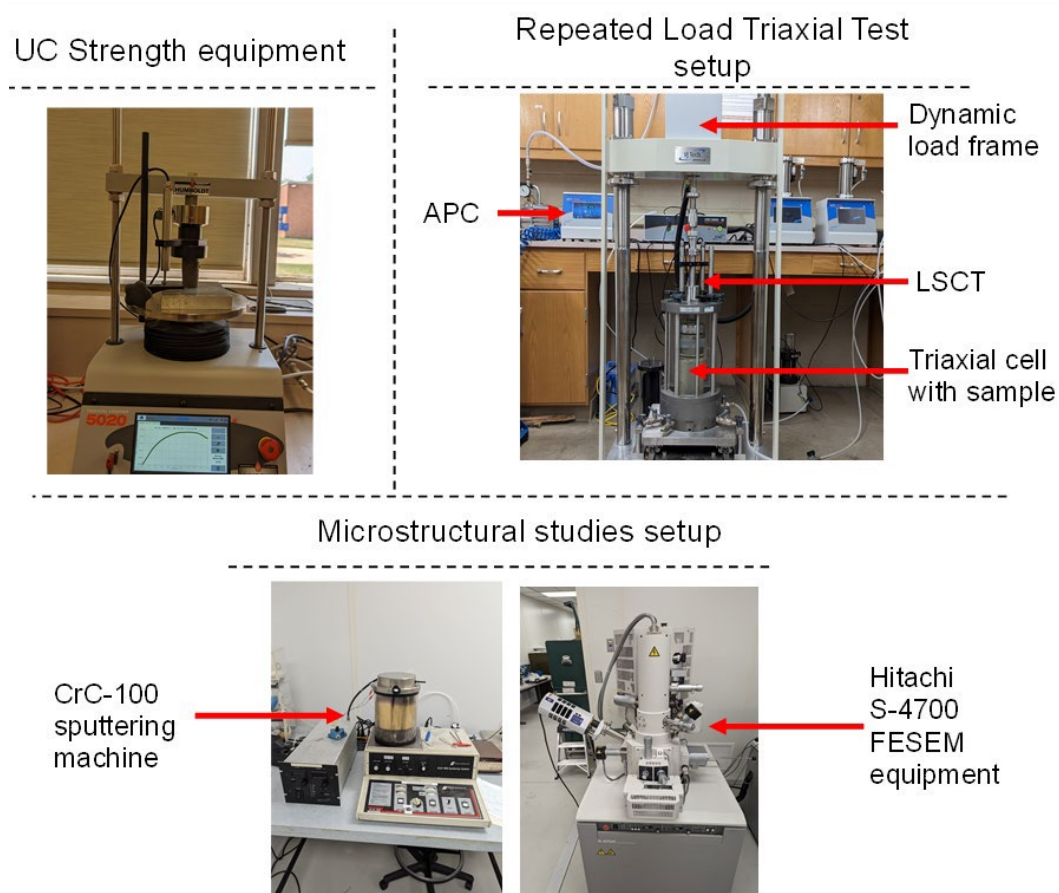


Figure 6.3 Equipment used for UCS, RLT tests, and microstructural studies

6.4.1 Strength Studies

Unconfined compressive strength (UCS) tests were performed on both untreated and treated soils to provide an initial assessment of soil strength to quantify the effect of treatment and curing periods according to the protocols outlined in ASTM D2166-16. The UC tests were also conducted after selected F-T cycles to assess the durability of control and treated soil. In these tests, cylindrical soil samples were subjected to strain-controlled uniaxial loads at a strain rate of 1%/minute until failure (Chang et al. 2015; Lu et al. 2020). The failure of the specimen represents the UCS of the soil, which corresponds to the peak stress value in the stress-strain curve obtained from the UCS test.

6.4.2 Determination of Stiffness Properties

Repeated load triaxial (RLT) tests were carried out in this study on both untreated soil and soils treated with cement and biopolymer following the recommendations of AASHTO T307-99 (2003). The RLT testing setup simulates the stress increment caused by traffic loads on subgrade soils. This is achieved by applying a predetermined cyclic loading sequence under varying confining stress conditions, effectively simulating the in-situ overburden pressure (Puppala 2008). A cyclic triaxial apparatus was used to conduct these experiments. The test sequence for the RLT test for subgrade soil and stabilized soil was selected as type 2 soil as per AASHTO T307-99 (2003), which is applicable for cohesive soils. The axial deviator stress is composed of two distinct components: the seating stress, and the cyclic deviator stress. The seating stress accounts for approximately 10% of the total deviator stress applied, and its primary function is to ensure proper contact between the load actuator and the upper surface of the specimen. The cyclic deviator stress is administered in the form of a haversine-shaped waveform, in accordance with the stipulations outlined by AASHTO T307-99 (2003) and (NCHRP 2004). Each loading and unloading cycle within the cyclic load sequence spans 0.1 seconds, followed by a relaxation period lasting 0.9 seconds, in line with the recommendations set forth by AASHTO T307-99 (2003).

Four different dosages (a) 3% cement, (b) 6% cement, (c) 1.5% biopolymer, and (d) a combination of 3% cement and 1.5% biopolymer were used for the study to understand the influence of cement and biopolymers on the mechanical properties of the soils based on a preliminary study. The potential for the use of biopolymers as a co-additive was also verified by mixing 3% cement with 1.5% biopolymer. For each treatment, the curing period selected for the study was 7 and 28 days.

6.4.3 Study of Swelling and Shrinkage Properties

The one-dimensional (1-D) or vertical swell test and the linear shrinkage test were conducted to quantify the expansive characteristics i.e., swelling and shrinkage of control and treated soil. In this study, the 1-D swell pertains to the percentage expansion demonstrated by soil after absorbing water under a confining pressure of 1 kPa. This expansion is assessed according to ASTM D4546-14e1 guidelines, and the samples employed in the 1-D swell tests were compacted under static conditions within a ring-shaped mold at their OMC, achieving a compaction level of 95% of their MDD. This process resulted in specimens with a diameter of 2.5 inches (63.5 mm) and a height of 1.13 inches (28.7 mm). The tests were conducted after curing for 2 hours and the readings were collected for a period of 48 hours.

The assessment of linear shrinkage of soils with drying was carried out in accordance with TEX-107-E guidelines. This was done to determine the extent of shrinkage in untreated soils versus soils treated with cement and biopolymer. The soil particles that were finer than the 425- μm (US # 40) sieve were subjected to specific amounts of the stabilizer treatment.

$$LS = 100 \times \frac{L_W - L_D}{L_W} \quad (1)$$

Where LS represents linear shrinkage presented as a percentage, L_W corresponds to the length of the wet soil bar, which measures 5 inches (127 mm), while L_D refers to the length of the dry soil bar. The control soil, cement- and biopolymer-treated soils were tested using the linear shrinkage test after a curing period of 2 hours for different dosages.

6.4.4 pH Test

Soil pH represents the level of acidity or alkalinity within the soil and serves as a valuable indicator for assessing the solubility of soil minerals and the mobility of ions within the soil. The pH tests for the control soil and stabilized soil were conducted in accordance with TEX-128-E using an Orion Star A211 pH meter, which uses 4-point calibration.

6.4.5 Study of the Microstructural Changes

Microscopic studies were performed using the Field Emission Scanning Electron Microscopy (FE-SEM) on control and treated soils. The aim was to qualitatively analyze the soil morphology and alterations in soil microstructure resulting from treatment and to identify the possible presence of biopolymer gels. The FE-SEM analysis was carried out using a Hitachi S-4700 FE-SEM instrument on cubic specimens. To maintain the microstructure of the specimens and obtain higher-quality images, the desiccator technique with slow removal of water content was employed for drying the specimens. Due to the non-conductive nature of soil and biopolymers, a layer of gold sputter coating was applied to the specimens using a CrC-100 sputtering machine. Visual comparison of images obtained from FE-SEM for control and treated specimens was conducted to discern microscopic morphological changes that might indicate the existence of reaction products and the development biopolymer matrix.

6.4.6 Freeze-Thaw Test

Following the conclusion of the curing period of 28 days, the soil specimens were placed inside a freeze-thaw chamber, where precise control over humidity and temperature was maintained, and the freeze-thaw system used for the study is illustrated in Figure 6.4.

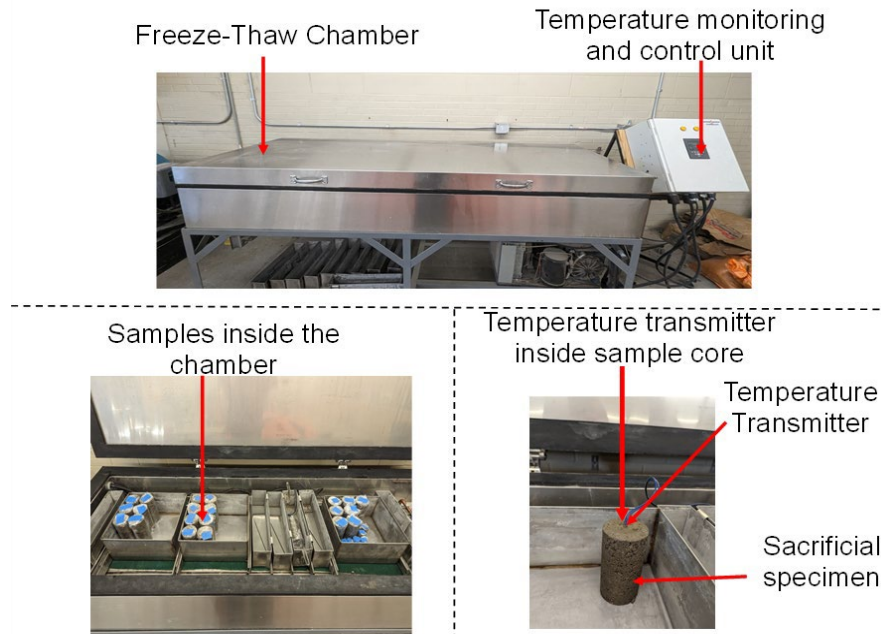


Figure 6.4 Experimental Set-up for the freeze-thaw cycles

A closed system was employed for the freeze-thaw test, replicating field conditions where no external water supply is present apart from the moisture already within the soil voids (Lu et al. 2020). To achieve this closed condition, the samples were sealed before freeze-thaw testing. The specimens for the UCS and

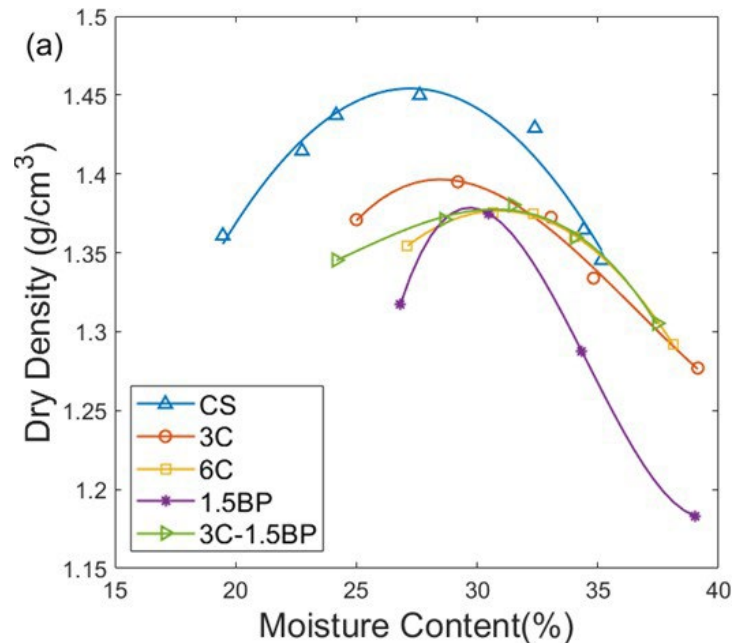
the resilient modulus test were subjected to 0, 1, 4, 8, and 12 repeated freeze-thaw cycles, Solanki et al. (2013) used a similar number of cycles for cement-treated soil. One freeze-thaw cycle consisted of a freezing period of 12 hours with a minimum temperature of -20°C , and the following 12 hours thawing period with a maximum temperature of 20°C . Several previous studies such as Lu et al. (2020) and Tiwari et al. (2021) adopted the 24-hour duration for a complete freeze-thaw cycle. The samples were weighed to determine the mass loss, and the water content and volume changes were measured at the end of the selected F-T cycles.

6.5 Combined Effect of Cement and Biopolymers in Soil Stabilization

The test results for the control (CS), 3% and 6% cement-treated (3C and 6C), and biopolymer-treated (1.5BP) soils and soils with a combination of cement and biopolymer (3C-1.5BP) were analyzed for identifying the changes to the physical, mechanical, chemical, and soil morphology. The test results helped to develop an understanding of the combined effect of the addition of cement and biopolymer.

6.5.1 Change in Compaction Characteristics

The compaction curves corresponding to various additives are depicted in Figure 6.5a for the Harvard miniature compaction tests and in Figure 6.5b for the standard compaction tests. A consistent pattern of diminishing maximum dry density can be observed as additives are introduced. Notably, the MDD values obtained from the standard Proctor tests are lower than those obtained from the Harvard miniature proctor tests which is due to the higher compaction energy per unit volume for the Harvard miniature compaction tests, while the OMC for the control and treated soils follows an inverse trend. This is consistent with the observations of other studies due to the difference in soil structure in both methods (Ltifi et al. 2014; Sridharan and Sivapullaiah 2005). The addition of biopolymer results in the most pronounced reduction in MDD when compared to the forms of control and treated soils.



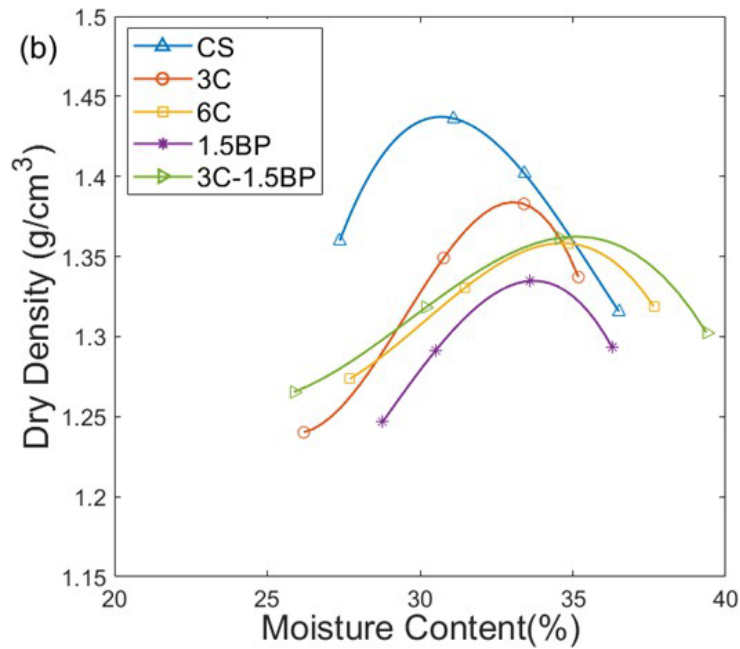


Figure 6.5 Compaction curves for control and treated soil from (a) Harvard miniature compaction and (b) Standard proctor compaction tests

6.5.2 Comparison of Stabilization Effect of Soil Treatment

The effectiveness of additives on the plasticity of soil was investigated. Expansive soils are characterized by their higher clay content, and elevated moisture levels, and typically exhibit liquid limit (LL) values exceeding 50. Even though soil mineralogy should be used to identify the expansive nature of the soil, the plasticity index (PI) serves as the most common indicator of the expansive nature of the soil. It has been recommended that soils with PI values of 18 or lower usually demonstrate good performance (Ross and Adaska. 2020). In contrast, extremely expansive soils exhibit considerably higher PI values (Ross and Adaska. 2020). Figure 6.6a demonstrates the impact of cement and biopolymers on the Atterberg limits of highly plastic clayey soil after two hours of mixing. It is evident that as the dosage of cement and biopolymers increases, both the liquid limit and plastic limit show a continuous rise, while the plastic limit remains relatively stable. This increase in the liquid limit and plasticity index can be attributed to the heightened viscosity of the pore fluid due to the introduction of biopolymers. These findings align with the results of Chen et al. (2013), who similarly reported an elevation in the consistency limits of mine tailings when treated with GG biopolymers. It can be seen in Figure 6.6b that 6% cement and co-additives (3C-1.5BP) successfully reduced the PI to a value lower than 18% which can lead to better performance.

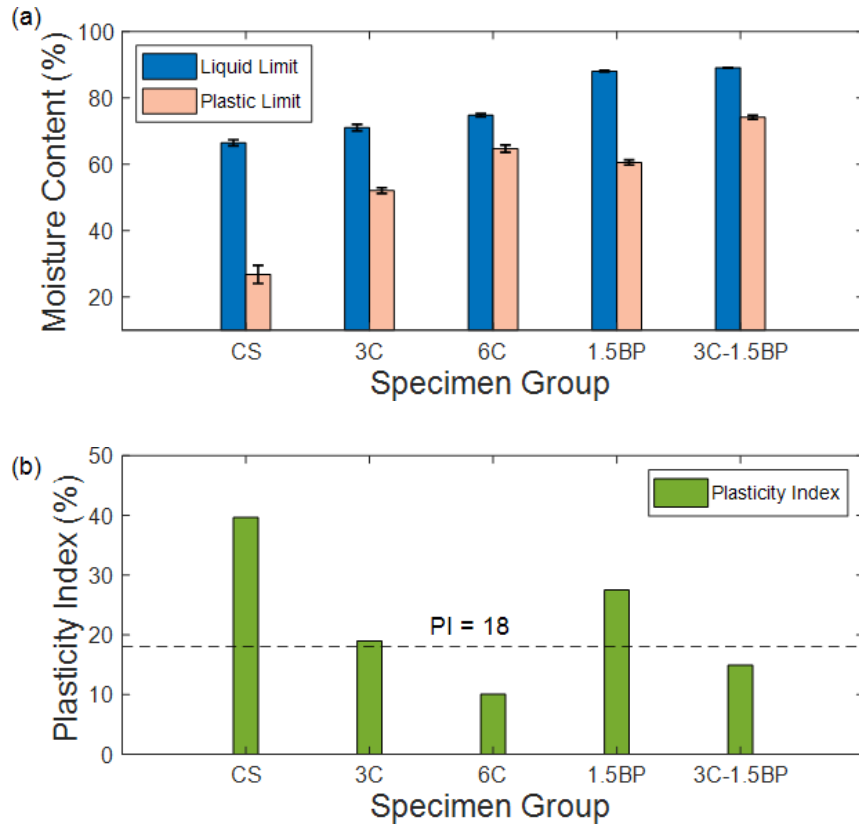


Figure 6.6 Comparison of (a) Atterberg limit and (b) plasticity index with different treatment methods for soils

6.5.3 Change in pH Due to Additives

The effectiveness of additives on the pH of soil was investigated. A correlation between increased pH values and soil shear strength was presented in previous studies (Goodarzi et al. 2016). The initial pH of the control soil used in the current study was determined to be 7.7. Subsequently, the pH levels were determined for the cement- and biopolymer-treated soils as per Tex-128-E for various dosages at intervals of 0 days (2 hours), 7 days, and 14 days, and the pH variation is presented in Figure 6.7. It is well-known that pozzolanic reactions in cement result in high values of pH. However, the biopolymer-treated soil was found to be mildly acidic, and as a co-additive with cement, the biopolymer was observed to not have a significant effect on the pH value. In other words, the pH of 3% cement (3C) and co-additives (3C-1.5BP) were observed to have similar pH values. Hence, the pH of treated soil is governed by the concentration of cement. A trend in modest reduction of soil pH with curing for 14 days can be observed in Figure 6.7. The addition of cement caused the increase in pH and with curing the pH showed a decreasing trend. The biopolymer used in the study was non-ionic and acidic in nature, which can be confirmed by several studies (Dehghan et al. 2019; Moghal and Vydehi 2021). Thus, biopolymer stabilization reduced the pH of the soil to less than 7.0 and created acidic conditions.

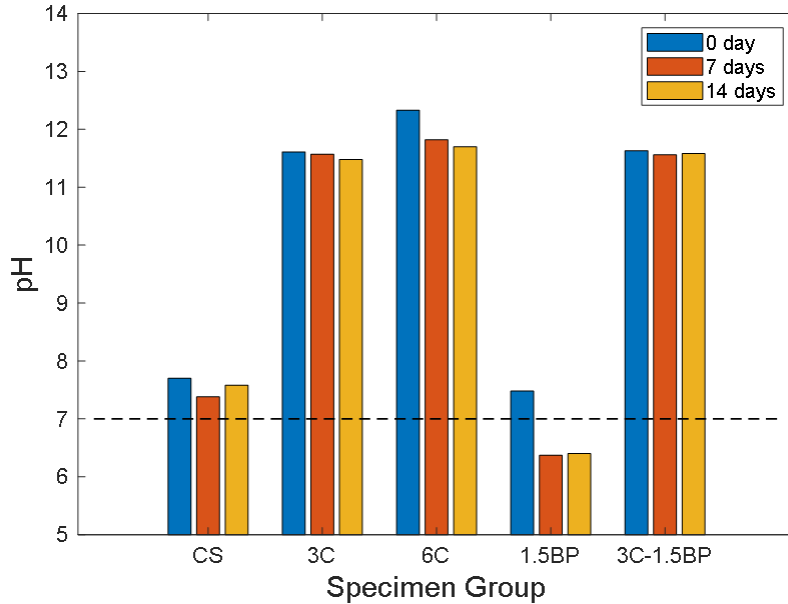


Figure 6.7 Variation of pH with treatment for different curing periods (0 days, 7 days & 14 days)

6.5.4 Swelling-shrinkage Characteristics of Treated Soil Compared to Control Soil

Cement treatment had a notable impact on mitigating the swelling potential of expansive soils, as shown in Figure 6.8a. The untreated soil displayed a moderate swelling potential, characterized by a vertical swell strain of approximately 5.2%. However, a substantial decrease in the vertical swell strain was observed within two hours of curing with cement, this rapid reduction in swelling potential can be attributed to the swift exchange of cations between the cement and clay minerals, which reduces the water absorption capacity of the clay minerals and reduction of soil plasticity with the introduction of cement.

In contrast, biopolymer treatment results in the formation of hydrogels, which results in a higher swelling potential of soils. Hydrogels are intricate, highly crosslinked structures known for their high water-absorbing capabilities (Reddy et al. 2018). They possess greatly enhanced hydrophilic properties, which contribute to their high swelling potential (Sharma et al., 2018). After longer exposure to hydrated condition (600 minutes = 10 hours), an increase in 1D-swell strain was also observed for cement-treated soil. The 1D swell for 6% cement-treated soil even exceeded that of 3% cement-treated soil (after 2000 minutes) due to the probable formation of ettringite. The soil treated solely with the biopolymer showed higher swelling potential than untreated soil due to the formation of hydrogels. Hence, soil stabilization using only biopolymers may not be suitable.

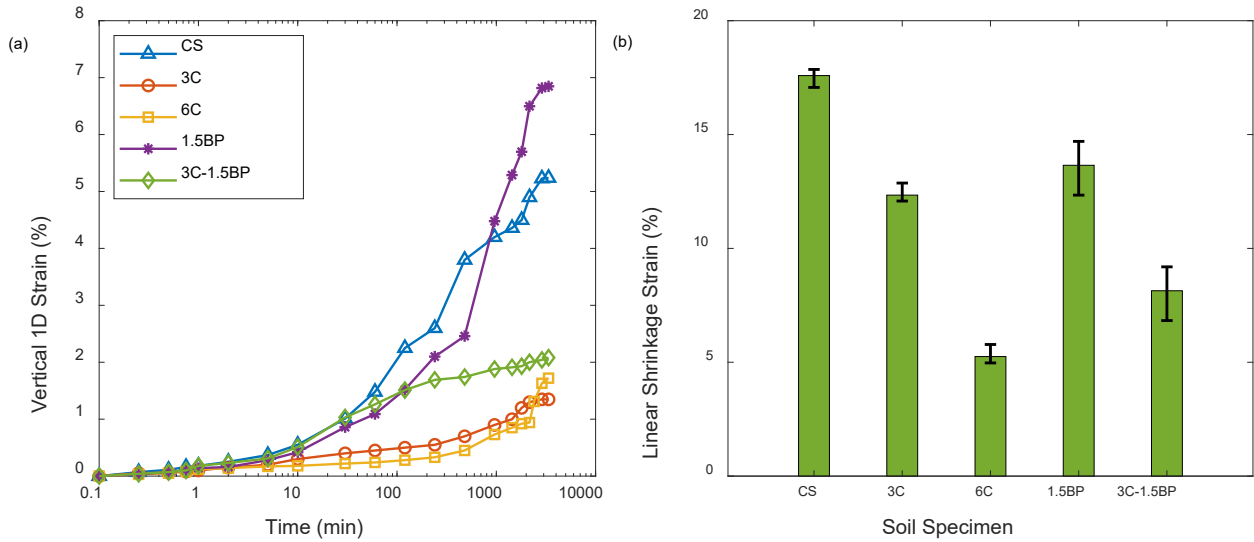


Figure 6.8 Comparison of (a) 1D-swell and (b) linear shrinkage strain with treatment of different types

A decrease in linear shrinkage was noted in both soils treated with cement and biopolymer, as indicated in Figure 6.8b. The linear shrinkage of the control soil was observed to be 17.6%. However, when biopolymer alone was added as a stabilizer, it did not lead to a significant reduction in soil shrinkage. The substantial reduction in linear shrinkage of expansive soils was achieved with increased stabilizer dosages. Specifically, the addition of 6% cement and a combination of 3% cement and 1.5% biopolymer for a short curing period of 2 hours resulted in a significant reduction in shrinkage by 70% and 54%, respectively.

The effect of stabilization on the swelling potential and curing period is illustrated in Figure 6.9. The swelling strains for 6C and 3C-1.5BP treatment after 14 days of curing were reduced by 96% and 95.8%, respectively. The swelling of biopolymer treatment was reduced by 76.9% and 81.8% for 7 days and 14 days of curing, respectively. The formation of the biopolymer network in biopolymer-treated soil could have contributed to the reduction of swelling strain.

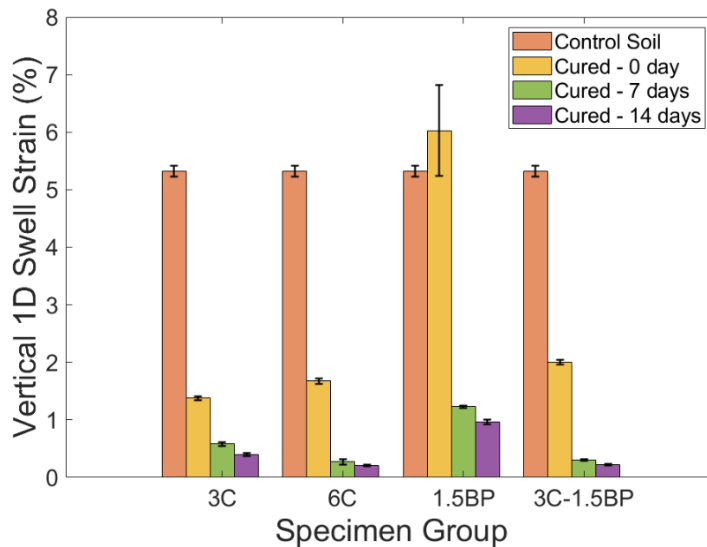


Figure 6.9 Variation of the swelling strain of different treatments with curing

6.5.5 Effect of Stabilization on the Strength Characteristics

The unconfined compressive strength (UCS) is a critical geotechnical parameter for cohesive soils that must be thoroughly characterized to assess the suitability of a particular soil for construction applications. While it does not directly translate to field-bearing capacity, it does provide insight into changes in shear strength caused by the addition of stabilizers. Figure 6.10 presents the unconfined compressive strength (UCS) of both the control soil and the soil treated with biopolymer (BP) after a 7-day curing period. The results reveal an initial increase in UCS with BP content ranging from 0.5% to 1.5%. However, a significant drop in UCS is observed with a 2.5% BP addition. This reduction in UCS compared to control soil aligns with findings from prior studies involving guar gum as a biopolymer, which reported a similar decrease in soil strength for certain polymer concentrations during shorter curing periods (Bozyigit et al. 2023; Sujatha and Saisree 2019). Therefore, a 1.5% polymer content was chosen as the co-additive content for subsequent studies involving freeze-thaw analysis as it had the maximum UC strength compared to other biopolymer content.

Figure 6.10 illustrates the UCS of expansive soil with different dosages of cement and biopolymer. The UCS of the untreated soil was observed to be 268.5 kPa, and the introduction of 1.5% biopolymer increased strength by 2.3%, and 17.1%, after 7 days and 28 days respectively.

Generally, the addition of cement as a stabilizer improves the properties of the expansive soil. The formation of hydrated calcium silicate (C-S-H) during the curing process is responsible for the increased strength (Peethamparan et al. 2009). The C-S-H gel acts as a binding agent for soil particles, improving the soil cementation and resulting in enhancing the cohesive properties of the soil. Increasing cement content by 3% to 6% leads to improvements in soil strength. The maximum UCS after 28 days can be observed in 6% cement samples which showed a 3.5 times strength increase compared to control soil. The specific surface properties, coupled with its electrokinetic charges, enable interactions between the soil particles and the biopolymer employed in this study (Chang et al. 2015). This interaction produces a strong biopolymer-soil matrix, which contributes to overall strength improvement as seen in Figure 6.11 for 28 days cured biopolymer specimens.

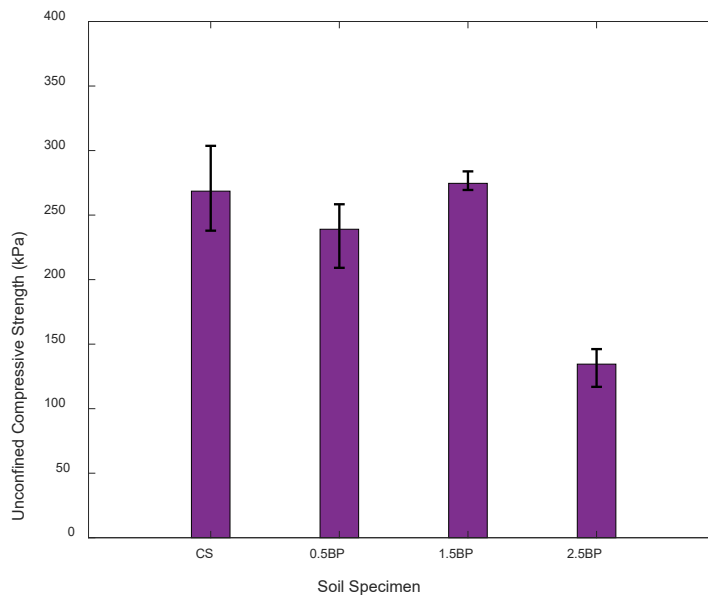


Figure 6.10 Unconfined compressive strength for different biopolymer content after 7 days of curing

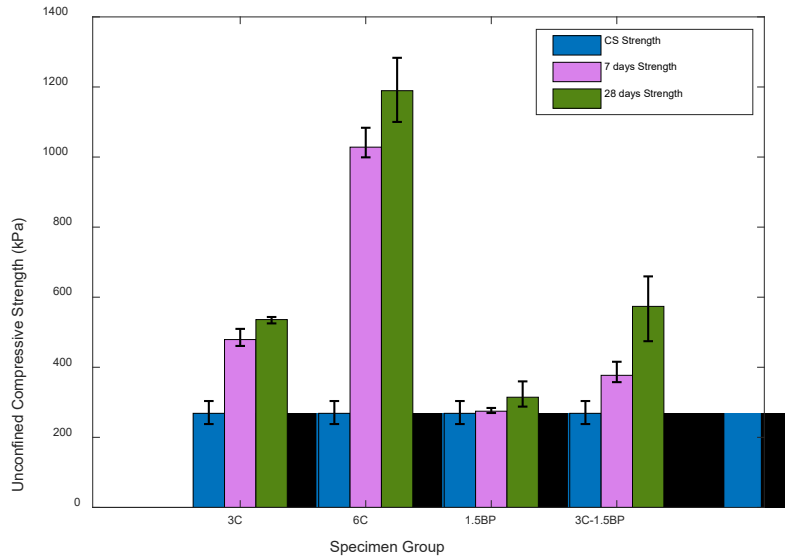
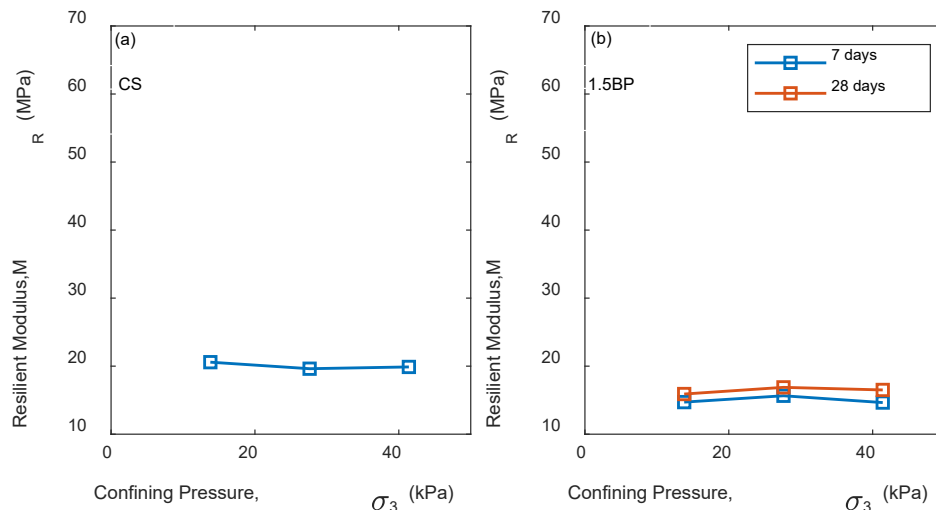


Figure 6.11 Unconfined Compressive Strength (UCS) test results of the treated soil for a curing period of 7 and 28 days compared to control soil

6.5.6 Effect of Cement- and Biopolymer-treatment on the Resilient Modulus

Resilient modulus (M_R) is an important material property that is used to quantify the stiffness of subgrade soil in order to aid in pavement design, as discussed earlier. M_R was chosen from test sequence 8 out of 15 test sequences, which had a confining pressure of 27.6 kPa and a maximum deviatoric stress of 41.4 kPa. This sequence closely simulates real-world traffic loading, with an equivalent single axle load (ESAL) of 80 kN and tire inflation pressure (TIP) of 241.32 kPa. A similar calculation was conducted by Moazami and Muniandy (2021). Kim & Siddiki (2006) investigated the relationship between M_R and UCS using confining pressure and peak deviatoric stress values of 13.6 kPa (2 psi) and 41.4 kPa (6 psi), respectively. The variation of resilient modulus (M_R) with confining pressure for different stabilizer dosages for a constant peak deviatoric stress of 41.4 kPa for a curing period of 7 days and 28 days is shown in Figure 6.12. The addition of cement increases the resilient modulus of expansive soil significantly. In contrast, the presence of biopolymer as the lone stabilizer has a detrimental impact on M_R due to the formation of hydrogels. However, when cement and biopolymer are combined with soil, M_R increases significantly with the curing period, signifying an increase in stiffness at a low strain level.



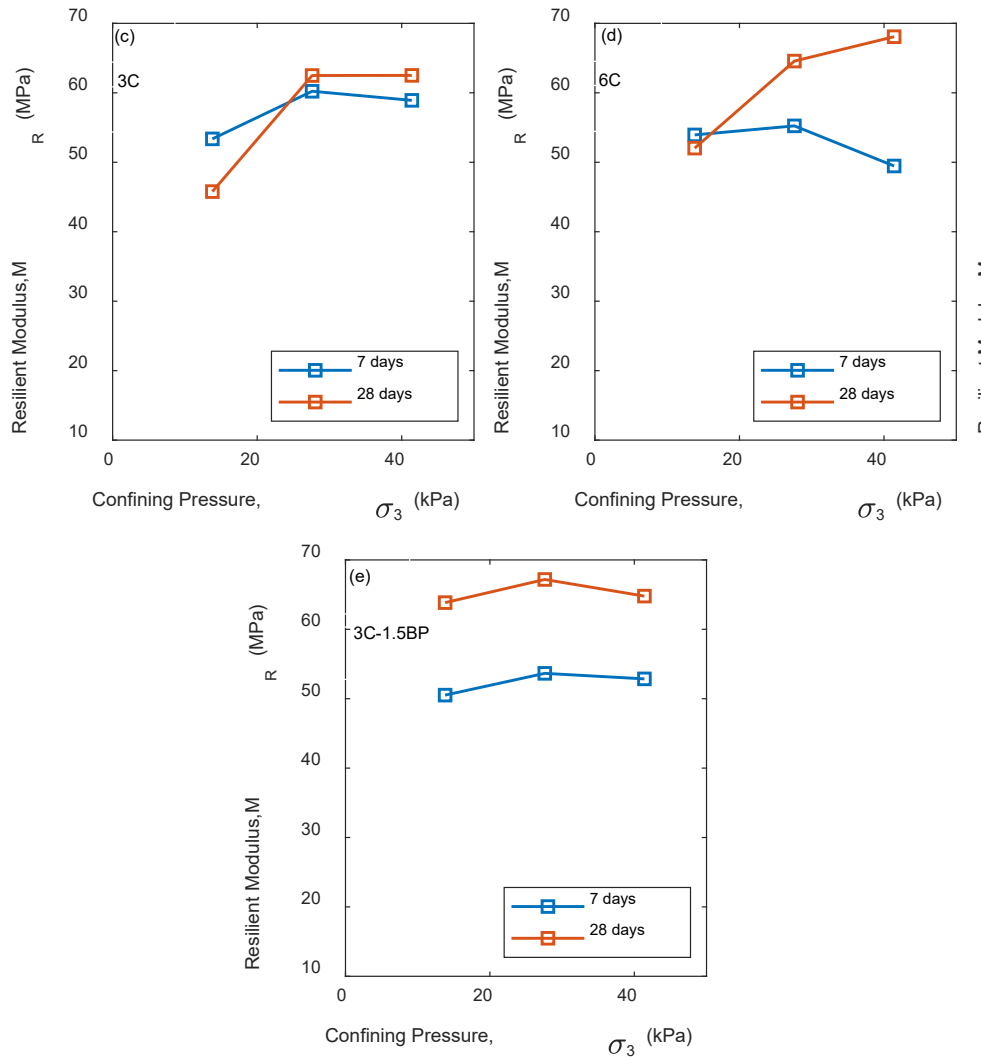


Figure 6.12 Variation of resilient modulus (M_R) with confining pressure for constant peak deviatoric stress ($\sigma_d = 41.4$ kPa) for: a) CS, b) 1.5BP, c) 3C, d) 6C, e) 3C-1.5BP

The variation of M_R values of samples treated with different stabilizers and dosages for different curing periods have been compared against that of the control soil samples and shown in Figure 6.13 for test sequence number 8. The M_R of the untreated soil was found to be 19.6 MPa. A reduction of 13.9% in M_R was observed for the addition of 1.5% biopolymer after 28 days which can be attributed to much less MDD of the specimens and the lack of bonding of the soil particles. The increase in the viscoelastic properties of the pore fluid for the addition of biopolymer can also contribute to the reduction in M_R of biopolymer-treated soil. For this test sequence, the M_R was observed to be the highest for the combination of 3% cement and 1.5% biopolymer after 28 days of curing. An increase of 7.5% in M_R can be observed with the addition of biopolymer in 3% cement content for 28 days of curing. A slight increase of 3.3% increase of M_R was observed for cement content, increasing from 3% to 6% for 28 days of curing. A minor reverse trend can be observed for the curing period of 7 days which can be due to the possible formation of two opposing phenomena of microcracking and the formation of C-S-H gel.

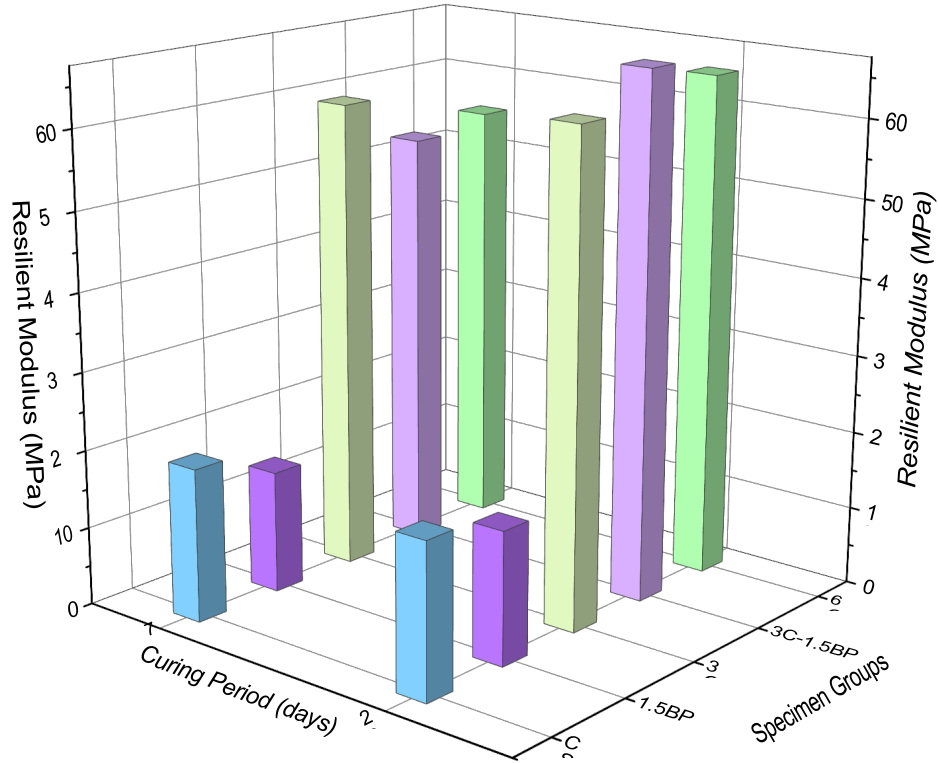


Figure 6.13 Resilient modulus (M_R) test results for constant confining pressure ($\sigma_3 = 27.6$ kPa) and deviatoric stress ($\sigma_d = 41.4$ kPa) of the control and treated soil for different curing periods

6.5.7 Microstructural Studies of the Treated Soil

Microstructural characterization studies involving FE-SEM were conducted on untreated and treated soil samples to gain insights into the morphological alterations brought about by the development of new reaction products. Figure 6.14 presents FE-SEM images of untreated soil, specimens treated with 3% cement (3C), 6% cement (6C), 1.5% biopolymer (1.5BP), and a combination of 3% cement and 1.5% biopolymer (3C-1.5BP) after a 28-day curing period. In Figure 6.14a, the untreated soil displays open pore structures with clay particles. Notably, needle-shaped ettringite crystals are evident in the 3C and 6C samples after 28 days, though the formation is much less in 3C specimens.

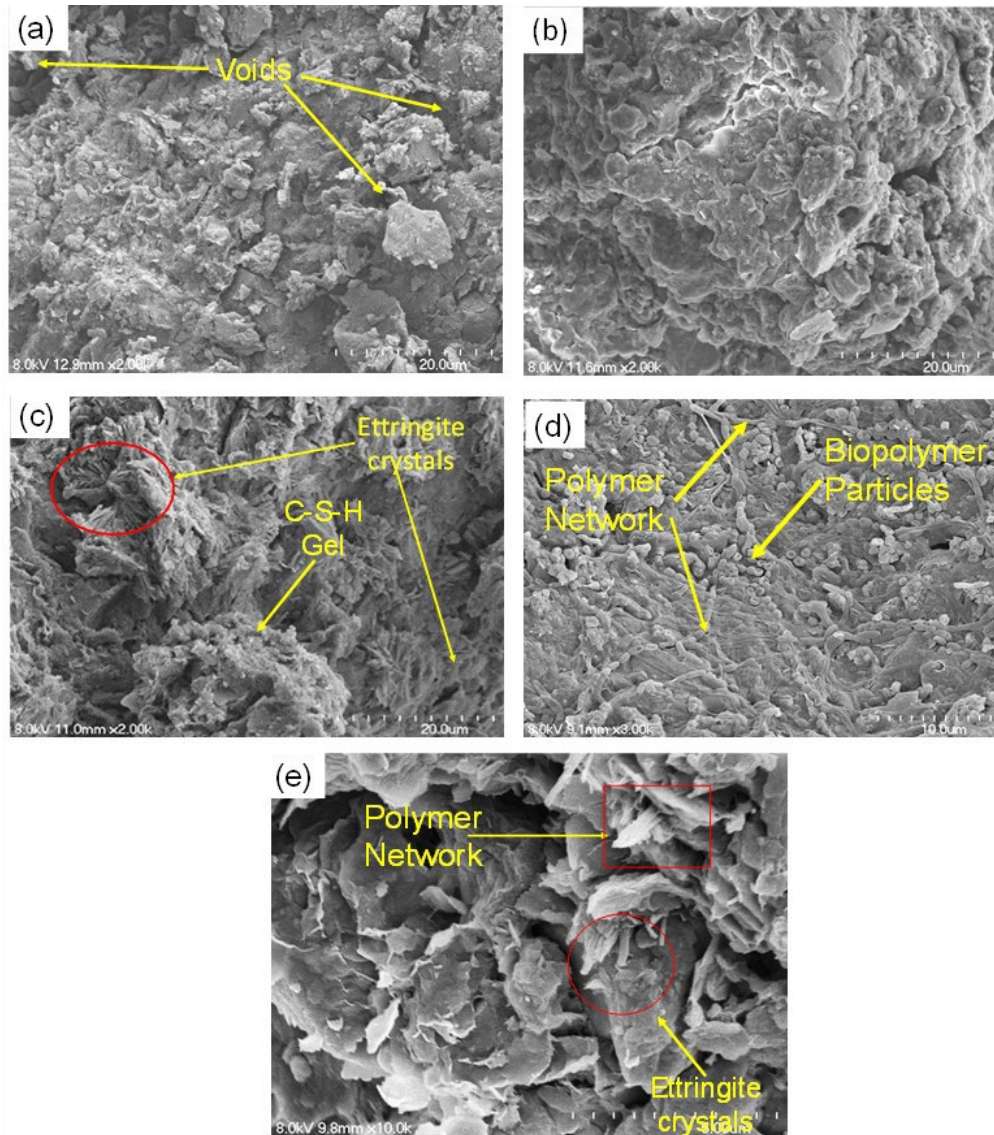


Figure 6.14 Field Emission Scanning Electron Microscopy (FE-SEM) images: (a) CS (2k Mag.), (b) 3C (2k Mag.), (c) 6C (2k Mag.), (d) 1.5BP (3k Mag.), and (e) 3C-1.5BP (10k Mag.)

The nucleation and growth of these ettringite crystals, following moisture intrusion, could be a key factor contributing to the increased swelling observed in the 6% cement-treated specimens compared to the 3% cement-treated specimens. Figure 6.14d reveals the formation of a polymer network, although it is noteworthy that after 28 days, this network appears to be incomplete. The formation of both the C-S-H gel and polymer network can be observed in the co-additive specimen in Figure 6.14e, the ettringite crystal formation can also be seen in 3C-1.5BP.

6.5.8 Study on the Effect of the Freeze-thaw (F-T) Cycles

The freeze-thaw (F-T) cycle is a complicated multi-physical process characterized by the flow of pore water due to thermal gradients towards regions of lower temperatures under uniform pressure conditions (Konrad 1989). It is apparent that as the frequency of freeze-thaw cycles increases, a progressive increase in water loss is there, resulting in a fall in the water content of soil samples. This phenomenon is well-documented and primarily attributed to two multi-physical mechanisms: the evaporation of liquid

moisture and the sublimation of solid ice. During thawing, the transformation of surface ice into liquid form occurs gradually, although only a portion of this surface water is drawn back into the samples, driven by the counteracting temperature gradient (Jong and Kachanoski 1988).

The changes in the parameters like water content, volume, and mass of the specimens with F-T cycles were assessed using Equation 6.2.

$$\delta_p = \frac{\Delta P}{P_o} = 100 \times \frac{(P_N - P_o)}{P_o} \quad (6.2)$$

where, δ_p is the comparative changes in the parameters (water content, volume, and mass) measured for the F-T cycles, P_o represents the initial parameter, and P_N is the parameter value after N number of F-T cycles.

Furthermore, Figure 6.15a provides observable evidence that the treatment of samples with cement and biopolymer leads to a significant reduction in moisture content loss. When exposed to F-T cycles, even though the volume of water increases upon freezing, the expansive soil undergoes contraction during freezing and expansion while thawing, due to the presence of available water in liquid form during thawing. This phenomenon is part of a complex thermo-hydro-mechanical process that is influenced by a variety of factors, including the phase change of ice to water, water loss, freezing temperatures, and the initial moisture content at the time of molding (Lu et al. 2019). A plot of volumetric strains against the selected number of F–T cycles is illustrated in Figure 6.15b. It is observed that there is less change in the volume of treated-expansive soil during F-T cycles. The incorporation of cement causes a hydration reaction, which limits the water adsorption capacity of treated soils. Subsequently, the hydration product interacts with the particles of the expansive soil, reducing its swelling and shrinkage tendencies. It can also be noticed that a higher stabilizer dosage corresponds to a smaller volume change, indicating that increased dosages of cement have a beneficial effect. Mass loss serves as a measure of the durability of the treated soil. After brushing off the soil particles that separated from the standard specimens resulting from F-T cycles, the mass of the specimens in each group was recorded. Mass loss gradually increases with each F-T cycle for all groups as shown in Figure 6.15c. The samples treated with 1.5% biopolymer (1.5 BP) exhibited the lowest mass loss, which could be attributed to the effective water retention capability of biopolymer, which helps to prevent desiccation cracks and mass separation during higher F-T cycles.

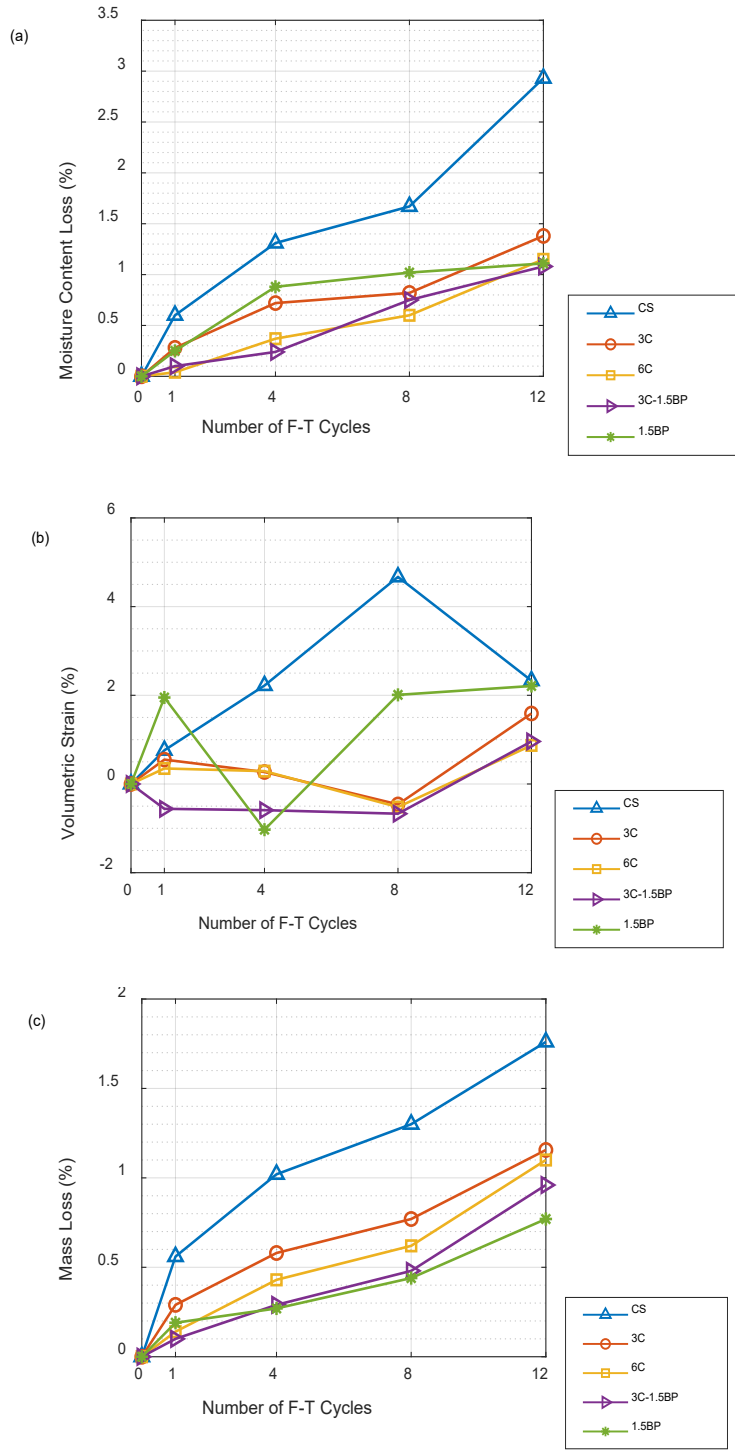


Figure 6.15a. Moisture content loss, **b.** Volumetric strain, and **c.** Mass loss with F-T cycles for untreated and treated soil

The variation of unconfined compressive strength (UCS) of expansive soil samples treated with cement and biopolymer after freeze-thaw (F-T) cycles is depicted in Figure 6.16. The durability of the treated specimens is contingent on their UCS values observed after various F-T cycles. UCS values were documented after the 1st, 4th, 8th, and 12th F-T cycles to gauge the endurance of the treated soil samples.

The presence of cement led to increased strength and stiffness in the specimens by forming a stable spatial network structure (Lu et al. 2019). However, during F-T cycles, the specimens experience non-reversible volumetric changes, causing the bond of calcium silicate hydrate (CSH) gel to break and resulting in a reduction in strength with increasing F-T cycles. It was observed that lower concentrations of cement content yielded less CSH gel, leading to a higher loss of strength. Conversely, higher concentrations of CSH gel produced a robust soil-cement matrix, resulting in minimal UCS strength loss during the F-T cycles. Similarly, the development of hydrogel and polymer networks initially increased the strength, but it was significantly less as compared to the cement-treated soil. The biopolymer addition reduced the decrease in the strain at failure due to the adverse effect of the F-T cycles. This can be attributed to the higher ductility of the biopolymer-treated soil due to the formation of the polymer network and better water retention capacity due to the hydrogel.

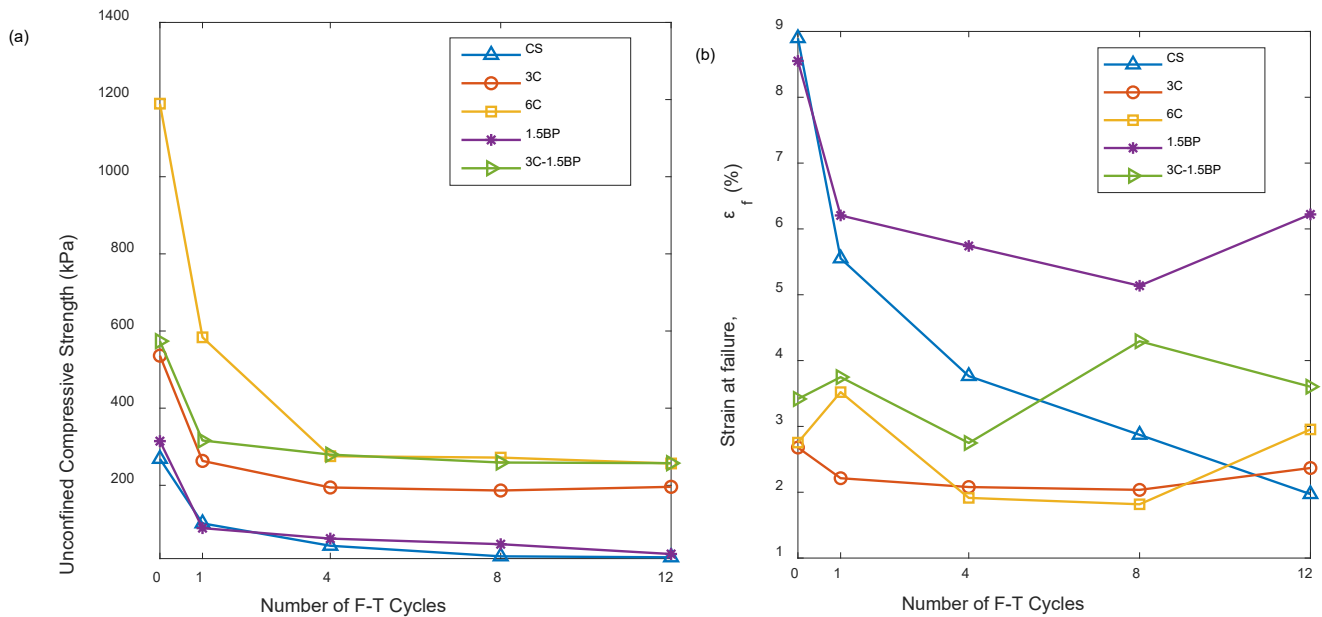


Figure 6.16 Variation of **a.** UCS, and **b.** Strain at failure, ϵ_f with F-T cycles for untreated and treated soil

In this study, RLT tests were conducted to determine the impact of cement and biopolymer treatment on the resilient modulus (M_R) of the soil specimens. The results of the RLT tests for samples subjected to 12 Freeze-Thaw (F-T) cycles were compared with those after 28 days of curing with no F-T cycles. Figure 6.17 illustrates the changes in M_R for the third, eighth, and thirteenth test sequences, considering untreated soil, cement-, and co-additive-stabilized soil, along with the number of F-T cycles. Control samples experienced a reduction in resilient modulus values after exposure to 12 F-T cycles, with an average decrease of 71.2% for the eighth load sequence. The addition of cement significantly improves the resilient modulus of expansive soil, indicating effective cementation between soil particles facilitated by cement hydration products.

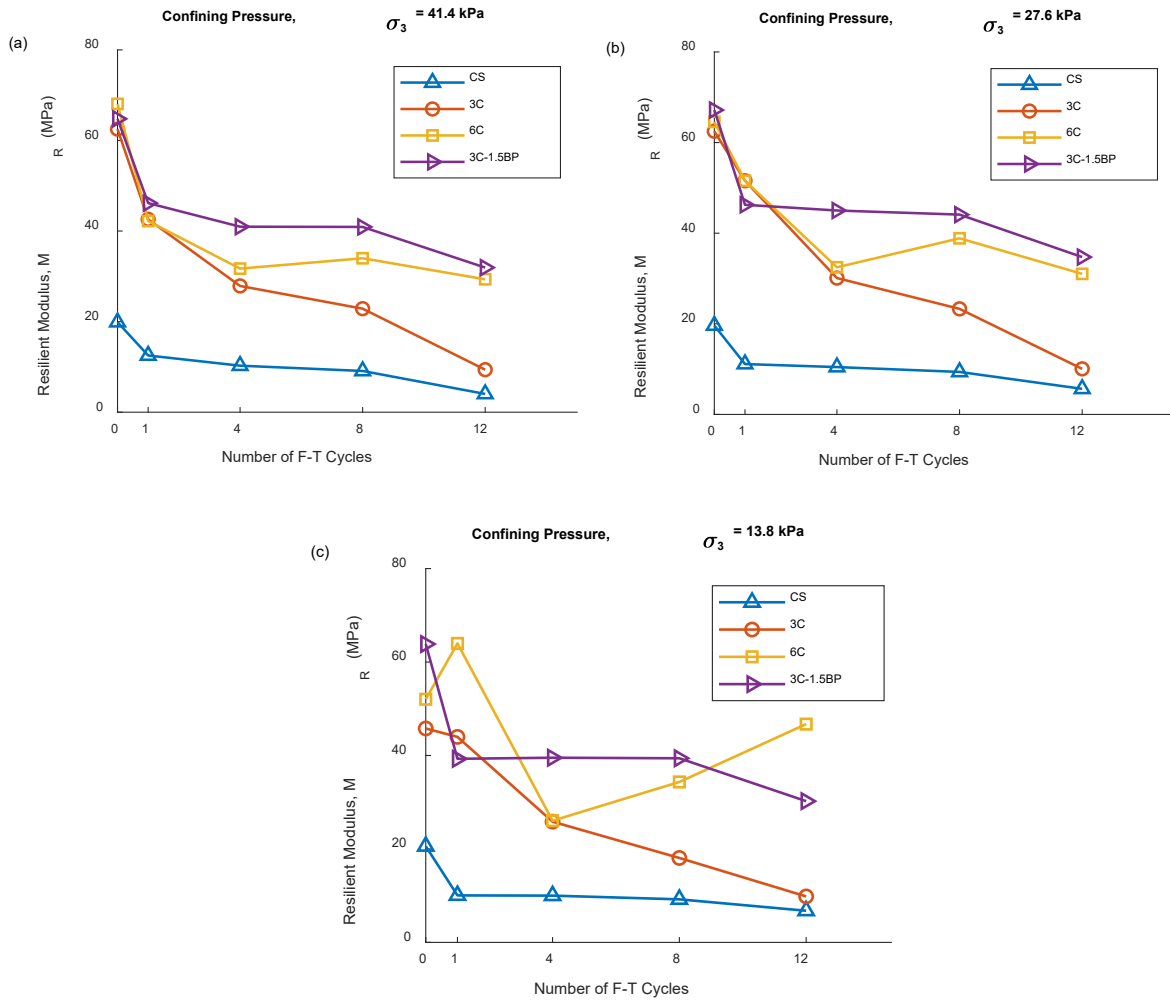


Figure 6.17 Variation of M_R with confining stresses: **a.** 41.4 kPa, **b.** 27.6 kPa, and **c.** 13.8 kPa with F-T cycles for control and treated soil for a peak deviatoric stress of 41.4 kPa

However, the resilient modulus experiences a decline during F-T cycles due to degradation caused by freeze-thaw weathering. Soil treated with higher cement content exhibits a smaller decrease in M_R over a higher number of F-T cycles. Samples treated with co-additives exhibited better resilient modulus performance compared to other treated specimens under freeze-thaw conditions.

6.6 Summary

This study investigated, for the first time, the effects of freezing and thawing processes on the mechanical properties of biopolymer as a co-additive to cement for pavement subgrade applications. Previous studies have mainly concentrated on the behaviors of cement-stabilized soil, and those studies mostly computed the resilient modulus from the UCS strength after F-T cycles using empirical relations. Based on the experimental results and the subsequent discussion, the following conclusions can be drawn:

- The addition of cement and biopolymer proved effective in reducing the plastic characteristics of the sulfate-rich expansive soil. Notably, the study revealed effective stabilization by incorporating 6% cement and 3% cement with 1.5% biopolymer by reducing the plasticity index to less than 18%.
- The UCS of the soil was found to be increasing with the increase in cement content and more than with biopolymer treatment, however, the one-dimensional swelling for 6% cement-treated specimen showed an increase in swelling after a long period due to the probable formation of ettringite which can be observed in FE-SEM images.
- The biopolymer addition as the co-additive made the specimens more ductile, which will allow the subgrade to undergo more deformation without failing under traffic load. This should be explored as a separate study.
- The effectiveness of the incorporation of a biopolymer as a co-additive to cement for the subgrade was verified by determining the resilient modulus (M_R). Among the combinations of stabilizers tested in this experimental program, the co-additive stabilized soil after 28 days of curing was found to have the highest M_R for the 8th test sequence of RLT tests.
- The addition of biopolymer as a co-additive for F-T cycles was found to retain the ductile nature and strength of the specimens after repeated F-T cycles. This might be suitable for levee design where higher ductility would prevent the fully softened state from being reached in biopolymer-stabilized soils.
- The RLT tests on the specimens after repeated F-T cycles were conducted on the control and treated soils. The co-additive stabilized soil can be seen to prevent the degradation of M_R compared to the cement-stabilized soil.

The experimental study found the promising effect of stabilization of subgrade on the resistance against freezing-thawing by the employment of the co-addition of cement and biopolymer. Future investigations regarding the long-term benefits of biopolymer-stabilized soil and soils where both cement and biopolymers are used for stabilization need to be investigated to understand the response of civil infrastructure built on such stabilized soils.

7. CONCLUSIONS

7.1 Findings from the current study

A series of studies were conducted to demonstrate the impact of extreme weather and resulting extreme climatic conditions like droughts and flooding on critical civil infrastructure like dams and levees. This report highlights different aspects of this problem through the need for an unsaturated soil mechanics laboratory with advanced suction-controlled shearing device, repeated load triaxial setup, and other devices to determine the soil water characteristics curve. This problem of addressing extreme weather or designing extreme weather adaptive infrastructure also needs a good understanding of soil chemistry and knowledge of different forms of mechanical, chemical, or biological soil stabilization techniques. Overall, the report presents different studies that highlight the successful installation and calibration of an advanced suction-controlled triaxial device and the use of traditional and novel soil stabilization techniques to stabilize sulfate-rich soils in different climatic conditions. The major findings of this study are stated below.

- To study the effects of extreme weather on earthen civil infrastructure like levees, pavements, and dams, it is essential to understand the difference between saturated and unsaturated soils by considering the mechanics involved in governing the behavior of unsaturated soils.
- A suction-controlled triaxial testing device integrated with an axis-translational technique is able to determine the shear strength of saturated and unsaturated soils which is imperative to understand the variation of shear strength of soils over fluctuations of moisture regime.
- Using axis-translational techniques sandy, silty, and low-plasticity clayey soils may be completely analyzed in a suction-controlled triaxial system, however, the higher suction levels as induced in high-plasticity clayey soils may be beyond the current standards of suction control in triaxial systems.
- During extreme climatic conditions, such as prolonged droughts, slopes built with expansive soil tend to form desiccation cracks due to the shrinkage of soil. With subsequent precipitation, the stability of the slope was found to be reduced due to the formation of the desiccated surface layer which allowed water to penetrate through the cracks to deeper layers and form a weakened layer.
- Extreme weather prediction models were used and a 23% increase in the maximum daily precipitation and a 31% increase in the number of extreme precipitation events for SSP5-8.5 at the end of the century compared to historical precipitation between 1981 and 2010 was observed. In the future, the intensity of precipitation is predicted to be higher, with shorter intervals between the occurrence of extreme precipitation events. This may result in higher stresses in civil infrastructure such as embankments as compared to the original designs. The cyclic wetting and drying of critical infrastructure due to such anticipated extreme events should be considered for analysis and design.
- The addition of cement and biopolymer proved effective in reducing the plastic characteristics and increased the strength of the sulfate-rich expansive soil. Notably, the study revealed effective stabilization by incorporating 6% cement and 3% cement with 1.5% biopolymer by reducing the plasticity index to less than 18%.
- The biopolymer addition as the co-additive made the specimens more ductile, which will induce the property to undergo deformation more without failing to subgrade of pavement under traffic load. This should be explored as a separate study.

- The effectiveness of the incorporation of a biopolymer as a co-additive to cement for the subgrade was verified by determining the resilient modulus (M_R).
- The addition of biopolymer as a co-additive for F-T cycles was found to retain the ductile nature and strength of the specimens after repeated F-T cycles. This might be suitable for levee design where higher ductility would prevent the fully softened state from being reached in biopolymer-stabilized soils.

7.2 Recommendations for Future studies

The following studies are recommended for the future to enhance our understanding of the impacts of extreme weather on civil infrastructure and identify ways to develop a sustainable and resilient design of extreme weather adaptive system.

- The development of advanced systems to control suction beyond 1.5 MPa may be required for high-plasticity clayey soils.
- Additional studies need to be conducted to understand the impact of other parameters such as temperature and solar radiation for different scenarios of extreme weather to quantify the potential impact of extreme weather on the resilience of earthen structures in different regions. Subsequently, sustainable measures need to be investigated and implemented to mitigate such issues by the end of the century. The incorporation of thermal and environmental stresses caused by extreme weather should be considered in the design of new structures, as such change is expected to have a negative impact on earthen infrastructures like dams, levees, and pavements throughout their lifespan.
- The experimental study found the promising effect of stabilization of subgrade on the resistance against freezing-thawing by the employment of the co-addition of cement and biopolymer. Future investigations regarding the long-term benefits of biopolymer-stabilized soil and soils where both cement and biopolymers are used for stabilization need to be investigated to understand the response of civil infrastructure built on such stabilized soils.

8. REFERENCES

- AASHTO. 2008. *Mechanistic-empirical pavement design guide: a manual of practice*. Washington, DC.
- AASHTO T307-99. 2003. *Standard Method of Test for Determining the Resilient Modulus of Soils and Aggregate Materials*. Washington, DC.
- Acharya, R., A. Pedarla, T. V. Bheemasetti, and A. J. Puppala. 2017. "Assessment of Guar Gum Biopolymer Treatment toward Mitigation of Desiccation Cracking on Slopes Built with Expansive Soils." *Transportation Research Record: Journal of the Transportation Research Board*, 2657 (1): 78–88. <https://doi.org/10.3141/2657-09>
- Ahangar-Asr, A., A. Johari, and A. A. Javadi. 2012. "An evolutionary approach to modelling the soil–water characteristic curve in unsaturated soils." *Comput Geosci*, 43: 25–33. Elsevier. <https://doi.org/10.1016/j.cageo.2012.02.021>
- Almazroui, M., M. N. Islam, F. Saeed, et al., J. D. Campbell, S. Kamil, I. U. Rashid, M. B. Sylla, T. Stephenson, M. Taylor, and M. Barlow. 2021. "Projected Changes in Temperature and Precipitation Over the United States, Central America, and the Caribbean in CMIP6 GCMs." *Earth Systems and Environment*, 5 (1): 1–24. <https://doi.org/10.1007/s41748-021-00199-5>
- Alonso, E. E., A. Gens, and C. H. Delahaye. 2003. "Influence of rainfall on the deformation and stability of a slope in overconsolidated clays: A case study." *Hydrogeol J*, 11 (1): 174–192. <https://doi.org/10.1007/s10040-002-0245-1>
- Alonso, E. E., A. Gens, and A. Josa. 1990. "A constitutive model for partially saturated soils." *Géotechnique*, 40 (3): 405–430. <https://doi.org/10.1680/geot.1990.40.3.405>
- Alonso, E. E., E. Romero, C. Hoffmann, and E. García-Escudero. 2005. "Expansive bentonite-sand mixtures in cyclic controlled-suction drying and wetting." *Eng Geol*, 81 (3): 213–226. <https://doi.org/10.1016/j.enggeo.2005.06.009>
- ASTM D6836-16. 2016. "Standard Test Methods for Determination of the Soil Water Characteristic Curve for Desorption Using Hanging Column, Pressure Extractor, Chilled Mirror Hygrometer, or Centrifuge." ASTM International, West Conshohocken, PA.
- Ayeldeen, M., and M. Kitazume. 2017. "Using fiber and liquid polymer to improve the behaviour of cement-stabilized soft clay." *Geotextiles and Geomembranes*, 45 (6): 592–602. <https://doi.org/10.1016/j.geotexmem.2017.05.005>
- Banerjee, A. 2017. "Response of Unsaturated Soils under Monotonic and Dynamic Loading over moderate Suction States." Doctoral Dissertation. Department of Civil Engineering, University of Texas at Arlington, Arlington, Texas
- Banerjee, A., A. J. Puppala, S. S. C. Congress, S. Chakraborty, W. J. Likos, and L. R. Hoyos. 2020a. "Variation of Resilient Modulus of Subgrade Soils over a Wide Range of Suction States." *Journal of Geotechnical and Geoenvironmental Engineering*, 146 (9). [https://doi.org/10.1061/\(ASCE\)GT.1943-5606.0002332](https://doi.org/10.1061/(ASCE)GT.1943-5606.0002332)
- Banerjee, A., A. J. Puppala, S. S. C. Congress, Chakraborty S., and A. Pedarla. 2021. "Recent Advancements in Predicting the Behavior of Unsaturated and Expansive Soils." *Lecture Notes in Civil Engineering*, Patel et al., ed., 1–21. Singapore: Springer
- Banerjee, A., A. J. Puppala, and L. R. Hoyos. 2020b. "Suction-controlled multistage triaxial testing on clayey silty soil." *Eng Geol*, 265. <https://doi.org/10.1016/j.enggeo.2019.105409>

- Banerjee, A., A. J. Puppala, L. R. Hoyos, W. J. Likos, and U. D. Patil. 2020c. “Resilient Modulus of Expansive Soils at High Suction Using Vapor Pressure Control.” *Geotechnical Testing Journal*, 43 (3): 720–736. <https://doi.org/10.1520/GTJ20180255>
- Bishop, A. W. 1959. “The principal of effective stress.” *Teknisk ukeblad*, 39: 859–863.
- Bishop, A. W., and D. J. Henkel. 1962. *The measurement of soil properties in the triaxial test*. London: E. Arnold.
- Bishop, A. W., and G. E. Blight. 1963. “Some Aspects of Effective Stress in Saturated and Partly Saturated Soils.” *Géotechnique*, 13 (3): 177–197. <https://doi.org/10.1680/geot.1963.13.3.177>
- Bishop, A. W., and B. I. Donald. 1961. “The experimental study of partly saturated soil in the triaxial apparatus.” *Proc. 5th International Conference on Soil Mechanics and Foundation Engineering, Paris, France*, 13–21. Paris, France.
- Biswas, N., A. J. Puppala, and S. Chakraborty. 2023. “Role of Nano- and Crystalline Silica to Accelerate Chemical Treatment of Problematic Soil.” *Journal of Geotechnical and Geoenvironmental Engineering*, 149 (7). <https://doi.org/10.1061/JGGEFK.GTENG-10999>
- Biswas, N., A. J. Puppala, M. A. Khan, S. S. C. Congress, A. Banerjee, and S. Chakraborty. 2021. “Evaluating the performance of wicking geotextile in providing drainage for flexible pavements built over expansive soils.” *Transp Res Rec*, 208–221
- Blatz, J., and J. Graham. 2000. “A system for controlled suction in triaxial tests.” *Geotechnique*, 50 (4): 465–469. <https://doi.org/10.1680/geot.2000.50.4.465>
- Bocking, K. A., and D. G. Fredlund. 1980. “Limitations of the axis translation technique.” *Proceedings 4th International Conference on Expansive Soil*.
- Bouazza, A., W. P. Gates, and P. G. Ranjith. 2009. “Hydraulic conductivity of biopolymer-treated silty sand.” *Géotechnique*, 59 (1): 71–72. <https://doi.org/10.1680/geot.2007.00137>
- Bozyigit, I., H. O. Zingil, and S. Altun. 2023. “Performance of eco-friendly polymers for soil stabilization and their resistance to freeze–thaw action.” *Constr Build Mater*, 379 (March): 131133. Elsevier Ltd. <https://doi.org/10.1016/j.conbuildmat.2023.131133>
- Bugge, W. A., and R. R. . Bartelsmeyer. 1961. *Soil Stabilization with Portland Cement. Highway Research Board*.
- Burrage, R. E., J. B. Anderson, M. A. Pando, V. O. Ogunro, and M. A. Cottingham. 2012. “A Cost Effective Triaxial Test Method for Unsaturated Soils.” *Geotechnical Testing Journal*, 35 (1): 50–59. <https://doi.org/10.1520/GTJ103600>
- Cabarkapa, Z., and T. Cuccovillo. 2006. “Automated Triaxial Apparatus for Testing Unsaturated Soils.” *Geotechnical Testing Journal*, 29 (1): 21–29. <https://doi.org/10.1520/GTJ12310>
- Cary, C. E., and C. E. Zapata. 2011. “Resilient Modulus for Unsaturated Unbound Materials.” *Road Materials and Pavement Design*, 12 (3): 615–638. <https://doi.org/10.1080/14680629.2011.9695263>
- Chakraborty, S., A. J. Puppala, and N. Biswas. 2022. “Role of crystalline silica admixture in mitigating ettringite-induced heave in lime-treated sulfate-rich soils.” *Géotechnique*, 72 (5): 438–454. <https://doi.org/10.1680/jgeot.20.P.154>
- Chang, I., and G. C. Cho. 2019. “Shear strength behavior and parameters of microbial gellan gum-treated soils: from sand to clay.” *Acta Geotech*, 14 (2): 361–375. Springer Berlin Heidelberg. <https://doi.org/10.1007/s11440-018-0641-x>
- Chang, I., J. Im, A. K. Prasadhi, and G.-C. Cho. 2015. “Effects of Xanthan gum biopolymer on soil strengthening.” *Constr Build Mater*, 74: 65–72. <https://doi.org/10.1016/j.conbuildmat.2014.10.026>

- Chang, I., M. Lee, A. T. P. Tran, S. Lee, Y. M. Kwon, J. Im, and G. C. Cho. 2020. "Review on biopolymer-based soil treatment (BPST) technology in geotechnical engineering practices." *Transportation Geotechnics*, 24 (June). <https://doi.org/10.1016/j.trgeo.2020.100385>
- Chen, R., L. Zhang, and M. Budhu. 2013. "Biopolymer Stabilization of Mine Tailings." *Journal of Geotechnical and Geoenvironmental Engineering*, 139 (10): 1802–1807. [https://doi.org/10.1061/\(ASCE\)GT.1943-5606.0000902](https://doi.org/10.1061/(ASCE)GT.1943-5606.0000902)
- Chiu, C. F., and C. W. W. Ng. 2003. "A state-dependent elasto-plastic model for saturated and unsaturated soils." *Géotechnique*, 53 (9): 809–829. <https://doi.org/10.1680/geot.2003.53.9.809>
- Cho, S. E., and S. R. Lee. 2002. "Evaluation of Surficial Stability for Homogeneous Slopes Considering Rainfall Characteristics." *Journal of Geotechnical and Geoenvironmental Engineering*, 128 (9): 756–763. [https://doi.org/10.1061/\(ASCE\)1090-0241\(2002\)128:9\(756\)](https://doi.org/10.1061/(ASCE)1090-0241(2002)128:9(756))
- Church, M., and M. J. Miles. 1987. "Meteorological antecedents to debris flow in southwestern British Columbia; Some case studies." *Reviews in Engineering Geology, Vol. VII - Debris Flows/Avalanches: Process, Recognition, and Mitigation.*, Reviews in Engineering Geology, J. E. Costa and G. F. Wiczeorek, eds., 63–80. Boulder, Colorado, USA: Geological Society of America
- Coulomb, C. A. 1776. "Essai sur une application des règles de maximis et minimis a` quelques proble`mes de statique relatifs a` l'architecture." *Mem. Math. Phys. Acad. R. Sci. Paris*, 7: 343–382
- Croft, J. B. 1967. "The Influence of Soil Mineralogical Composition on Cement Stabilization." *Géotechnique*, 17 (2): 119–135. <https://doi.org/10.1680/geot.1967.17.2.119>
- Croney, D., and J. D. Coleman. 1954. "Soil structure in relation to soil suction (pF)." *Journal of Soil Science*, 5 (1): 75–84. <https://doi.org/10.1111/j.1365-2389.1954.tb02177.x>
- Cui, Y. J., and P. Delage. 1996. "Yielding and plastic behaviour of an unsaturated compacted silt." *Géotechnique*, 46 (2): 291–311. <https://doi.org/10.1680/geot.1996.46.2.291>
- Dehghan, H., A. Tabarsa, N. Latifi, and Y. Bagheri. 2019. "Use of xanthan and guar gums in soil strengthening." *Clean Technol Environ Policy*, 21 (1): 155–165. Springer Berlin Heidelberg. <https://doi.org/10.1007/s10098-018-1625-0>
- Dronamraju, V. S. 2008. "Studies on Field Stabilization Methods to Prevent Surficial Slope Failures of Earthfill Dams." Doctoral Dissertation, Department of Civil and Environmental Engineering, The University of Texas at Arlington, Arlington, TX.
- Edlefsen, N. E., and A. B. C. Anderson. 1943. "Thermodynamics of soil moisture." *Hilgardia*, 15 (2): 31–298. <https://doi.org/10.3733/hilg.v15n02p031>
- Escario, V., and J. Sáez. 1986. "The shear strength of partly saturated soils." *Géotechnique*, 36 (3): 453–456. <https://doi.org/10.1680/geot.1986.36.3.453>
- Fatehi, H., D. E. L. Ong, J. Yu, and I. Chang. 2021. "Biopolymers as Green Binders for Soil Improvement in Geotechnical Applications: A Review." *Geosciences (Basel)*, 11 (7): 291. <https://doi.org/10.3390/geosciences11070291>
- Fredlund, D. G. 1973. "Volume Change Behavior of Unsaturated Soils." Doctoral Dissertation. University of Alberta, Edmonton, Alberta, Canada.
- Fredlund, D. G. 1987. "The stress state for expansive soils." *Proc. 6th Int. Conf. on Expansive Soils, Keynote Address*, 1–9. New Delhi, India.

- Fredlund, D. G. 2000. "The 1999 R.M. Hardy Lecture: The implementation of unsaturated soil mechanics into geotechnical engineering." *Canadian Geotechnical Journal*, 37 (5): 963–986.
<https://doi.org/10.1139/t00-026>
- Fredlund, D. G., and N. R. Morgenstern. 1977. "Stress State Variables for Saturated and Unsaturated Soils." *Journal of Geotechnical and Geoenvironmental Engineering*, 103 (5): 447–466.
[https://doi.org/doi:10.1061/40802\(189\)202](https://doi.org/doi:10.1061/40802(189)202)
- Fredlund, D. G., and H. Rahardjo. 1993. *Soil Mechanics for Unsaturated Soils*. New York: Wiley.
- Fredlund, D. G., H. Rahardjo, and M. D. Fredlund. 2012. *Unsaturated Soil Mechanics in Engineering Practice*. Hoboken, New Jersey: John Wiley and Sons, Inc.
- Fredlund, D. G., and A. Xing. 1994. "Equations for the soil-water characteristic curve." *Canadian Geotechnical Journal*, 31 (4): 521–532. <https://doi.org/10.1139/t94-061>
- Gallipoli, D., a. Gens, R. Sharma, and J. Vaunat. 2003. "An elasto-plastic model for unsaturated soil incorporating the effects of suction and degree of saturation on mechanical behaviour." *Géotechnique*, 44 (June): 123–135. <https://doi.org/10.1680/geot.53.1.123.37251>
- van Genuchten, M. T. 1980. "A Closed-form Equation for Predicting the Hydraulic Conductivity of Unsaturated Soils1." *Soil Science Society of America Journal*, 44 (5): 892.
<https://doi.org/10.2136/sssaj1980.03615995004400050002x>
- Ghosh, D., and A. Banerjee. 2025. "Microscale and Macroscale characterization of biopolymer-stabilized sulfate-rich expansive soils" *ASCE Journal of Materials in Civil Engineering*, 37(5), doi: 10.1061/JMCEE7/MTENG-18188
- Ghosh, D., and A. Banerjee. 2024. "Uncovering the Impact of Freeze–Thaw Cycles on Resilient Modulus of Cement-Stabilized Sulfate-Rich Subgrade Soil." *Proc. Cold Regions Engineering 2024*, 484–494. Reston, VA: American Society of Civil Engineers. <https://doi.org/10.1061/9780784485460.045>
- Ghosh, D., A. Banerjee, S. Chakraborty, and U. D. Patil. 2024. "Impact of Biopolymers on Slope Stability of an Embankment in Steady and Transient States." *Proc. IFCEE 2024*, 61–70. Reston, VA: American Society of Civil Engineers. <https://doi.org/10.1061/9780784485415.007>
- Giancoli, D. C. 1985. *Physics: Principles with Applications*. Englewood Cliffs, N.J.: Prentice-Hall.
- Gibbs, J. 1873. "A Method of Geometrical Representation of the Thermodynamic Properties of Substances by Means of Surfaces." *Transactions of the Connecticut Academy of Arts and Sciences*, 382–404
- Giorgi, F., and X.-J. Gao. 2018. "Regional earth system modeling: review and future directions." *Atmospheric and Oceanic Science Letters*, 11 (2): 189–197.
<https://doi.org/10.1080/16742834.2018.1452520>
- Goodarzi, A. R., H. R. Akbari, and M. Salimi. 2016. "Enhanced stabilization of highly expansive clays by mixing cement and silica fume." *Appl Clay Sci*, 132–133: 675–684.
<https://doi.org/10.1016/j.clay.2016.08.023>
- Gould, S., P. Rajeev, J. Kodikara, X.-L. Zhao, S. Burn, and D. Marlow. 2012. "A New Method for Developing Equations Applied to the Water Retention Curve." *Soil Science Society of America Journal*, 6 (3): 806–814. The Soil Science Society of America, Inc.
<https://doi.org/10.2136/sssaj2011.0260>

- Gross, J., and W. Adaska. 2020. *Guide to Cement Stabilized Subgrade Soils*. PCA Special Report SR1007P, Washington, DC: Portland Cement Association.
- Gulhati, S. K. , and D. J. Satija. 1981. “Shear Strength of Partially Saturated Soils.” *Proc. 10th International Conference on Soil Mechanics and Foundation Engineering*, Vol.1, 609-612. Stockholm, Sweden.
- He, S., X. Yu, A. Banerjee, and A. J. Puppala. 2018. “Expansive Soil Treatment with Liquid Ionic Soil Stabilizer.” *Transportation Research Record: Journal of the Transportation Research Board*, 2672 (52): 185–194. <https://doi.org/10.1177/0361198118792996>
- Hilf, J. W. 1956. “An investigation of Pore-Water pressure in compacted cohesive soils.” University of Colorado, Boulder.
- Holtz, R. D., and W. D. Kovacs. 1981. *Introduction to Geotechnical Engineering*. Prentice-Hall, Inc.
- Houston, S. L., N. Perez-Garcia, and W. N. Houston. 2008. “Shear Strength and Shear-Induced Volume Change Behavior of Unsaturated Soils from a Triaxial Test Program.” *Journal of Geotechnical and Geoenvironmental Engineering*, 134 (11): 1619–1632. [https://doi.org/10.1061/\(ASCE\)1090-0241\(2008\)134:11\(1619\)](https://doi.org/10.1061/(ASCE)1090-0241(2008)134:11(1619))
- Houston, W. N., H. B. Dye, C. E. Zapata, Y. Y. Perera, and A. Harraz. 2006. “Determination of SWCC Using One Point Suction Measurement and Standard Curves.” *Unsaturated Soils 2006*, 1482–1493. Reston, VA: American Society of Civil Engineers.
- Hoyos, L. R. 1998. “Experimental and computational modeling of unsaturated soil behavior under true triaxial stress states.” Doctoral Dissertation. Georgia Institute of Technology, Atlanta, Georgia.
- Im, J., A. T. P. Tran, I. Chang, and G. C. Cho. 2017. “Dynamic properties of gel-type biopolymer-treated sands evaluated by resonant column (RC) tests.” *Geomechanics and Engineering*, 12 (5): 815–830. <https://doi.org/10.12989/gae.2017.12.5.815>
- Ishikawa, T., T. Tokoro, K. Ito, and S. Miura. 2010. “Testing methods for hydro-mechanical characteristics of unsaturated soils subjected to one-dimensional freeze-thaw action.” *Soil Science Society of America Journal*, 50 (3): 431–440. <https://doi.org/10.3208/sandf.50.431>
- Ishikawa, T., Y. Zhang, T. Tokoro, and S. Miura. 2014. “Medium-size triaxial apparatus for unsaturated granular subbase course materials.” *Soils and Foundations*. <https://doi.org/10.1016/j.sandf.2013.12.007>
- Ivanov, V., and J. Chu. 2008. “Applications of microorganisms to geotechnical engineering for bioclogging and biocementation of soil in situ.” *Rev Environ Sci Biotechnol*, 7 (2): 139–153. <https://doi.org/10.1007/s11157-007-9126-3>
- Jang, J., N. Biswas, A. J. Puppala, S. S. C. Congress, M. Radovic, and O. Huang. 2022. “Evaluation of Geopolymer for Stabilization of Sulfate-Rich Expansive Soils for Supporting Pavement Infrastructure.” *Transp Res Rec*, 2676 (9): 230–245. <https://doi.org/10.1177/03611981221086650>
- Jennings, J. E. B., and J. B. Burland. 1962. “Limitations to the Use of Effective Stresses in Partly Saturated Soils.” *Géotechnique*, 12 (2): 125–144. <https://doi.org/10.1680/geot.1962.12.2.125>
- Jong, E. de, and R. G. Kachanoski. 1988. “Drying of Frozen Soils.” *Can J Soil Sci*, 68 (4): 807–811. <https://doi.org/10.4141/cjss88-079>

- Kayadelen, C., O. Sivrikaya, T. Taşkıran, and H. Güneyli. 2007. “Critical-state parameters of an unsaturated residual clayey soil from Turkey.” *Eng Geol*, 94 (1–2): 1–9. <https://doi.org/10.1016/j.enggeo.2007.05.008>
- Khalili, N., and M. H. Khabbaz. 2002. “A unique relationship for chi for the determination of the shear strength of unsaturated soils.” *Geotechnique*, 52 (1): 76–77
- Khosravi, A., N. Alsherif, C. Lynch, and J. McCartney. 2011. “Multistage Triaxial Testing to Estimate Effective Stress Relationships for Unsaturated Compacted Soils.” *Geotechnical Testing Journal*, 35 (1): 1–7
- Kim, D., and N. Siddiki. 2006. *Simplification of Resilient Modulus Testing for Subgrades*. West Lafayette, IN
- Kim, T.-H., and S. Sture. 2008. “Capillary-induced tensile strength in unsaturated sands.” *Canadian Geotechnical Journal*, 45 (5): 726–737. <https://doi.org/10.1139/T08-017>
- Konrad, J. M. 1989. “Physical processes during freeze-thaw cycles in clayey silts.” *Cold Reg Sci Technol*, 16 (3): 291–303. [https://doi.org/10.1016/0165-232X\(89\)90029-3](https://doi.org/10.1016/0165-232X(89)90029-3)
- Kumar, P., A. Banerjee, S. S. Chandra Congress, and A. J. Puppala. 2021. “Effect of Future Extreme Precipitation on Expansive Soil Embankments.” *IFCEE 2021*, 255–266. Reston, VA: American Society of Civil Engineers
- Ladd, R. 1978. “Preparing Test Specimens Using Undercompaction.” *Geotechnical Testing Journal*, 1 (1): 16–23. <https://doi.org/10.1520/GTJ10364J>
- Laloui, L. 2010. *Mechanics of Unsaturated Geomaterials*. London and New York: ISTE and John Wiley & Sons, Inc
- Latifi, N., S. Horpibulsuk, C. L. Meehan, M. Z. Abd Majid, M. M. Tahir, and E. T. Mohamad. 2017. “Improvement of Problematic Soils with Biopolymer—An Environmentally Friendly Soil Stabilizer.” *Journal of Materials in Civil Engineering*, 29 (2). [https://doi.org/10.1061/\(ASCE\)MT.1943-5533.0001706](https://doi.org/10.1061/(ASCE)MT.1943-5533.0001706)
- Leong, E. C., T. T. Nyunt, and H. Rahardjo. 2013. “Triaxial Testing of Unsaturated Soils.” *Multiphysical Testing of Soils and Shales*, Springer Series in Geomechanics and Geoengineering, L. Laloui and A. Ferrari, eds., 33–44. Berlin, Heidelberg: Springer Berlin Heidelberg
- Leong, E. C., and H. Rahardjo. 1997. “Review of Soil-Water Characteristic Curve Equations.” *Journal of Geotechnical and Geoenvironmental Engineering*, 123 (12): 1106–1117
- Leshchinsky, B., F. Vahedifard, H. B. Koo, and S. H. Kim. 2015. “Yumokjeong Landslide: an investigation of progressive failure of a hillslope using the finite element method.” *Landslides*, 12 (5): 997–1005. <https://doi.org/10.1007/s10346-015-0610-5>
- Li, L., and X. Zhang. 2015. “A new triaxial testing system for unsaturated soil characterization.” *Geotechnical Testing Journal*, 38 (6): 823–839. <https://doi.org/10.1520/GTJ20140201>
- Li, L., X. Zhang, G. Chen, and R. Lytton. 2015. “Measuring Unsaturated Soil Deformations during Triaxial Testing Using A Photogrammetry-Based Method.” *Canadian Geotechnical Journal*, 53 (3): 472–489. <https://doi.org/10.1139/cgj-2015-0038>
- Likos, W., and N. Lu. 2003. “Automated Humidity System for Measuring Total Suction Characteristics of Clay.” *Geotechnical Testing Journal*, 26 (2): 179–190. <https://doi.org/10.1520/GTJ11321J>
- Little, D., B. Herbert, and S. Kunagalli. 2005. “Ettringite Formation in Lime-Treated Soils: Establishing Thermodynamic Foundations for Engineering Practice.” *Transportation Research Record: Journal of the Transportation Research Board*, 1936 (1): 51–59. <https://doi.org/10.3141/1936-07>

- Little, D. N., and S. Nair. 2009. *Recommended Practice for Stabilization of Sulfate-Rich Subgrade Soils*. Washington, D.C.: Transportation Research Board
- Liu, C., C. Berard, and L. Deng. 2023. “Engineering behavior of cement-treated stiff clay subjected to freezing/thawing cycles.” *Cold Reg Sci Technol*, 206 (December 2022): 103743. Elsevier B.V. <https://doi.org/10.1016/j.coldregions.2022.103743>
- Ltifi, M., T. Abichou, and J. P. Tisot. 2014. “Effects of Soil Aging on Mechanical and Hydraulic Properties of a Silty Soil.” *Geotechnical and Geological Engineering*, 32 (4): 1101–1108. <https://doi.org/10.1007/s10706-014-9784-1>
- Lu, N., T.-H. Kim, S. Sture, and W. J. Likos. 2009. “Tensile Strength of Unsaturated Sand.” *J Eng Mech*, 135 (12): 1410–1419. [https://doi.org/10.1061/\(ASCE\)EM.1943-7889.0000054](https://doi.org/10.1061/(ASCE)EM.1943-7889.0000054)
- Lu, N., and W. J. Likos. 2004. *Unsaturated Soil Mechanics*. Hoboken, N.J.: J. Wiley.
- Lu, N., and W. J. Likos. 2006. “Suction Stress Characteristic Curve for Unsaturated Soil.” *Journal of Geotechnical and Geoenvironmental Engineering*, 132 (2): 131–142. [https://doi.org/10.1061/\(ASCE\)1090-0241\(2006\)132:2\(131\)](https://doi.org/10.1061/(ASCE)1090-0241(2006)132:2(131))
- Lu, Y., S. Liu, E. Alonso, L. Wang, L. Xu, and Z. Li. 2019. “Volume changes and mechanical degradation of a compacted expansive soil under freeze-thaw cycles.” *Cold Reg Sci Technol*, 157 (October 2018): 206–214. <https://doi.org/10.1016/j.coldregions.2018.10.008>
- Lu, Y., S. Liu, Y. Zhang, Z. Li, and L. Xu. 2020. “Freeze-thaw performance of a cement-treated expansive soil.” *Cold Reg Sci Technol*, 170 (October 2019): 102926. Elsevier. <https://doi.org/10.1016/j.coldregions.2019.102926>
- Ma, T., C. Wei, H. Wei, and W. Li. 2016. “Hydraulic and Mechanical Behavior of Unsaturated Silt: Experimental and Theoretical Characterization.” *International Journal of Geomechanics*, 16 (6). [https://doi.org/10.1061/\(ASCE\)GM.1943-5622.0000576](https://doi.org/10.1061/(ASCE)GM.1943-5622.0000576)
- Manzanal, D., J. A. Fernández Merodo, and M. Pastor. 2011. “Generalized plasticity state parameter-based model for saturated and unsaturated soils. Part II: Unsaturated soil modeling.” *Int J Numer Anal Methods Geomech*, 35: 1899–1917. <https://doi.org/10.1002/nag.983>
- Marshall, C. E. 1964. *The Physical Chemistry and Mineralogy of Soils. Vol. 1: Soil Materials*. New York: Wiley.
- McCleskey, L. K., A. J. Puppala, S. V Dronamraju, and L. Perrin. 2008. “Remedial Measures Planned to Prevent Surficial Failures.” *GeoEdmonton*, 21–24. Edmonton, Alberta: Canadian Geotechnical Society.
- Meinshausen, M., Z. R. J. Nicholls, J. Lewis, M. J. Gidden, E. Vogel, et al. (2020). The shared socio-economic pathway (SSP) GHG concentrations and their extensions to 2500. *Geoscientific Model Development*, 13(8), 3571–3605. <https://doi.org/10.5194/gmd-13-3571-2020>
- Mitchell, J. K., and K. Soga. 2005. *Fundamentals of Soil Behavior*. Hoboken, New Jersey: John Wiley & Sons
- Moazami, D., and R. Muniandy. 2021. “Determination of rutting performance of asphalt pavements considering realistic tire-pavement contact area.” *International Journal of Pavement Research and Technology*, 14 (6): 764–770. <https://doi.org/10.1007/s42947-020-0187-9>
- Moghal, A. A. B., and K. V. Vydehi. 2021. “State-of-the-art review on efficacy of xanthan gum and guar gum inclusion on the engineering behavior of soils.” *Innovative Infrastructure Solutions*, 6 (2). <https://doi.org/10.1007/s41062-021-00462-8>
- Morgenstern, N. R., and V. E. Price. 1965. “The Analysis of the Stability of General Slip Surfaces.” *Géotechnique*, 15 (1): 79–93. <https://doi.org/10.1680/geot.1965.15.1.79>

- Mudgil, D., S. Barak, and B. S. Khatkar. 2014. "Guar gum: processing, properties and food applications—A Review." *J Food Sci Technol*, 51 (3): 409–418. <https://doi.org/10.1007/s13197-011-0522-x>
- Murray, E. J., and V. Sivakumar. 2010. *Unsaturated Soils: A fundamental interpretation of soil behaviour*. John Wiley & Sons.
- Nazzal, M. D., and L. N. Mohammad. 2010. "Estimation of Resilient Modulus of Subgrade Soils for Design of Pavement Structures." *Journal of Materials in Civil Engineering*, 22 (7): 726–734. [https://doi.org/10.1061/\(asce\)mt.1943-5533.0000073](https://doi.org/10.1061/(asce)mt.1943-5533.0000073)
- NCHRP. 2004. *Guide for Mechanistic-Empirical Design of New and Rehabilitated Pavement Structures, Part2; Design Inputs, NCHRP 1-37A, Final Report*.
- Nelson, J. D., and D. J. Miller. 1997. *Expansive Soils: problems and practice in foundation and pavement engineering*. John Wiley & Sons.
- Ng, C. W. W., Y. Cui, R. Chen, and P. Delage. 2007. "The axis-translation and osmotic techniques in shear testing of unsaturated soils: A comparison." *Soils and Foundations*, 47 (4): 675–684. <https://doi.org/10.3208/sandf.47.675>
- Ng, C. W. W., L. T. Zhan, and Y. J. Cui. 2002. "A new simple system for measuring volume changes in unsaturated soils." *Canadian Geotechnical Journal*, 39 (3): 757–764. <https://doi.org/10.1139/t02-015>
- Nishimura, S. 2021. "A model for freeze-thaw-induced plastic volume changes in saturated clays." *Soils and Foundations*, 61 (4): 1054–1070. <https://doi.org/10.1016/j.sandf.2021.05.008>
- Nishiumura, T., J. Koseki, D. Fredlund, and H. Rahardjo. 2012. "Microporous Membrane Technology for Measurement of Soil-Water Characteristic Curve." *Geotechnical Testing Journal*, 35 (1): 1–8. <https://doi.org/10.1520/GTJ103670>
- Olive, W. W., A. F. Chleborad, C. W. Frahme, J. Schlocker, R. R. Schneider, and R. L. Schuster. 1989. *Swelling clays Map of the Conterminous United States*. Reston, VA.
- Olson, R. E., and L. J. Langfelder. 1965. "Pore Water Pressures in Unsaturated Soils." *Journal of the Soil Mechanics and Foundations Division*, 91 (4): 127–150. <https://doi.org/10.1061/JSFEAQ.0000753>
- O'Neill, B. C., J. Lamarque, and D. Lawrence. 2014. "Developing Climate Model Comparisons." *Eos, Transactions American Geophysical Union*, 95 (49): 462–462. <https://doi.org/10.1002/2014EO490008>
- Pathania, D., R. Katwal, and G. Sharma. 2016. "Fabrication, Characterization and Cytotoxicity of Guar Gum/Copper Oxide Nanocomposite: Efficient Removal of Organic Pollutant." *Materials Science Forum*, 842: 88–102. <https://doi.org/10.4028/www.scientific.net/MSF.842.88>
- Patil, U. D. 2014. "Response of Unsaturated Silty Sand over a Wider Range of Suction States using a Novel Double-Walled Triaxial Testing System." Doctoral Dissertation. University of Texas at Arlington, Arlington, TX.
- Patil, U. D., L. R. Hoyos, M. Morvan, and A. J. Puppala. 2018. "Bounding surface-based modeling of compacted silty sand exhibiting suction dependent postpeak strain softening." *Int J Numer Anal Methods Geomech*, 42 (14): 1741–1761. <https://doi.org/10.1002/nag.2837>

- Patil, U. D., L. R. Hoyos, and A. J. Puppala. 2016a. "Characterization of Compacted Silty Sand Using a Double-Walled Triaxial Cell With Fully Automated Relative-Humidity Control." *Geotechnical Testing Journal*, 39 (5): 20150156. <https://doi.org/10.1520/GTJ20150156>
- Patil, U. D., L. R. Hoyos, and A. J. Puppala. 2016b. "Modeling Essential Elastoplastic Features of Compacted Silty Sand via Suction-Controlled Triaxial Testing." *International Journal of Geomechanics*, 16 (6). [https://doi.org/10.1061/\(ASCE\)GM.1943-5622.0000726](https://doi.org/10.1061/(ASCE)GM.1943-5622.0000726)
- Peethamparan, S., J. Olek, and S. Diamond. 2009. "Mechanism of stabilization of Na-montmorillonite clay with cement kiln dust." *Cem Concr Res*, 39 (7): 580–589. Elsevier Ltd. <https://doi.org/10.1016/j.cemconres.2009.03.013>
- Pereira dos Santos, C., G. J. Bruschi, J. R. G. Mattos, and N. C. Consoli. 2022. "Stabilization of gold mining tailings with alkali-activated carbide lime and sugarcane bagasse ash." *Transportation Geotechnics*, 32: 100704. Elsevier Ltd. <https://doi.org/10.1016/j.trgeo.2021.100704>
- Peron, H., T. Hueckel, L. Laloui, and L. B. Hu. 2009. "Fundamentals of desiccation cracking of fine-grained soils: experimental characterisation and mechanisms identification." *Canadian Geotechnical Journal*, 46 (10): 1177–1201. <https://doi.org/10.1139/T09-054>
- Petry, T. M., and D. N. Little. 2003. "Review of Stabilization of Clays and Expansive Soils in Pavements and Lightly Loaded Structures - History, Practice, and Future." *Perspectives in Civil Engineering: Commemorating the 150th Anniversary of the American Society of Civil Engineers*, 14 (December): 307–320. [https://doi.org/10.1061/\(asce\)0899-1561\(2002\)14:6\(447\)](https://doi.org/10.1061/(asce)0899-1561(2002)14:6(447))
- Pham, H. Q., D. G. Fredlund, and S. L. Barbour. 2003. "A practical hysteresis model for the soil – water characteristic curve for soils with negligible volume change." *Geotechnique*, 53 (2): 293–298. <https://doi.org/10.1680/geot.2003.53.2.293>
- Pietsch, W., and H. Rumpf. 1967. "Haftkraft, Kapillardruck, Flüssigkeitsvolumen und Grenzwinkel einer Flüssigkeitsbrücke zwischen zwei Kugeln." *Chemie Ingenieur Technik*, 39 (15): 885–893. <https://doi.org/10.1002/cite.330391502>
- Puppala, A. J. 2008. *Estimating stiffness of subgrade and unbound materials for pavement design*. Washington, DC.: NCHRP Synthesis 382, Transportation Research Board.
- Puppala, A. J., and A. Cerato. 2009. "Heave distress problems in chemically-treated sulfate-laden materials." *Geo-Strata — Geo Institute of ASCE*, 10 (2): 28-30,32.
- Puppala, A. J., J. A. Griffin, L. R. Hoyos, and S. Chomtid. 2004. "Studies on Sulfate-Resistant Cement Stabilization Methods to Address Sulfate-Induced Soil Heave." *Journal of Geotechnical and Geoenvironmental Engineering*, 130 (4): 391–402. [https://doi.org/10.1061/\(asce\)1090-0241\(2004\)130:4\(391\)](https://doi.org/10.1061/(asce)1090-0241(2004)130:4(391))
- Puppala, A. J., N. Intharasombat, and R. K. Vempati. 2005. "Experimental Studies on Ettringite-Induced Heaving in Soils." *Journal of Geotechnical and Geoenvironmental Engineering*, 131 (3): 325–337. [https://doi.org/10.1061/\(ASCE\)1090-0241\(2005\)131:3\(325\)](https://doi.org/10.1061/(ASCE)1090-0241(2005)131:3(325))
- Puppala, A. J., A. Pedarla, A. Pino, and L. R. Hoyos. 2017. "Diffused Double-Layer Swell Prediction Model to Better Characterize Natural Expansive Clays." *J Eng Mech*, 143 (9): 1–10. [https://doi.org/10.1061/\(ASCE\)EM.1943-7889.0001292](https://doi.org/10.1061/(ASCE)EM.1943-7889.0001292)

- Puppala, A. J., K. Punthutaecha, and S. K. Vanapalli. 2006. "Soil-Water Characteristic Curves of Stabilized Expansive Soils." *Journal of Geotechnical and Geoenvironmental Engineering*, 132 (6): 736–751. [https://doi.org/10.1061/\(asce\)1090-0241\(2006\)132:6\(736\)](https://doi.org/10.1061/(asce)1090-0241(2006)132:6(736))
- Puppala, A. J., E. Wattanasanticharoen, and K. Punthutaecha. 2003. "Experimental evaluations of stabilisation methods for sulphate-rich expansive soils." *Proceedings of the Institution of Civil Engineers - Ground Improvement*, 7 (1): 25–35. <https://doi.org/10.1680/grim.2003.7.1.25>
- Qi, J., P. A. Vermeer, and G. Cheng. 2006. "A review of the influence of freeze-thaw cycles on soil geotechnical properties." *Permafrost Periglacial Process*, 17 (3): 245–252. <https://doi.org/10.1002/ppp.559>
- Qi, S. C., and S. K. Vanapalli. 2016. "Numerical study on expansive soil slope stability considering the cracks and coupling effects." *Unsaturated Soil Mechanics from Theory to Practice - Proceedings of the 6th Asia-Pacific Conference on Unsaturated Soils*, (October 2015): 621–628. <https://doi.org/10.1201/b19248-103>
- Qi, S., and S. Vanapalli. 2015. "Stability Analysis of an Expansive Clay Slope: A Case Study of Infiltration-Induced Shallow Failure of an Embankment in Regina, Canada." *International journal of geohazards and environment*, (December): 7–19. <https://doi.org/10.15273/ijge.2015.01.003>
- Rahardjo, H., O. B. Heng, and L. E. Choon. 2004. "Shear strength of a compacted residual soil from consolidated drained and constant water content triaxial tests." *Canadian Geotechnical Journal*, 41: 421–436. <https://doi.org/10.1139/t03-093>
- Rahardjo, H., T. T. Lim, M. F. Chang, and D. G. Fredlund. 1995. "Shear strength characteristics of a residual soil with suction." *Canadian Geotechnical Journal*, 32: 60–77.
- Rahardjo, H., T. H. Ong, R. B. Rezaur, and E. C. Leong. 2007. "Factors Controlling Instability of Homogeneous Soil Slopes under Rainfall." *Journal of Geotechnical and Geoenvironmental Engineering*, 133 (12): 1532–1543. [https://doi.org/10.1061/\(ASCE\)1090-0241\(2007\)133:12\(1532\)](https://doi.org/10.1061/(ASCE)1090-0241(2007)133:12(1532))
- Rampino, C., C. Mancuso, and F. Vinale. 1999. "Laboratory testing on an unsaturated soil: equipment, procedures, and first experimental results." *Canadian Geotechnical Journal*, 36 (1): 1–12. <https://doi.org/10.1139/t98-093>
- Rampino, C., C. Mancuso, and F. Vinale. 2000. "Experimental behaviour and modelling of an unsaturated compacted soil." *Canadian Geotechnical Journal*, 37 (4): 748–763. <https://doi.org/10.1139/t00-004>
- Reddy, N. G., B. H. Rao, and K. R. Reddy. 2018. "Biopolymer amendment for mitigating dispersive characteristics of red mud waste." *Géotechnique Letters*, 8 (3): 201–207. <https://doi.org/10.1680/jgele.18.00033>
- Richards, L. A. 1931. "Capillary conduction of liquids through porous mediums." *Physics (College Park Md)*, 1 (5): 318–333. <https://doi.org/10.1063/1.1745010>
- Richter, I., and H. Tokinaga. 2020. "An overview of the performance of CMIP6 models in the tropical Atlantic: mean state, variability, and remote impacts." *Clim Dyn*, 55 (9–10): 2579–2601. <https://doi.org/10.1007/s00382-020-05409-w>
- Robinson, J. D., and F. Vahedifard. 2016. "Weakening mechanisms imposed on California's levees under multiyear extreme drought." *Clim Change*, 137 (1–2): 1–14. <https://doi.org/10.1007/s10584-016-1649-6>
- Robinson, J. D., F. Vahedifard, and A. AghaKouchak. 2017. "Rainfall-triggered slope instabilities under a changing climate: comparative study using historical and projected precipitation extremes." *Canadian Geotechnical Journal*, 54 (1): 117–127. <https://doi.org/10.1139/cgj-2015-0602>

- Rojas, J. C., C. Mancuso, and F. Vinale. 2008. "A modified triaxial apparatus to reduce testing time: Equipment and preliminary results." 2 (1975): 103–109. <https://doi.org/10.1201/9780203884430.ch8>
- Rosone, M., C. Airò Farulla, and A. Ferrari. 2016. "Shear strength of a compacted scaly clay in variable saturation conditions." *Acta Geotech*, 11 (1): 37–50. <https://doi.org/10.1007/s11440-015-0379-7>
- Ross, J., and W. Adaska. 2020. *Guide to Cement-Stabilized Subgrade Soils*. Portland Cement Association (PCA), Washington, DC.
- Rout, R. K., P. Ruttanapormakul, S. Valluru, and A. J. Puppala. 2012. "Resilient Moduli Behavior of Lime-Cement Treated Subgrade Soils." *GeoCongress 2012: State of the Art and Practice in Geotechnical Engineering*, 1428–1437.
- Saeedy, H. S., and M. A. Mollah. 1988. "Application of multistage triaxial test to Kuwaiti soils." *Advanced Triaxial Testing of Soil and Rock, ASTM STP 977*, R. T. Donaghe, R. C. Chaney, and M. L. Silver, eds., 363–375. American Society for Testing and Materials, Philadelphia.
- Saleh, A. A., and S. G. Wright. 1997. *Shear Strength Correlations and Remedial Measure Guidelines for Long-Term Stability of Slopes Constructed of Highly Plastic Clay Soils*. Austin, TX.
- Samuel, R. A. 2019. "Synthesis of metakaolin-based geopolymer and its performance as sole stabilizer of expansive soils." Doctoral Dissertation, University of Texas at Arlington, Arlington, TX.
- Scavuzzo, R. 1984. *Use of the Harvard Miniature Apparatus for obtaining moisture-unit weight relationships of soils*. Denver, Colorado.
- Schubert, H. 1984. "Capillary Forces—Modeling and Application in Particulate Technology." *Powder Technol*, 37 (1): 105–116. [https://doi.org/10.1016/0032-5910\(84\)80010-8](https://doi.org/10.1016/0032-5910(84)80010-8)
- Schuurman, Ir. E. 1966. "The Compressibility of an Air/Water Mixture and a Theoretical Relation Between the Air and Water Pressures." *Géotechnique*, 16 (4): 269–281. <https://doi.org/10.1680/geot.1966.16.4.269>
- Sharma, G., S. Sharma, A. Kumar, A. H. Al-Muhtaseb, M. Naushad, A. A. Ghfar, G. T. Mola, and F. J. Stadler. 2018. "Guar gum and its composites as potential materials for diverse applications: A review." *Carbohydr Polym*, 199 (May): 534–545. <https://doi.org/10.1016/j.carbpol.2018.07.053>
- Sharma, R. S. 1998. "Mechanical behaviour on unsaturated highly expansive clays." Doctoral Dissertation, University of Oxford, Oxford, U.K.
- Sherwood, P. T. 1962. "Effect of sulfates on cement- and lime-stabilized soils." *Highway Research Board*, 41 (353): 98–107.
- Solanki, P., M. Zaman, and R. Khalife. 2013. "Effect of Freeze-Thaw Cycles on Performance of Stabilized Subgrade." *In Sound Geotechnical Research to Practice: Honoring Robert D. Holtz II*, 566–580.
- Soranzo, M. 1988. "Results and interpretation of multistage triaxial compression tests." *Advanced triaxial testing of soil and rock*, 353–362.
- Sridharan, A., and P. Sivapullaiah. 2005. "Mini Compaction Test Apparatus for Fine Grained Soils." *Geotechnical Testing Journal*, 28 (3): 240–245. <https://doi.org/10.1520/GTJ12542>
- Sujatha, E. R., and S. Saisree. 2019. "Geotechnical behaviour of guar gum-treated soil." *Soils and Foundations*, 59 (6): 2155–2166. <https://doi.org/10.1016/j.sandf.2019.11.012>
- Taher, Z. J., J. Scalia IV, and C. A. Bareither. 2020. "Comparative assessment of expansive soil stabilization by commercially available polymers." *Transportation Geotechnics*, 24 (March): 100387. Elsevier. <https://doi.org/10.1016/j.trgeo.2020.100387>

- Talluri, N., A. J. Puppala, S. S. C. Congress, and A. Banerjee. 2020. "Experimental Studies and Modeling of High-Sulfate Soil Stabilization." *Journal of Geotechnical and Geoenvironmental Engineering*, 146 (5). [https://doi.org/10.1061/\(ASCE\)GT.1943-5606.0002240](https://doi.org/10.1061/(ASCE)GT.1943-5606.0002240)
- Tami, D., H. Rahardjo, and E.-C. Leong. 2004. "Effect of Hysteresis on Steady-State Infiltration in Unsaturated Slopes." *Journal of Geotechnical and Geoenvironmental Engineering*, 130 (9): 956–967. [https://doi.org/10.1061/\(ASCE\)1090-0241\(2004\)](https://doi.org/10.1061/(ASCE)1090-0241(2004))
- Tang, C.-S., C. Zhu, Q. Cheng, H. Zeng, J.-J. Xu, B.-G. Tian, and B. Shi. 2021. "Desiccation cracking of soils: A review of investigation approaches, underlying mechanisms, and influencing factors." *Earth Sci Rev*, 216: 103586. <https://doi.org/10.1016/j.earscirev.2021.103586>
- Tang, G. X., J. Graham, J. Blatz, M. Gray, and R. K. N. D. Rajapakse. 2002. "Suctions, stresses and strengths in unsaturated sand-bentonite." *Eng Geol*. [https://doi.org/10.1016/S0013-7952\(01\)00108-9](https://doi.org/10.1016/S0013-7952(01)00108-9)
- Thom, R., V. Sivakumar, J. Brown, and D. Hughes. 2008. "A Simple Triaxial System for Evaluating the Performance of Unsaturated Soils Under Repeated Loading." *Geotechnical Testing Journal*, 31 (2): 107–114. <https://doi.org/10.1520/GTJ100963>
- Thrasher, B., W. Wang, A. Michaelis, F. Melton, T. Lee, and R. Nemani. 2022. "NASA Global Daily Downscaled Projections, CMIP6." *Sci Data*, 9 (1): 262. <https://doi.org/10.1038/s41597-022-01393-4>
- Tiwari, N., N. Satyam, and A. J. Puppala. 2021. "Strength and durability assessment of expansive soil stabilized with recycled ash and natural fibers." *Transportation Geotechnics*, 29 (March). <https://doi.org/10.1016/j.trgeo.2021.100556>
- Vahedifard, F., C. C. Goodman, V. Paul, and A. AghaKouchak. 2024. "Amplifying feedback loop between drought, soil desiccation cracking, and greenhouse gas emissions." *Environmental Research Letters*, 19 (3): 031005. <https://doi.org/10.1088/1748-9326/ad2c23>
- Vahedifard, F., F. H. Jasim, F. T. Tracy, M. Abdollahi, A. Alborzi, and A. AghaKouchak. 2020. "Levee Fragility Behavior under Projected Future Flooding in a Warming Climate." *Journal of Geotechnical and Geoenvironmental Engineering*, 146 (12). [https://doi.org/10.1061/\(ASCE\)GT.1943-5606.0002399](https://doi.org/10.1061/(ASCE)GT.1943-5606.0002399)
- Vanapalli, S. K., D. G. Fredlund, D. E. Pufahl, and A. W. Clifton. 1996. "Model for the prediction of shear strength with respect to soil suction." *Canadian Geotechnical Journal*, 33 (3): 2. <https://doi.org/10.1139/t96-060>
- Vann, J. D., and S. L. Houston. 2021. "Field Soil Suction Profiles for Expansive Soil." *Journal of Geotechnical and Geoenvironmental Engineering*, 147 (9). [https://doi.org/10.1061/\(ASCE\)GT.1943-5606.0002570](https://doi.org/10.1061/(ASCE)GT.1943-5606.0002570)
- Vardon, P. J. 2015. "Climatic influence on geotechnical infrastructure: A review." *Environmental Geotechnics*, 2 (3): 166–174. <https://doi.org/10.1680/envgeo.13.00055>
- Yang, S.-R., H.-D. Lin, J. H. S. Kung, and W.-H. Huang. 2008. "Suction-Controlled Laboratory Test on Resilient Modulus of Unsaturated Compacted Subgrade Soils." *Journal of Geotechnical and Geoenvironmental Engineering*, 134 (9): 1375–1384. [https://doi.org/10.1061/\(ASCE\)1090-0241\(2008\)134:9\(1375\)](https://doi.org/10.1061/(ASCE)1090-0241(2008)134:9(1375))
- Yong, R. N., and V. R. Ouhadi. 2007. "Experimental study on instability of bases on natural and lime/cement-stabilized clayey soils." *Appl Clay Sci*, 35 (3–4): 238–249. <https://doi.org/10.1016/j.clay.2006.08.009>
- Zhang, Y., T. Ishikawa, T. Tokoro, and T. Nishimura. 2014. "Influences of degree of saturation and strain rate on strength characteristics of unsaturated granular subbase course material." *Transportation Geotechnics*, 1 (2): 74–89. <https://doi.org/10.1016/j.trgeo.2014.04.001>